

5-2014

Mimicking Early Stages Of Diagenesis In Modern Metasequoia Leaves Implications For Plant Fossil Lagerstätten

Caitlyn Witkowski
Bryant University

Follow this and additional works at: <https://digitalcommons.bryant.edu/msglobalenv>

Recommended Citation

Witkowski, Caitlyn, "Mimicking Early Stages Of Diagenesis In Modern Metasequoia Leaves Implications For Plant Fossil Lagerstätten" (2014). *Master of Science in Global Environmental Studies*. Paper 1.
<https://digitalcommons.bryant.edu/msglobalenv/1>

This Thesis is brought to you for free and open access by the Graduate Theses at DigitalCommons@Bryant University. It has been accepted for inclusion in Master of Science in Global Environmental Studies by an authorized administrator of DigitalCommons@Bryant University. For more information, please contact dcommons@bryant.edu.

5-2014

Mimicking Early Stages Of Diagenesis In Modern Metasequoia Leaves Implications For Plant Fossil Lagerstätten

Caitlyn Witkowski
Bryant University

Follow this and additional works at: <http://digitalcommons.bryant.edu/msglobalenv>

Recommended Citation

Witkowski, Caitlyn, "Mimicking Early Stages Of Diagenesis In Modern Metasequoia Leaves Implications For Plant Fossil Lagerstätten" (2014). *Master of Science in Global Environmental Studies*. Paper 1.
<http://digitalcommons.bryant.edu/msglobalenv/1>

This Dissertation is brought to you for free and open access by the Graduate Theses at DigitalCommons@Bryant University. It has been accepted for inclusion in Master of Science in Global Environmental Studies by an authorized administrator of DigitalCommons@Bryant University. For more information, please contact dcommons@bryant.edu.

Bryant University
The Graduate Program
College of Arts and Sciences

**MIMICKING EARLY STAGES OF DIAGENESIS IN MODERN *METASEQUOIA* LEAVES:
IMPLICATIONS FOR PLANT FOSSIL *LAGERSTÄTTEN***

A Thesis in Global Environmental Studies

by

Caitlyn R. Witkowski

Department of Science and Technology


Submitted in Partial Fulfillment of the Requirements for the Master of Science Degree

May 2014

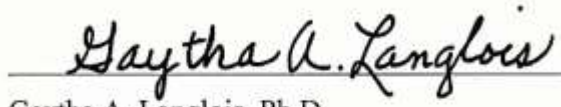
© 2014 Caitlyn R. Witkowski

Committee for the Master of Science Degree in Global Environmental Studies

The thesis of Caitlyn R. Witkowski was reviewed and approved by the following members:


_____ 5/23/2014
Hong Yang, Ph.D.
Charles J. Smiley Chair Professor of Environmental Sciences
Thesis Advisor


_____ 5/27/2014
Qin Leng, Ph.D.
Professor of Biology


_____ 5/30/2014
Gaytha A. Langlois, Ph.D.
Chair, Science and Technology Department
Graduate Director, MSGES


_____ 5/30/2014
Dan McNally, Ph.D.
Associate Professor of Environmental Sciences

*Signatures are on file with the Arts and Sciences Associate Dean of Graduate Studies

Abstract

Remarkably well-preserved plants from rich fossil deposits (known as *lagerstätten*) provide insights into paleoenvironmental and paleoclimatic reconstructions. However, it is difficult to distinguish whether proxy signals from fossil *lagerstätten* represent original environmental information or modified data due to degradation. To better understand molecular and morphological changes of plant leaves over time, modern *Metasequoia*, a well-studied “living fossil,” was degraded to mimic early stages of diagenesis and then compared with its ancient counterpart. Two sample series were used: 1) a laboratory decay experiment with samples in a closed, controlled environment and 2) a natural decay experiment with samples collected from an open lacustrine environment. Morphological and anatomical changes during early diagenesis are evident in both decay series, as seen through SEM observations and through a new quantitative pixel-count evaluation method. The molecular and isotopic results indicate that the removal of polysaccharides collapses cellulose-based primary-walled parenchymatous cells, while cells with lignin-strengthened secondary cells walls remain intact much later in the decay process. This supports previous hypotheses that polysaccharide is significant in maintaining the three-dimensional structures found in plant fossil *lagerstätten*. Both modern laboratory and natural decay series show that diagenesis occurs quickly, suggesting that fossil samples must have been rapidly buried in order to avoid microbial growth. Therefore, given the overall fidelity of *Metasequoia* fossil *lagerstätten*, the approximately -24‰ $\delta^{13}\text{C}$ values recorded in arctic Cenozoic *Metasequoia* fossils are likely due to physiological response to different ancient atmospheric conditions, and not due to microbial-based tissue decay during early diagenesis.

摘要

超常保存的植物化石在古环境与古气候重建中具有重要意义。然而，超常保存的植物化石中的信息究竟源自原始环境因素还是由降解造成，要准确区分却非易事。为了更准确了解植物分子和形态特征在降解过程中的变化，本项研究以现代水杉（已被广泛研究的一种“活化石”植物）叶为材料模拟植物降解在早期成岩作用中的变化，并与化石水杉进行比较。本研究设计了两个降解系列，分别为（1）实验室封闭环境下的降解和（2）室外湖相环境中的自然开放式降解。通过扫描电子显微镜观察和新建立的以计算机分析为基础的定量形态分析，我们在两个系列的样品中均观测到了植物组织明显的逐步降解变化。结合分子和同位素检测结果我们发现，植物叶中多糖分子被微生物分解后，叶中只具有初生细胞壁（主要由多糖组成）的薄壁细胞即发生坍塌，而具有由木质素加固的次生细胞壁的厚壁细胞其降解则被大大延迟。该结果证明多糖在保持植物化石的三维结构中起到了关键性作用。此外，两个现代降解系列都表明微生物降解在成作用的最早期即快速发生，保存了原始三维结构的超常保存的植物化石，在沉积后应经历了极迅速的掩埋，得以避免微生物对多糖分子的分解。考虑到超常保存的植物化石的高保真度，新生代北极区超常保存的水杉化石中的碳同位素值（约-24‰）很可能反映了植物对当时古大气环境和同位素的记录，而并非由于成岩作用过程中的微生物降解所致。

Table of Contents

Abstract	iii
Illustrations	vii
Tables	vii
Equations	vii
Figures	viii
Abbreviations	x
Chapter 1. Introduction	12
Chapter 2. Materials	18
2.1 Microbial strains for laboratory degradation	18
2.2 <i>Metasequoia</i> leaf samples	20
2.2.1 Modern <i>Metasequoia</i> leaves for laboratory decay experiments	21
2.2.2 Modern <i>Metasequoia</i> leaves from a natural decay environment	21
2.2.3 Fossil <i>Metasequoia</i> leaves	22
Chapter 3. Molecular Analyses	23
3.1 Introduction	23
3.1.1 Gas chromatography	24
3.1.2 Mass-spectrometry	26
3.1.3 Combined GC-MS methodologies	27
3.1.4 Pyrolysis	28
3.1.5 UV/vis	29
3.2 Methods	30
3.2.1 Py-GC-MS	30
3.2.2 MBTH assay	33
3.3 Results	34
3.3.1 Py-GC-MS	34
3.3.2 MBTH Assay	40
Chapter 4. Isotopic Analyses	41
4.1 Introduction	41
4.2 Methods	44
4.3 Results	45

Chapter 5. SEM Observations.....	48
5.1 Introduction	48
5.2 Methods.....	50
5.3 Results.....	51
Chapter 6. Pixel-Count Evaluation	58
6.1 Introduction	58
6.2 Methods.....	61
6.3 Results	65
Chapter 7. Discussion	78
7.1 Quantified degradation.....	78
7.1.1 Quantification	78
7.1.2 Automation	81
7.1.3 Reliability	82
7.1.4 Limitations.....	86
7.2 Molecular evidence for plant decay and preservation.....	89
7.2.1 Explaining molecular degradation of <i>Metasequoia</i> samples.....	89
7.2.2 The effects of open versus closed systems on the removal of carbohydrates	93
7.2.3 Polysaccharide concentration as a structural keystone.....	96
7.3 Insights for paleobotanical studies	99
7.3.1 Cross-examination.....	99
7.3.2 Implications for molecular mechanisms.....	101
7.3.3 Impact on fossilization.....	103
Chapter 8. Conclusion.....	106
Acknowledgements.....	108
References.....	109
Appendix A – Flow Charts	117
Appendix B – Standards	120
Appendix C – NMR Results	121
Appendix D – Polysaccharide in Lab Decay	122

Illustrations

Tables

Table 1. *Metasequoia* leaf samples used for the current study, showing their sample number, age, location, and brief descriptions. AHI—Axel Heiberg Island; CL—Clarkia; EI—Ellesmere Island; MA—Mt Auburn Cemetery; WH—Wuhan. 20

Table 2. A master list of polysaccharide pyrolysates and their respective abundances found in *Geotrichum candidum* laboratory decay series of *Metasequoia glyptostroboides* leaves from Day 0 through Day 25, as well as the fragment ions (frag) for the compounds based on the mass-to-charge ratios (m/z). 37

Table 3. Leaf tissue bulk carbon and nitrogen isotopes ($\delta^{13}\text{C}$ and $\delta^{15}\text{N}$, respectively), weight percent carbon and weight percent nitrogen (wt% C and wt% N), and the weight ratio of carbon to nitrogen for fossil (*Metasequoia occidentalis*), modern natural decay (*Metasequoia glyptostroboides*), and modern laboratory decay (*Metasequoia glyptostroboides*) samples (N/A=not available). 45

Equations

Equation 1. Absorbance of a sample as related to the transmittance. 29

Equation 2. Notation for the stable carbon isotope ratio. 42

Equation 3. Notation for the stable nitrogen isotope ratio. 43

Equation 4. Bhattacharyya distance. 63

Equation 5. Relationship between plant tissue carbon isotope value $\delta^{13}\text{C}$ and intercellular CO_2 concentrations. 105

Figures

- Figure 1.** Flow diagram of pyrolysis-gas chromatography-mass spectrometry in which a sample is vaporized under instant heat in pyrolysis, the sample compounds are separated in a silica-lined column in gas chromatography, and then the compounds are bombarded with electrons and identified based on their mass-to-charge ratios in the mass spectrometer..... 26
- Figure 2.** Mass spectra (m/z) and molecular structures of major polysaccharide pyrolysates identified in *Metasequoia* leaves. 32
- Figure 3.** Total ion chromatogram of consortium laboratory decay series of *Metasequoia glyptostroboides*, with polysaccharide peaks labeled in correspondence with the master list in Table 2. (A) Day 0, (B) Day 12, and (C) Day 25 samples..... 38
- Figure 4.** Change in the abundance of polysaccharide pyrolysates over 25 days in *Geotrichum candidum* laboratory decay series of *Metasequoia glyptostroboides* leaves. (A) Relative abundance of levoglucosan over time as determined by Py-GC-MS. (B) Quantitative change in bulk polysaccharide in mol/g over time as determined by MBTH assay 39
- Figure 5.** Leaf bulk tissue $\delta^{13}\text{C}$ of natural decay (black) and *Geotrichum candidum* laboratory decay (gray) samples of *Metasequoia glyptostroboides*, in order of increasing degradation..... 46
- Figure 6.** Flow diagram of scanning electron microscopy, starting from the electron gun and moving through to the electron detector and data collection. 49
- Figure 7.** SEM observations of the transverse sections of the laboratory decay *Metasequoia glyptostroboides* leaf series introduced with *Geotrichum candidum*, showing the control sample (Day 0, A through C), and the decay series from Day 4 (D), Day 9 (E and F), Day 21 (G through J), and Day 25 (K through L) samples. J and L show the lateral sides of leaves with the leaf interiors full filled by fungal hyphae, while or other images show the mid-vein area in the image center. 53
- Figure 8.** SEM observations of *Metasequoia glyptostroboides* leaf surfaces. (A) The inner surface of the clean cuticular membrane of the lower leaf epidermis of M-M-83-B1, showing the mid-vein area in the center and two stomatal zones. Leaf margins are not shown (image, courtesy of Qin Leng, Vienna University on May 2006). (B), (C), and (D) show external different views of leaf lower surface of Day 9 laboratory decay samples introduced with to *Geotrichum candidum*, at which time the fungal hyphae have infiltrated the leaf cuticle via stomata (arrows)..... 57
- Figure 9.** Example of the hemocytometer-like computer pixel-count evaluation method. (A) Pixel size of a selected region of interest on a SEM photograph on the transverse section of a *Metasequoia* leaf mid-vein. (B) 40x40 pixel grid cell used for both the conventional manual method and the computer pixel-count evaluation method..... 59

- Figure 10.** GMM of pixel values for *Geotrichum candidum* laboratory decay of *Metasequoia glyptostroboides*, where 0 represents black and 1.0 represents white. (A) Day 9 (image in upper right) shows a bimodal distribution of mostly black and white. (B) Day 21 (image in upper right) shows more unimodal distribution of mostly gray. 66
- Figure 11.** Scatterplot of the mean from the first peak against the mean of the second peak from the GMM distributions from the pixel-count evaluation. Red represents not degraded and green represents degraded samples. 68
- Figure 12.** Bhattacharyya distance of GMM distributions from pixel-count evaluation using all samples (laboratory decay, natural decay, and fossil) showing degraded (blue) and not degraded (red). Day 5 (green) are seen in (A) region of interest, (C) histogram, and (E) scatterplot. Day 25 (green) are seen in (B) region of interest, (D) histogram, and (F) scatterplot. 70
- Figure 13.** Pixel-count evaluation conducted on strips of the image for Day 0. (A) GMM showing the distributions of pixel values. (B) Strip image with Bhattacharyya distance. 73
- Figure 14.** Pixel-count evaluation conducted on strips of the image for Day 25. (A) GMM showing the distributions of pixel values. (B) Strip image with Bhattacharyya distance. 74
- Figure 15.** Pixel-count evaluation conducted on strips of the images for Day 5 (A and B) and Day 25 (C and D) of the consortium laboratory decay. (A) and (C) show the original image, whereas (B) and (D) show the strips color-coded based on how well-preserved (white) or poorly-preserved (black) the sample is, based on the Bhattacharyya distance. 75
- Figure 16.** Bhattacharyya distance from the pixel-count evaluation method for consortium laboratory decayed, *Geotrichum candidum* laboratory decayed, and natural decayed series, as well as fossil *Metasequoia* leaves. 77
- Figure 17.** Different photo conditions to test the pixel-count evaluation effectiveness. (A) and (C) are low and high brightness for Day 5 consortium laboratory decay sample. (B) and (D) are low and high brightness for Day 25 consortium laboratory decay sample. The scale on the graph ranges from 0 (black) to 255 (white) pixel values. 83
- Figure 18.** The same image of consortium laboratory decay Day 5 and Day 25 plot on the same graph, with not degraded (red) and degraded (green). (A) Traditional hemocytometer. (B) Computerized pixel-count evaluation method. 84

Abbreviations

CaCl ₂	Calcium chloride
CO ₂	Carbon dioxide
CuO	Copper (II) oxide
DG	Degraded <i>Metasequoia</i> leaf sample
DTT	Dithiothreitol
δ ¹³ C	Stable carbon isotope ratio of ¹³ C to ¹² C, reported in parts per mil (‰) in comparison with the Vienna-Pee Dee Belemnite (VPDB) standard
δ ¹⁵ N	Stable nitrogen isotope ratio of ¹⁵ N to ¹⁴ N, reported in part per mil (‰) in comparison with ambient air as a standard
DCM	Dichloromethane
FeNH ₄ (SO ₄) ₂	Ammonium iron (II) sulfate
GC	Gas chromatography
GlcNAc	N-Acetylglucosamine
GMM	Gaussian mixture model
Gu	Guaiacyl
HCl	Hydrochloric acid
H ₂ SO ₄	Sulfuric acid
IRMS	Isotope ratio mass spectrometry
KHPO ₄	Potassium hydrogen phosphate
Lv	Levoglucosan (aka 1,6-Anhydro-beta-glucopyranose)
MBTH	3-methyl-2-benzothiazolinone hydrazone
MeOH	Methanol

MgSO ₄	Magnesium sulfate
MS	Mass spectrometry
NaOH	Sodium hydroxide
Na ₂ HPO ₄	Disodium phosphate
NDG	Not degraded <i>Metasequoia</i> leaf sample (well-preserved)
NH ₄ Cl	Ammonium chloride
NMR	Nuclear magnetic resonance mass spectrometry
Py	Pyrolysis
Py-GC-MS	Pyrolysis-gas chromatography-mass spectrometry
SEM	Scanning electron microscope
TLE	Total lipid extraction
UV	Ultraviolet light
UV/vis	Ultraviolet/visible spectroscopy
Vp	Vinyl phenol

Chapter 1. Introduction

Because well-documented human history (approximately 4000 BCE) is remarkably short in geological terms, and direct environmental records are even shorter (from the late nineteenth century), indirect measurements, known as proxies, are necessary to understanding the past (Stocker and Mysak, 1992; Verschuren, 1999; McDermott, 2004; Moberg et al., 2005). There are many different proxies, such as tree rings, lake and ocean sediment cores, corals, forams, diatoms, and plant fossils to help reconstruct ancient climate and environments (Peulve et al., 1996; Uhl and Mosbrugger, 1999; Barber et al., 2003; Charman et al., 2006; Stevens et al., 2007).

The focus of this research is on plants, a major type of proxy often associated with fossil *lagerstätten*. Extraordinarily well-preserved fossil deposits (known as fossil *lagerstätten*) contain particularly useful information to be used as proxies because the fossils have high fidelity, often containing biological material indicative of the past. A single, well-preserved leaf can offer a snapshot of the environment and climate during a particular time period, as well as offer important information in plant systematics, physiology, and ecology (Dilcher, 2000; 2001; Barber et al., 2003; Friis et al., 2005). Some of the ways in which fossil plants record the past are through chemical and physical means (Hickey, 1973; Hickey and Wolfe, 1975; Dilcher, 2000).

There are two major chemical means in which plants can store information: molecularly and isotopically. Molecular chemical changes in the leaf composition and their implementation for environmental proxies are well-established (Doyle and Hickey, 1976; Blanchette et al.,

1991; Hughes, 1994; Endress and Igersheim, 2000; Soltis et al., 2002; Davies et al., 2004; Friis et al., 2005). Examination of early stages of degradation in modern organisms is significant in identifying molecular biomarkers in fossils and their preservation potential. *In situ* biomolecules and biomarkers in plant fossils are characteristic stable compounds that provide information on the climate and environment during the time in which that plant was buried, as well as offer insights across many studies, from fossil identification to understanding plant physiology to the condition of fossil preservation (Eglinton and Logan, 1991; Peulve et al., 1996; Briggs, 2003).

The second major chemical means for using plant fossils as proxies is isotopically, in which often examines variations in stable carbon, hydrogen, and nitrogen isotopes. For example, plant waxes demonstrate that stable carbon isotopes ($\delta^{13}\text{C}$) change when plants incorporate atmospheric carbon dioxide (CO_2) during plant photosynthesis, which give clues into ancient climates. Hydrogen isotopes (δD) change when plants incorporate environmental water into plant tissues, offering information on ancient water, as well as demonstrate latitude and coastal distance (Jahren and Sternberg, 2003; Yang et al., 2009; Yang and Leng, 2009; Yang et al., 2011; Sessions et al., 1999; Huang and Yang, 2003). Using only these two isotopes, an ancient environment much better understood.

The major physical means of using plant fossils as proxies is anatomically and morphologically. Anatomically, remarkably preserved three-dimensional structures offer insight into evolutionary history, as well as act as a clear comparison of environments among different time periods (Yang et al., 2007). Morphologically, physical variations in leaf

venation, leaf margin, leaf cuticle, etc. can provide insights for the climate and environment reconstruction. An example of using morphology for the understanding of proxies is the frequency of stomata (density, index, and number per leaf length). Stomata are the pores on the epidermis of the leaf that controls CO₂ intake and water loss, is closely related to atmospheric CO₂. In the past several decades, the relationship between the concentration of stomata and atmospheric CO₂ has widely been used to reconstruct ancient atmospheric CO₂ concentrations (Doyle and Hickey, 1976; Dilcher, 2001).

Despite the utility of environmental proxies in understanding the past, it is often difficult to distinguish whether molecular, isotopic, or morphological features have high fidelity. The detected features in fossils are either the original biological features or are possibly the results of degradation and exposure to different environments (Poinar and Stankiewicz, 1999; Yang et al., 2005; 2007). Understanding chemical and physical degradation in plant fossil proxies is significant because it helps us determine how cautiously we should use proxies when extracting information on ancient life and environments (Wolf, 1971; 1977; Liang et al., 2003; Briggs, 2003; Yang et al., 2005). The established hypothesis for the mechanism behind excellent morphological preservation is a microbial-restricted depositional environment, such as rapid burial, permafrost, or saline ponds (Eglinton and Logan, 1991; Briggs and Eglinton, 1994). Regardless of this hypothesis, however, the fidelity of preserved biomolecules is still unknown (Poinar and Stankiewicz, 1999; Yang et al., 2005; Gupta et al., 2009; Leng et al., 2010; Witkowski et al., 2012). Proxies offer a wealth of knowledge about the past, but must have high fidelity in order to be considered reliable.

Possibly offering an answer to the fidelity of plant proxies, previous studies have hypothesized that polysaccharides may play a key role in preserving three-dimensional structures of fossil plant cell walls, given that polysaccharides have been found more abundantly in morphologically better preserved fossils (Yang, 2005; Yang et al. 2005; 2006; 2007; Witkowski et al. 2012). In order to confirm this hypothesis and to determine the potential relationship between the amount of preserved molecular polysaccharides and the morphological preservation condition of three-dimensional cell wall structures, modern *Metasequoia glyptostroboides* (Hu and Cheng, 1948) leaves underwent molecular, isotopic, and morphological analyses and were compared to the fossil counterpart. Two modern decay series were conducted, one in which samples were collected from a natural outdoor environment (hereafter referred to as “natural decay”) and one in which samples were controlled in several laboratory decay experiments (hereafter referred to as “laboratory decay”).

M. glyptostroboides, the monospecific living species of the genus *Metasequoia* (Miki, 1941), is considered a “living fossil.” *Metasequoia* plants first appeared on the Earth in Cenomanian some 100 million years (Ma) ago in northern Eurasia and soon expanded to every continent in the Northern Hemisphere. They left abundant fossil remains spanning a long geological time window of approximately 100 Ma (Florin, 1962; Yang and Jin 2000, LePage, et al, 2005). During this long evolutionary history, *Metasequoia* have remained genetically (Yang and Jin, 2000; Li and Yang, 2003a; 2003b; Yang, 2005) and morphologically static (Yang et al., 2005; Leng et al., 2010). Because there is no genetic drift over time, modern *Metasequoia* organs can be effectively benchmarked to its fossil counterpart. All these features make

Metasequoia a “model” organism for studying plant evolution, phylogeny, and phytogeography, as well as ideal for studying the plants’ morphological, anatomical, and physiological adaptation. Furthermore, these genetically and morphologically static features also make *Metasequoia* ideal for studying environmental changes and aid in paleoenvironmental and paleoclimatic reconstruction (Leng et al., 2001; Leng et al., 2010; Yang et al., 2005).

In addition to its wide and abundant existence in fossil records, *Metasequoia* fossils are often found in fossil *lagerstätten*. They are not only extremely well-preserved morphologically, often with three-dimensional structures still intact, but are also extraordinarily well-preserved molecularly (Blanchette et al., 1991; Basinger, 1991; McIver and Basinger, 1999). *Metasequoia* has well-established analysis of morphological and biomolecular characteristics (Gupta and Pancoast, 2004; Yang et al., 2005, 2007; Gupta et al., 2009; Witkowski et al., 2012). These features make *Metasequoia* a “model” organism for the understanding of fossil taphonomy, a process leading to fossilization. As a result, we use *M. glyptostrobooides* leaves as the material in our study to mimic the early diagenesis process (the physical and chemical changes during the fossilization process) which will then be compared against known fossils.

Our multi-objective project’s first aim is to quantify degradation. The purpose of quantification is to more objectively and readily compare samples, better understand tissue decay, and apply an unbiased method across many different samples. The second aim is to identify the molecular mechanisms for degradation in biological materials, primarily through the use of pyrolysis-gas chromatography-mass spectrometry (Py-GC-MS) and 3-methyl-2-

benzothiazolinone hydrazone (MBTH) assay. Furthermore, isotopic data will allow us to understand how the environment played an effect on the degradation of samples. Finally, the most important and primary aim is to explain the remarkable three-dimensional preservation of fossils seen in morphological observations from molecular perspectives, as well as understanding the morphological demonstration of the preservation of certain biomolecules.

Through analyses at the molecular level, stable isotopic level, and morphological level, as well as applying both qualitative observations and quantitative measurements on different degrees of decay in both naturally decayed and laboratory decayed *M. glyptostroboides* leaf samples, we hope to compare the degradation of modern samples with their fossil counterparts to have a better understanding on the roles played by polysaccharides in the preservation of exceptional plant fossils. This research is pioneer in several ways. This is the first research to use quantitatively and qualitatively measured degradation of modern plants to understand implications for fossil plants. In fact, this is the first research to quantify morphological changes of any kind, offering a new computer-based method, and is the first to employ the MBTH assay for quantifying degradation of plants.

Chapter 2. Materials

2.1 Microbial strains for laboratory degradation

We conducted laboratory decay experiments by introducing polysaccharide-degrading microbes because polysaccharides are the most abundant biomolecules in nature and because previous hypotheses suggest that polysaccharide might maintain cell wall structures in plant fossils. Polysaccharides are mainly degraded by carbohydrate-active enzymes secreted by microbes, where different microbes produce enzymes committed to degrading specific polysaccharides (van den Brink and de Vries, 2011).

Laboratory experiments were carried out to determine the effectiveness of microbial strains for the degradation of polysaccharides. Growth experiments were conducted on a list of candidate strains generated on previous work (Wouters, 1966; Sietsma and Wouters, 1971; Trinci and Collinge, 1975; Yamanaka et al., 1993; van Fossen et al., 2008; van den Brink and de Vries, 2011). All strains were obtained from the Department of Microbiology at China University of Geosciences (CUG) and CUG collaborative laboratories. The list was narrowed to two fungal (ascomycete or sac fungal) species: *Geotrichum candidum* Link (Wouters, 1966; Sietsma and Wouters, 1971) and *Trichoderma reesei* (Simmons, 1977), the asexual industrial fungus which was confirmed by Kuhls et al (1996) by DNA analysis to be the anamorph of *Hypocrea jecorina* (Berk and Broome, 1875; Chaverri and Samuels, 2003). Two consortia were also used for comparison.

In each of the growth experiments, a microbial strain or a consortium was introduced to a medium in which levoglucosan (Lv) and agar were the only carbohydrate source. Lv was chosen because it has been confirmed to be the most common pyrolysis product (known as a pyrolysate) of cellulose and the most abundant pyrolysate in *Metasequoia* (Yang et al., 2005; 2007; Gupta et al., 2009; Witkowski et al., 2012). To make the medium, first, NH_4Cl (0.1% m/v), Na_2HPO_4 (1% m/v), KHPO_4 (0.15% m/v), and Lv (0.2% m/v) were combined in 50 mL of water and autoclaved. Then 2% agar was added, everything was autoclaved again, and finally MgSO_4 (0.1% m/v) and CaCl_2 (5% m/v) were added. Microbial growth was examined over a three-week period. After several experiments, four cultures were determined to be the most effective based on their visible grow on the Lv medium.

These four cultures were then independently introduced to *M. glyptostrobooides* leaves. A concentration of 0.5 mL of microbial strain in 1M NH_3NO_3 solution as a nitrogen source was added to 1g of fresh freeze-dried *M. glyptostrobooides* leaves in a petri dish. In total, twelve petri dishes were prepared and placed in a 30°C incubator to optimize microbial growth. Once a week, samples were supplied with 1 mL of autoclaved tap water. The water was autoclaved to prevent the introduction of additional microbial life. Every four to five days, two petri dishes from each set were removed from the incubator and placed into a freezer at -20°C to terminate microbial growth for future analyses. All experiments were carried out for a period of 25 days (d), which was deemed sufficient to mimic early stages of diagenesis through the removal of polysaccharide and judge differences in leaf degradation, while still short enough to modify and repeat the experiment.

2.2 *Metasequoia* leaf samples

Three groups of *Metasequoia* leaf samples were used for this study: 1) modern leaves for laboratory decay, 2) modern leaves sampled from a natural decay environment, and 3) fossil leaves from three localities. All samples are listed in Table 1.

Table 1. *Metasequoia* leaf samples used for the current study, showing their sample number, age, location, and brief descriptions. AHI—Axel Heiberg Island; CL—Clarkia; EI—Ellesmere Island; MA—Mt Auburn Cemetery; WH—Wuhan.

Sample No.	Age	Location	Type	Description
Clarkia	Miocene	CL	Fossil	
M-E-10	Eocene	AHI	Fossil	
M-E-10R	Eocene	AHI	Fossil	
M-P-15	Paleocene	EI	Fossil	
M-P-15R	Paleocene	EI	Fossil	
M-M-83-B1	Modern	MA	Natural	Green leaves from tree
M-M-83-B2	Modern	MA	Natural	Early senescence from tree
M-M-83-B3	Modern	MA	Natural	Late senescence from tree
M-M-83-B4	Modern	MA	Natural	Ground beneath tree
M-M-83-B5	Modern	MA	Natural	Pond, sediment-water interface
M-M-83-B6	Modern	MA	Natural	Pond, deep
Gc-D00	Modern	WH	Laboratory	<i>Geotrichum candidum</i> , Day 0
Gc-D04	Modern	WH	Laboratory	<i>Geotrichum candidum</i> , Day 4
Gc-D09	Modern	WH	Laboratory	<i>Geotrichum candidum</i> , Day 9
Gc-D21	Modern	WH	Laboratory	<i>Geotrichum candidum</i> , Day 21
Gc-D25	Modern	WH	Laboratory	<i>Geotrichum candidum</i> , Day 25
B-D00	Modern	WH	Laboratory	Consortium, Day 0
B-D05	Modern	WH	Laboratory	Consortium, Day 5
B-D12	Modern	WH	Laboratory	Consortium, Day 12
B-D17	Modern	WH	Laboratory	Consortium, Day 17
B-D20	Modern	WH	Laboratory	Consortium, Day 20
B-D25	Modern	WH	Laboratory	Consortium, Day 25

2.2.1 Modern *Metasequoia* leaves for laboratory decay experiments

Fresh green leaves from a mature *M. glyptostroboides* tree were collected from China University of Geosciences campus in Wuhan, Hubei, China (30°31'15.54"N, 114°23'59.16"E) during September 2011. All samples were taken from matured leafy branchlets at the exact same height (approximately 7m) from the middle portion of branches. Leafy branchlets were removed from the branch, cleaned with de-ionized water, and freeze-dried before storing in a -80°C freezer. On the day of the experiment, leafy branches were taken out from the freezer and remained sealed until they reached room temperature. Then, samples were open-exposed under an ultraviolet (UV) hood for 4 hours (h) for sterilization. The upper and lower surfaces were turned over every 30 minutes (min) to ensure that both sides were well exposed to UV light to terminate all microbial life. All glassware used in the experiment was autoclaved and all metal tools were cleaned with dichloromethane (DCM).

2.2.2 Modern *Metasequoia* leaves from a natural decay environment

M. glyptostroboides leaf samples were collected from a natural decay environment, representing a sequence of various stages of leaf senescence and tissue decay from the Mt. Auburn Cemetery, MA, USA (42°22'21"N, 71°08'33"W) during the fall through winter of 2004 by Hong Yang. Details of the natural decay samples and their physical environments were previously published in Gupta et al. (2009). Briefly, three samples (M-M-83-B1 through 3) were directly collected from the south side of the tree to represent samples from green (M-M-83-B1) through the onset of color change (M-M-83-B2) to orange-red leaves (M-M-83-B3) before falling. M-M-83-B4 samples are fallen leaves of the same year collected from the ground directly under the same tree. Samples M-M-83-B5 through 6 were

obtained from the pond sediments directly under the same tree that M-M-83-B1 through 4 are from. They were collected using an environmental dredge. Sample M-M-83-B5 was collected from the water-sediment interface, whereas M-M-83-B6 was obtained within sediments representing deposition of the previous years. The pond is a small and quiet aqueous environment with little water disturbance and with a single *M. glyptostroboides* tree growing aside, thus samples M-M-83-B5 and 6 are highly likely to be from the same tree of samples M-M-83-B1 through 4. After collecting, all samples were stored in a -80°C freezer at Bryant University before being analyzed.

2.2.3 Fossil *Metasequoia* leaves

The term ‘fossil’ is used to describe ancient samples, although only early stages of diagenesis may be found and actual fossilization has not yet occurred. Fossil leaves of *M. occidentalis* (Newberry) Chaney used for comparative study with modern decayed samples were collected from three fossil localities. 1) Samples labeled Clarkia were collected by the author in August 2013 from the UIMM P-33 site of the Miocene Clarkia fossil site near Clarkia, Idaho, USA (46°59'29.3"N, 116°16'35.8"W). 2) Samples labeled M-P-15 were collected by Christopher Williams from the late Paleocene-early Eocene lignite beds at the top of Member 2The Iceberg Bay Formation at Stenkul Fiord, Ellesmere Island, Canadian Arctic Archipelago (77°20'58"N, 83°26'08"W). 3) Samples labeled M-E-10 were also collected by Christopher Williams from the Upper Coal Member in the Buchanan Lake Formation at Axel Heiberg Island, Canadian Arctic Archipelago (79°54'55.8"N, 89°01'26.8"W). Detailed descriptions of these fossil samples as well as their geological settings were previously published (Yang et al., 2005; Witkowski et al., 2012).

Chapter 3. Molecular Analyses

3.1 Introduction

As explained in Chapter 1, the two major types of chemical analyses for studying environmental proxies are molecular and isotopic. This chapter includes an introduction to the instrumentation, the methods, and the results for molecular analyses. Initially, only pyrolysis-gas chromatography-mass spectrometry (Py-GC-MS) was the only instrumentation planned for molecular analysis in this study, but due to unusual results, other methods were also introduced, including 3-methyl-2-benzothiazolinone hydrazone (MBTH) assay and nuclear magnetic resonance mass spectrometry (NMR). Because there are few results for NMR, this technology will not be explained in great detail (results in Appendix C).

Thus, Py-GC-MS and MBTH assay were the two major molecular tools used for analyzing the degradation in modern and fossil *Metasequoia* leaves for this study. The addition of the MBTH assay provided insights into the Py-GC-MS results. Py-GC-MS provides semi-quantitative relative abundances of both bulk polysaccharide and individual compounds, whereas the colorimetric MBTH assay provides quantitative and highly replicable abundances of bulk polysaccharides. The former is frequently used for examining fossil materials because of its sensitivity with trace material, whereas the latter has rarely been applied to paleobotany, despite its common use in other fields.

3.1.1 Gas chromatography

Chromatography, a common technique for separating mixtures, dissolves an analyte in a mobile phase and pushes the resulting fluid through a stationary phase based on the compound's partition coefficient. The partition coefficient, also known as the distribution coefficient, is a ratio of the compound in the mobile and in the stationary phases; the coefficient can vary based on the compound's properties, especially on the polarity (Martin and Synge, 1941; Conder, 2000). Silica gel, the most commonly used stationary phase and approximately 40-65 μm in size, has hydroxyl (OH) groups that give the gel unique stationary phase properties (Sigma-Aldrich, 2014). In normal phase chromatography, silica gel is used because it has high polarity and unique bonding properties; this causes non-polar components to elute first, which helps quickly and effectively separate major compounds (Still et al., 1978; Okamoto et al., 1981).

Gas chromatography (GC) differs from liquid chromatography in that instead of using a liquid mobile phase, a carrier gas stream is used as the mobile phase to push the analyte through a column with silica gel lining (as opposed to a packed column as seen in column chromatography). Although hydrogen is the most efficient carrier gas for separation, our experiments use helium gas because it is inert, non-flammable (unlike highly combustible hydrogen), and has comparable efficiency to hydrogen for most experiments (Shetty et al., 1993). As compounds move through the column, some exhibit adsorption to the column walls. The strength of adsorption, due to the partition coefficient and other physical properties of the molecules, affects how long the compounds are retained in the column (Martin and Synge, 1941). Thus, the time that it takes a compound to exit the column is referred to as the retention time.

When compounds reach the end of the column, they are detected and identified electronically. Although there are many types of detectors, such as catalytic combustion, electron capture, flame photometric, infrared, and photo-ionization detectors, the most commonly used are the flame ion detector (FID) and the thermal conductivity detector (TCD). FID is a destructive detector that breaks chemical bonds and is more sensitive to hydrocarbons, whereas TCD is a nondestructive detector that is more sensitive to water; chemists often use both for their complementing strengths (Gupta et al., 2009). In this research, mass spectrometry (MS, see 3.1.2) is instead used as a combinational instrumentation method (Figure 1).

Compounds are detected and graphically represented on an adjacent computer by a series of peaks which show abundance versus retention time; the samples can then be either analyzed via peak height or peak area (Yang et al., 2005; Gupta et al., 2009). Peak height gives a more qualitative understanding of the general abundance in the sample, and is recognizable by eye. Peak area, which is used in this research, is a semi-quantitative measurement that is particularly useful for large polysaccharides (levoglucosan, for example) which have relatively small peak heights, but large overall abundance due to peak area (Witkowski et al., 2012).

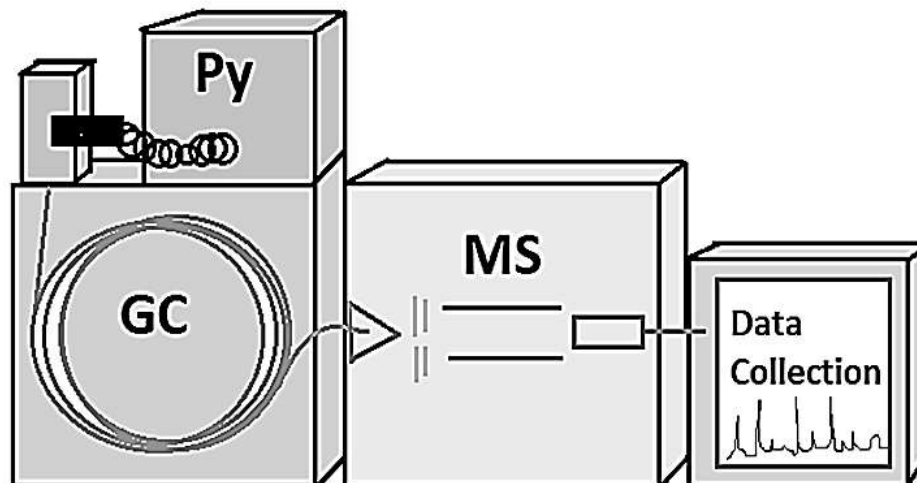


Figure 1. Flow diagram of pyrolysis-gas chromatography-mass spectrometry in which a sample is vaporized under instant heat in pyrolysis, separated in a silica-lined column in gas chromatography, and then identified based on their mass-to-charge ratios in the mass spectrometer.

3.1.2 Mass-spectrometry

Mass spectrometry (MS) identifies and analyzes compounds based on their mass-to-charge ratios (m/z). The specifics of the instrumentation can vary greatly depending on the type of mass spectrometry; thus, the instrumentation explained here will be of those used in this research (Shetty et al., 1993). Once the analyte enters the MS, compounds are ionized via chemical ion-molecule reactions during collisions in the ion source component; both positive and negative ions can be obtained. The ionized compounds are then accelerated and subjected to an electromagnetic field, where they are then separated and sorted based on their m/z in the mass analyzer module ions of the same m/z are equally deflected, which helps demonstrate the abundance of specific compounds in a given sample. Once separated, ions are measured on a detector (usually an electron multiplier) and graphically represented on an adjacent computer (Audi, 2006), as seen in Figure 1.

The graphical representation, known as mass spectra, indicates the quantity and abundance of each ion present in the sample. The resulting peaks each have a specific ion fragmentation pattern that indicates how key features of the compound break down (Pavia et al., 2006; Parkins, 2005). These masses and fragmentation patterns are then compared to already known, studied, and tested compounds (referred to as standards) from the National Institute of Standards and Technology (NIST) and from previous analysis of compounds with known molecular structures in order to confirm the identification of the given compound (Yang et al., 2005; NIST, 2010; Witkowski et al., 2012).

3.1.3 Combined GC-MS methodologies

In the 1950s, Roland Gohlke and Fred McLafferty developed the combined methodology of GC-MS (Gohlke and McLafferty, 1993). As a unified technique, in which compounds that are separated through the GC column are introduced to MS based upon their retention times, the two components dramatically increased the quality of compound identification. Combined, GC-MS reduces the potential error found in either individual machine, complementing each other's weaknesses; the likeliness of a compound eluding detection in both pieces of equipment becomes highly unlikely when the two are combined (Gudzinowicz, 1977; Shetty et al., 1993). As GC-MS decreases in price and increases in accessibility, precision, and accuracy, it has become increasingly popular and is now one of the most efficient forms of compound identification (McMaster and McMaster, 1998).

3.1.4 Pyrolysis

The current study uses the prefacing auxiliary instrument pyrolysis (Py) before the analyte is inserted into the combined GC-MS instrumentation (Figure 1). Pyrolysis subjects an analyte to high temperatures (610°C for this experiment) in the absence of oxygen and halogens. The high temperatures irreversibly and thermochemically decompose the solid organic material into a gaseous analyte. Pyrolysis decomposes large, bulky compounds at their weakest structural points into smaller molecules; this is useful because molecules that are too large, like proteins, can remain in the column and cause unresolved contamination in future run samples.

The benefit of using pyrolysis is that a solid sample can very quickly and readily be transformed to a volatile material capable of running on the GC-MS without solubilizing solid materials into either a liquid or gas which can be extremely difficult and time-consuming. Furthermore, Py-GC-MS is also extremely useful for examining trace samples because it requires so little sample to be thermally decomposed, one of the reasons that it is so useful in archeology because fossils and ancient materials are both rare and in small quantity. The trace sensitivity of Py-GC-MS is particularly useful for studying *Metasequoia* fossils.

3.1.5 UV/vis

The MBTH assay requires the use of ultraviolet/visible spectroscopy (UV/vis). UV/vis considers color in terms of wave motion, quantifying color based on the absorption and reflectance in the visible light and adjacent ranges (near-UV and near-infrared). Light (c) is equivalent to the distance between two peaks (the wavelength, λ) multiplied by the amount of peaks passing a given point per second (the frequency, ν). UV/vis measures the intensity of light before and after it passes through a sample; the resulting ratio is referred to as transmittance ($\%T$). Transmittance is then translated into absorption (A), as seen in Equation 1.

Equation 1. Absorbance of a sample as related to the transmittance.

$$A = -\log\left(\frac{\%T}{100\%}\right)$$

The detected color is indicative of the chemicals present in the sample. For this research, MBTH is used to determine how much reducing sugar is in the *Metasequoia* leaf samples. According to the Anthon and Barrett (2001) method, an MBTH molecule condenses with aldehyde to form an adduct. The adduct then reacts with a second MBTH molecule under acid and oxidizing conditions to form a highly-colored blue product. The resulting color is then measured (620nm) by UV/vis to determine how much bulk sugar is in the sample. The “bluer” the sample is, the more reducing sugar is in the sample. UV/vis yields highly reproducible and accurate results, as well as offers simple, versatile, quick, and cost-effective means of measuring bulk sugar.

3.2 Methods

3.2.1 Py-GC-MS

A total lipid extraction (TLE) was performed prior to Py-GC-MS analysis for natural decay, laboratory decay, and fossil samples. Approximately 2 mg of sample were crushed and extracted via ultrasonication for 15min using 2:1(v/v) dichloromethane (DCM):methanol (MeOH) solvent (Yang et al., 2005; Witkowski et al., 2012) and concentrated using nitrogen. The entire TLE process was repeated three times. After samples were dried, precisely 0.5mg of the remaining sample was placed in a quartz tube with glass wool. All samples were run on the same machine under the same conditions with the same sample weight during the same several days. Two blanks were run in between each sample run in order to prevent contamination from the previous sample.

The sample inside the quartz tube was then inserted into the CDS 1500 with an interface of 250°C. The pyrolysis probe was set at 610°C for 15 seconds in a flow of helium gas. An Agilent 7890A GC with a 30m capillary column (250µm diameter and 0.25µm film thickness) was used with helium as the carrier gas. The GC oven was held at 40°C for 5min isothermal to 100°C at a rate of 10°C/min, and then finally increases to 300°C at a rate of 10°C/min. An Agilent 5975C Series GCMSD MS was operated in full scan mode at 70eV (Logan and Eglinton, 1994; Yang et al., 2005; Witkowski et al., 2012). Peaks were identified via the US National Bureau of Standards and Technology (NIST) mass spectral library and other references (Yang et al., 2005; Gupta et al., 2009; Witkowski et al., 2012).

Relative abundances of polysaccharides commonly found in *Metasequoia* were measured for comparative analyses among the 25 d span of samples. The 13 polysaccharide compounds include 2-methylfuran, acetic acid, 2-furaldehyde, 2-hydroxy-2-methyl-2-cyclopenten-1-one, 5-methyl-2-furfuraldehyde, 4-hydroxy-5,6-dihydro (2H) pyran-2-one, two Rhamnose markers, 3 hydroxy-2-methyl-(4H)-pyran-4-one, levoglucosan, and anhydrosugar (Figure 2), and are based on both the findings in this study and previously published work on the major polysaccharide-based products seen as pyrolysates (Yang et al., 2005; Gupta et al., 2009; Witkowski et al., 2012).

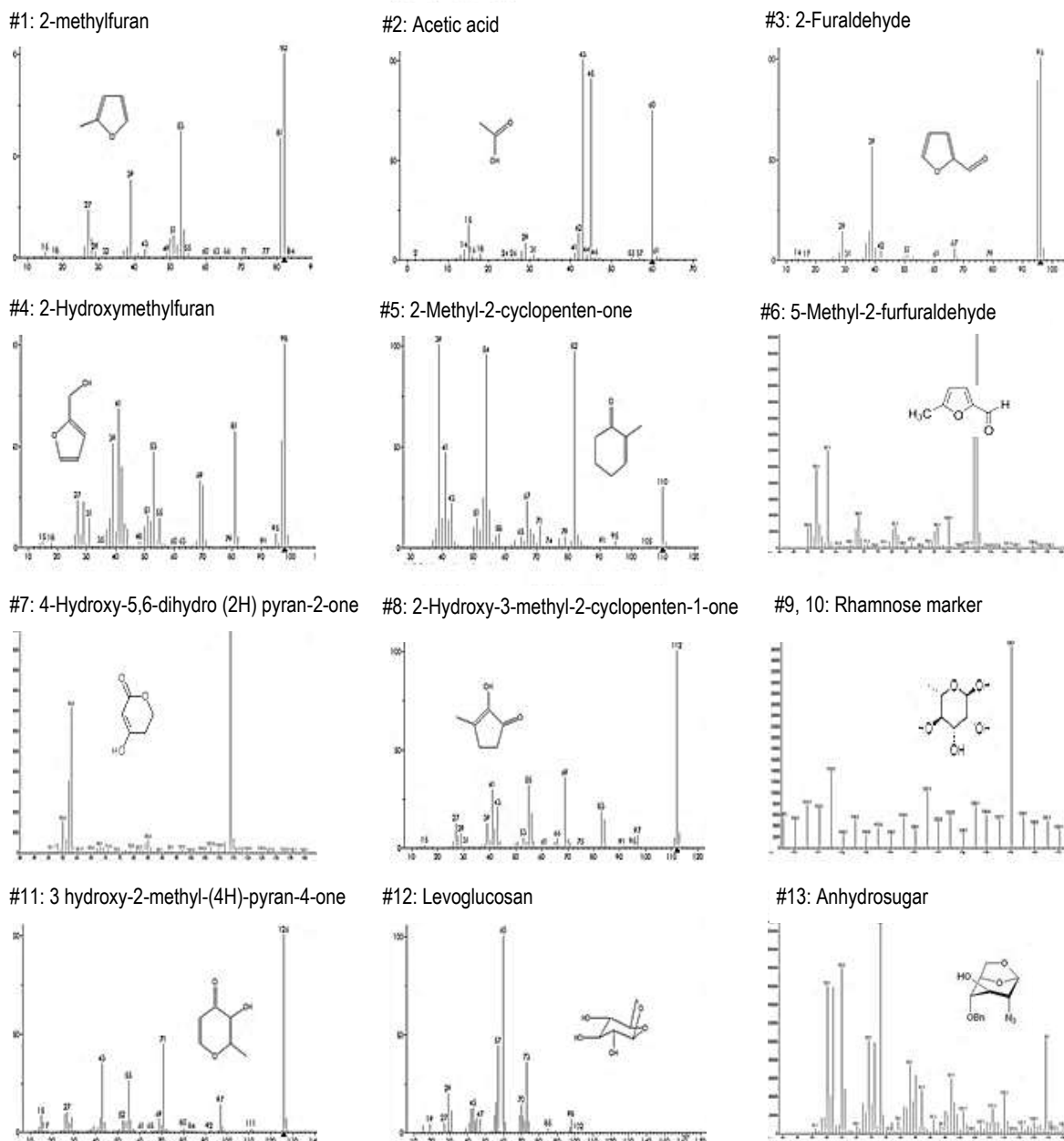


Figure 2. Mass spectra (m/z) and molecular structures of major polysaccharide pyrolysates identified in *Metasequoia* leaves.

3.2.2 MBTH assay

To better quantify the microbial-induced polysaccharide degradation in *M. glyptostroboides* leaf samples over time, the 3-methyl-2-benzothiazolinone hydrazone (MBTH) assay was conducted. MBTH assay is a colorimetric determination of total carbohydrate yields measured by ultraviolet–visible spectroscopy (UV/vis). Samples were hydrolyzed as seen in Opsahl and Benner (1999). 10mg of each sample were crushed to ensure more consistent results. The samples were then pretreated with 100 μ L of 12M sulfuric acid (H_2SO_4) for 2h to hydrolyze the samples. After this modification, methods were entirely based off Anthon and Barrett (2001).

After pretreatment, samples were diluted to 1.2M and hydrolyzed for 3h at 95°C. 1:100 diluted samples were mixed with 0.5M sodium hydroxide (NaOH) and 40 μ L MBTH reagent (equal volumes of 3mg/mL MBTH and 1 mg/mL DTT), and then heated at 80°C for 15min. As samples were removed from the heating block, 80 μ L solution containing ammonium iron (II) sulfate ($(FeNH_4(SO_4)_2) \cdot 12H_2O$), 0.5% H_2SO_4 , and 0.25M hydrochloric acid (HCl) was added, and then samples were left to process for 5min. As the organic carbon condenses with MBTH to form a sugar adduct and is then put under acid and oxidizing conditions, it forms a highly colored final product, which was then evaluated by UV/vis.

The method is highly replicable and reliable, as demonstrated by the high correlation lines in the standards run with the samples. A serial dilution of D-glucose (Glc) and a dilution of N-Acetylglucosamine (GlcNAc) were used as standards, each showing an R-square value of 0.9995 and 0.9992, respectively (see Appendix B).

3.3 Results

From the microbe experiments (2.1), *G. candidum* culture showed the most growth of all tested microbes and was thus the primary focus of this study. Other cultures showed similar but less obvious trends. One of the consortia was also used as a comparison in all of the techniques. All *Metasequoia* samples (laboratory decay, natural decay, and fossil) were examined using Py-GC-MS instrumentation and the MBTH assay. Both methods showed similar trends in the concentration of molecular polysaccharides in the laboratory decay series of *M. glyptostrobooides*.

3.3.1 Py-GC-MS

In Py-GC-MS analyses, relative abundances of peaks show trends of polysaccharide degradation in each sample series over retention time (Figure 3, Figure 4, and Table 2). Because the same amount of sample and the same method was used for each run and because the peak areas are used (as opposed to peak heights), Py-GC-MS is semi-quantitative. Using Py-GC-MS, common polysaccharide pyrolysates found in *M. glyptostrobooides* were measured for each series. Polysaccharides were based on the previously published compiled master lists (Yang et al., 2005; Witkowski et al., 2012).

The 13 compounds include 2-methylfuran, acetic acid, 2-furaldehyde, 2-hydroxy-2-methyl-2-cyclopenten-1-one, 5-methyl-2-furfuraldehyde, 4-hydroxy-5,6-dihydro (2H) pyran-2-one, two Rhamnose markers, 3 hydroxy-2-methyl-(4H)-pyran-4-one, levoglucosan, and anhydrosugar (Figure 4 and Table 2). Although 13 common polysaccharide pyrolysates in *M. glyptostrobooides* were measured, only 11 demonstrate complete data sets for the entire

laboratory decay series. The two compounds that were incomplete, 2-hydroxymethylfuran and anhydrosugar, have symbols to distinguish whether they were not well-separated enough for area abundance (“-”) or were completely absent (“0”).

Abundances via Py-GC-MS, as expected, were greatest in the control samples (Day 0). Py-GC-MS results of the two sample sets, the *G. candidum* laboratory decayed samples and the consortium laboratory decayed samples, showed similar results (data not shown). Figure 5 shows the complete chromatograms of the Day 0, Day 9, and Day 25 of the *G. candidum* laboratory decayed samples, in which there is a significant qualitative and quantitative decrease of pyrolysates, each of which are marked with numbers that correspond with the pyrolysate names in The second most common trend is that the compound abundances decrease in the first several days and then increases slightly above the initial abundance of polysaccharide pyrolysates, as seen in acetic acid, 2-furaldehyde, 2-methyl-2-cyclopentenone, 5-methyl-2-furfuraldehyde, and 3 hydroxy-2-methyl-(4H)-pyran-4-one. In the unusual case of 2-hydroxymethylfuran, there is no detectable abundance in Day 4, 9, and 21 samples, but there is in Day 25 samples at 1936 which exceeds the initial value of 1415 (Table 2).

Levoglucosan, one of the most abundant and most stable polysaccharide pyrolysates found in *Metasequoia* is a good representative of all polysaccharide fragments throughout the laboratory decay (shown in Figure 6A). As seen in Figure 6A and Table 2, there is a definite decrease in relative abundances from Day 0 samples at 20,166 to Day 4 samples at 8,349 to Day 9 at 5,888. There is then a definite increase when examining Day 21 samples at 9,845 to finally Day 25 samples at 14,105. Most compounds have this very same pattern in which the

sample decreases in the first several days and then increases slightly below the initial abundance of polysaccharide (Figure 6 and Table 2).

The second most common trend is that the compound abundances decrease in the first several days and then increases slightly above the initial abundance of polysaccharide pyrolysates, as seen in acetic acid, 2-furaldehyde, 2-methyl-2-cyclopenten-one, 5-methyl-2-furfuraldehyde, and 3 hydroxy-2-methyl-(4H)-pyran-4-one. In the unusual case of 2-hydroxymethylfuran, there is no detectable abundance in Day 4, 9, and 21 samples, but there is in Day 25 samples at 1936 which exceeds the initial value of 1415 (Table 2).

Table 2. A master list of polysaccharide pyrolysates and their respective abundances found in *Geotrichum candidum* laboratory decay series of *Metasequoia glyptostroboides* leaves from Day 0 through Day 25, as well as the fragment ions (frag) for the compounds based on the mass-to-charge ratios (m/z).

#	Compound Name	Frag (m/z)	0	4	9	21	25
1	2-Methylfuran	82, 81, 53	2806	890	1411	890	2669
2	Acetic acid	60	3511	1454	2842	1540	3769
3	2-Furaldehyde	96, 95, 39	2426	1192	1829	1066	3007
4	2-hydroxymethylfuran	98, 81, 43	1415	-	0	0	1936
5	2-methyl-2-cyclopenten-one	98, 55, 69	3053	674	1214	1216	3138
6	5-Methyl-2-furfuraldehyde	110, 53, 81	2407	718	1417	591	3056
7	4-hydroxy-5,6-dihydro (2H) pyran-2-one	114, 58	1127	754	957	343	666
8	2-hydroxy-3-methyl-2-cyclopenten-1-one	112, 55, 69	5225	705	1545	1110	4742
9	Rhamnose marker	128, 113	1819	973	1468	879	1084
10	Rhamnose marker	128, 57	1527	698	672	683	2017
11	3 hydroxy-2-methyl-(4H)-pyran-4-one	126, 42, 71	1686	302	1149	1050	2873
12	Levogluconan	60, 73	20166	8349	5888	9845	14105
13	Anhydrosugar	73, 60	7815	0	0	0	0

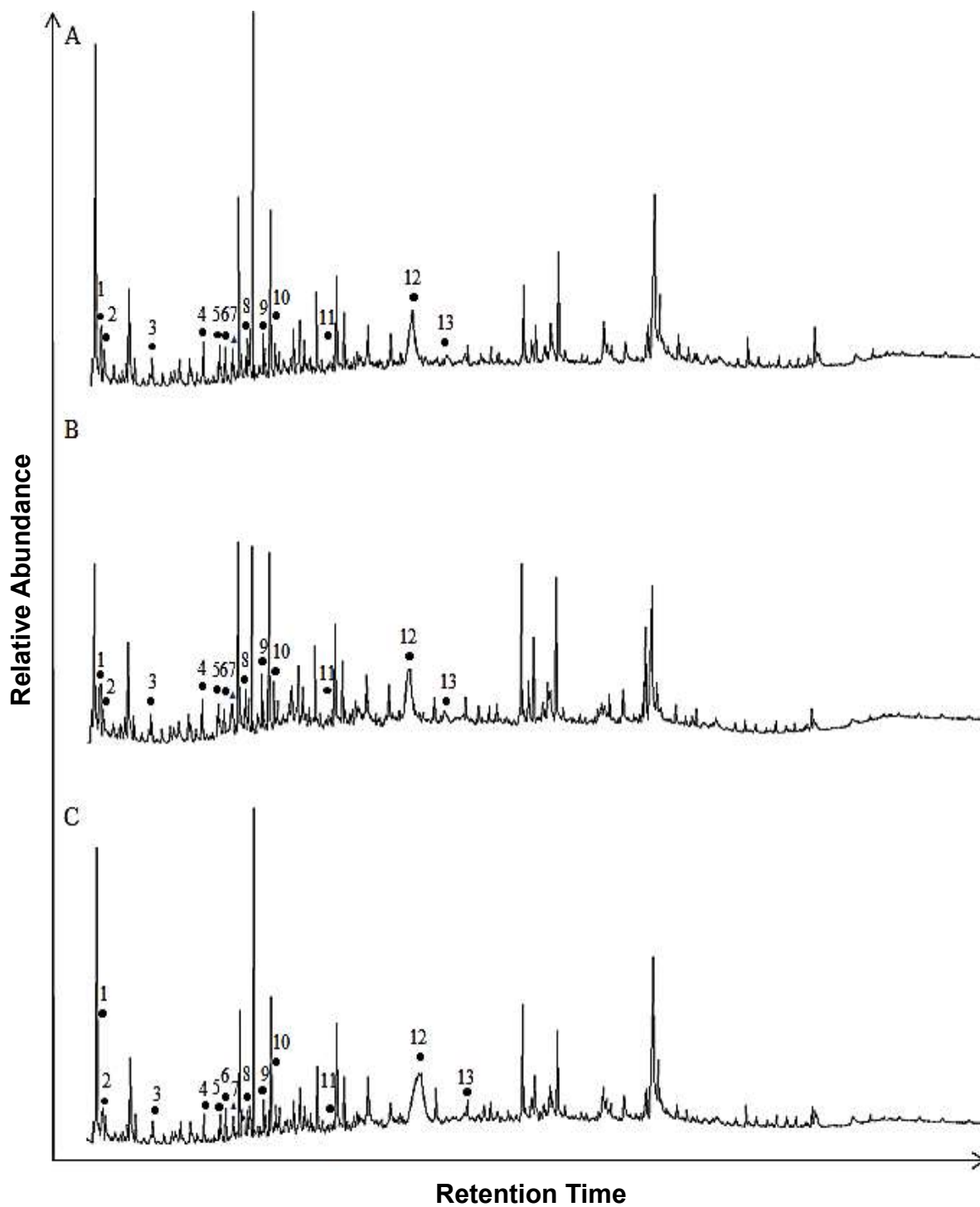


Figure 3. Total ion chromatogram of consortium laboratory decay series of *Metasequoia glyptostroboides*, with polysaccharide peaks labeled in correspondence with the master list in Table 2. (A) Day 0, (B) Day 12, and (C) Day 25 samples.

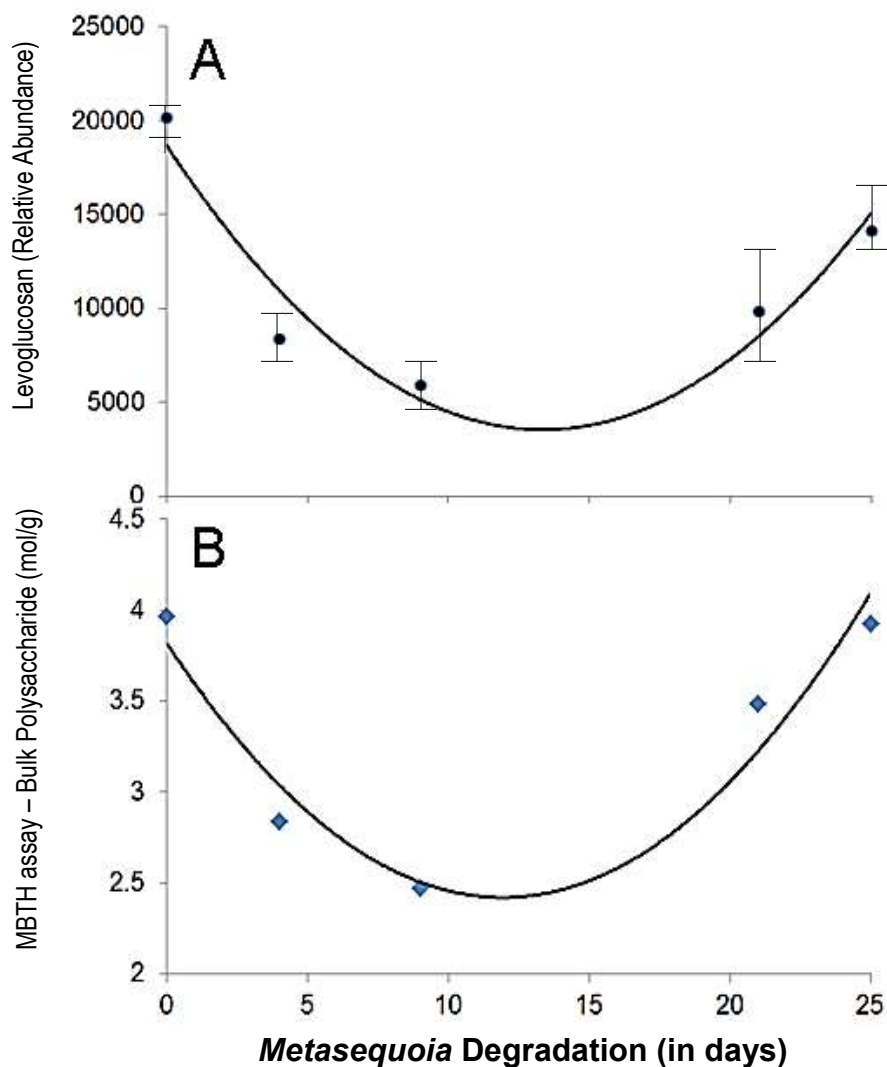


Figure 4. Change in the abundance of polysaccharide pyrolysates over 25 days in *Geotrichum candidum* laboratory decay series of *Metasequoia glyptostroboides* leaves. (A) Relative abundance of levoglucosan over time as determined by Py-GC-MS. (B) Quantitative change in bulk polysaccharide in mol/g over time as determined by MBTH assay (error within size of data point, see Appendix B).

3.3.2 MBTH Assay

Consistent with the results from Py-GC-MS, the MBTH sugar-reducing assay on laboratory decay samples resulted in a high initial sugar count on Day 0 samples, followed by a decrease in Day 4 samples and subsequent decrease in Day 9 samples. Also like the Py-GC-MS results, samples from Day 21 and 25 shows an increase in sugars (Figure 4B). This trend is consistent among the *G. candidum* laboratory decay series leaves, consortium laboratory decay series leaves, and natural decay series leaves (data not shown).

Fossil abundances were also examined using the MBTH assay. All three major types of fossil contained approximately the same amount of bulk sugar as the laboratory decay control and laboratory decay Day 25. In other words, fossils contained much higher abundance of polysaccharides than Day 4 and Day 9 of the laboratory decay where we see significant microbial decay. However, the fossils did not show degradation patterns based on their relative age, but instead correlative to their morphological preservation (Gupta et al., 2009; Witkowski et al., 2012). In other words, there was no age correlation, but samples that were better preserved morphologically showed greater polysaccharide abundances.

Data on the relative compound abundances for the natural decay series samples (Gupta et al., 2009) and the fossil samples (Yang et al., 2005) are previously published. Natural decay series samples showed a consistent decrease in polysaccharides, as expected based on age in the series, unlike the results of the laboratory decay.

Chapter 4. Isotopic Analyses

4.1 Introduction

As explained in Chapter 1, isotopic analysis is the second major chemical method for studying environmental proxies used in this research. Isotopic data was collected to help us to understand how the ancient environment and modern environments relate to one another, as well as how these isotopes may or may not play a role in the degradation of samples. This chapter covers an introduction to the instrumentation and theory of isotopes, the methods, and the results from isotopic studies.

Using the same methodologies for MS in 3.1.2, isotope ratio-mass spectrometry (IRMS) is a technology applied to explore naturally occurring isotopes in a given analyte. IRMS is used for this research because it has a multiple-collector analysis and gives high-quality peaks shapes, both of which are useful when examining trace samples such as fossil material (Felton, 2004; Yang and Leng, 2009; Kohn, 2010). Although IRMS can be used for radiogenic isotope geochemistry which examines the half-life of naturally radioactive elements, for the purposes of this research, it is used for stable isotope geochemistry which examines the isotope fractionation based on mass (Farquhar et al., 1989; Xiao et al., 2013). The classification of an element is based on the number of protons in each atom; although the amount of protons in a given element is always constant, occasionally there is a variant in the number neutrons, resulting in a different mass known as an isotope. The ratio between different masses from the isotopes is measured.

IRMS for bulk isotope analysis is achieved by converting the sample to a gaseous state, either by combusting and ionizing the bulk analyte or by chromatographically separating the analyte and converting them into requisite gases; the current research conducts the latter. Once the values are achieved, the isotope ratios of the element (expressed as a δ notation, see Equations 2 and Equation 3) and its isotope values are compared with a unanimously recognized standard. The sample's differentiation from the standard provides insight into environmental changes and conditions. In the current study, naturally occurring bulk carbon and bulk nitrogen isotopes are measured.

Carbon typically has twelve protons and twelve neutrons, but in a rare, naturally-occurring stable nitrogen isotope, it has twelve protons and thirteen neutrons. A ratio of carbon and its isotope in a sample is compared to the Vienna-Pee Dee Belemnite (VPDB) standard. In comparison with the standard, samples generally have negative ratios because samples are typically isotopically lighter than that of the standard (Equation 2). The following equation is used to express carbon isotope values in a δ notation ($\delta^{13}\text{C}$).

Equation 2. Notation for the stable carbon isotope ratio.

$$\delta^{13}\text{C} = \left(\frac{\left(\frac{^{13}\text{C}}{^{12}\text{C}} \right)_{\text{sample}}}{\left(\frac{^{13}\text{C}}{^{12}\text{C}} \right)_{\text{standard}}} - 1 \right) \times 1000$$

Nitrogen typically has fourteen protons and fourteen neutrons, but in a rare, naturally-occurring stable nitrogen isotope, it has fourteen protons and fifteen neutrons. A ratio of nitrogen and its isotope in a sample is compared to ambient air as the standard. To determine the isotope ratio for bulk nitrogen isotopes in a δ format ($\delta^{15}\text{N}$), Equation 3 is used.

Equation 3. Notation for the stable nitrogen isotope ratio.

$$\delta^{15}\text{N} = \left(\frac{\left(\frac{^{15}\text{N}}{^{14}\text{N}} \right)_{\text{sample}}}{\left(\frac{^{15}\text{N}}{^{14}\text{N}} \right)_{\text{standard}}} - 1 \right) \times 1000$$

4.2 Methods

Based on the methodology in Yang et al. (2011), air-dried and lipid-free fossil and modern natural decay leaf samples were ground to fine powder, weighed, and placed into 4×6 mm silver capsules. The capsules were then combusted for bulk isotope measurements on a Costech ECS 4010 EA elemental analyzer connected to a ThermoFinnigan DeltaPlus Advantage isotope ratio mass spectrometer at the Earth System Center for Stable Isotopic Studies (ESCSIS) of Yale University. Carbon and nitrogen elemental abundance were also measured simultaneously. Duplicate measurements were made for most of samples except for fossil samples which yielded only enough tissues for one measurement. All stable isotope values are reported in the δ notation (Equation 2 and Equation 3). The $\delta^{13}\text{C}$ values, compared with those of reference samples, were converted to those of V-PDB (Vienna-Pee Dee Belemnite) scale. The ESCSIS working standard was a house Cocoa ($\delta^{13}\text{C} = -28.42\text{‰}$, 48.7‰ C). The standard deviations of replicate samples are 0.05‰ for $\delta^{13}\text{C}$.

Bulk carbon isotope for the modern laboratory decay leaf samples were measured at the State Key Laboratory of Loess and Quaternary Geology, Institute of Earth Environment, Chinese Academy of Sciences in Xi'an, China. Samples were pretreated by washing leaves several times with deionized water, washing with HCl to remove carbonates, and washing again using deionized water until the pH increased to 6. Samples were air-dried overnight and then crushed. Samples were evacuated for 1h at 800°C and then sealed in the presence of CuO, Cu foil, and Ag foil. Cryogenic distillation purified and isolated the trapped CO₂, which was then measured using a MAT-251 offline gas mass spectrometer with a dual inlet system. The standard analytical error was less than 0.3‰ (Liu et al., 2005; Gupta et al., 2013).

4.3 Results

The *G. candidum* laboratory decay experiment showed little change in leaf bulk tissue stable carbon isotope ($\delta^{13}\text{C}$) over the 25 d period (Figure 5 and Table 3). Minor changes from Day 0 samples (-27.62‰) to Day 25 samples (-27.51‰) were detected. These “changes” fall within analytical error, suggesting little or no $\delta^{13}\text{C}$ change in modern laboratory samples. Stable nitrogen isotope ($\delta^{15}\text{N}$), as well as the weight percent carbon and nitrogen (wt% C and wt% N), were not measured for the laboratory decay series.

Table 3. Leaf tissue bulk carbon and nitrogen isotopes ($\delta^{13}\text{C}$ and $\delta^{15}\text{N}$, respectively), weight percent carbon and weight percent nitrogen (wt% C and wt% N), and the weight ratio of carbon to nitrogen for fossil (*Metasequoia occidentalis*), modern natural decay (*Metasequoia glyptostroboides*), and modern laboratory decay (*Metasequoia glyptostroboides*) samples (N/A=not available).

Sample No.	$\delta^{13}\text{C}$ (‰)	$\delta^{15}\text{N}$ (‰)	wt% C	wt% N	C/N
M-E-10	-24.46	0.23	33.36	0.50	67.06
M-E-10R	-23.73	0.61	42.23	0.45	93.01
M-P-15	-24.53	2.27	34.82	0.42	83.36
M-P-15R	-24.40	1.91	33.04	0.38	87.51
M-M-83-1	-27.88	3.73	49.90	1.90	26.27
M-M-83-2	-27.78	3.40	47.43	1.74	27.22
M-M-83-3	-28.40	3.25	48.17	0.99	48.64
M-M-83-4	-28.25	3.07	50.67	1.63	31.02
M-M-83-5	-28.20	3.70	34.20	1.50	22.82
M-M-83-6	-28.45	2.59	39.07	1.72	22.73
GC-D0	-27.62	N/A	N/A	N/A	N/A
GC-D4	-27.66	N/A	N/A	N/A	N/A
GC-D9	-27.66	N/A	N/A	N/A	N/A
GC-D21	-27.57	N/A	N/A	N/A	N/A
GC-D25	-27.58	N/A	N/A	N/A	N/A

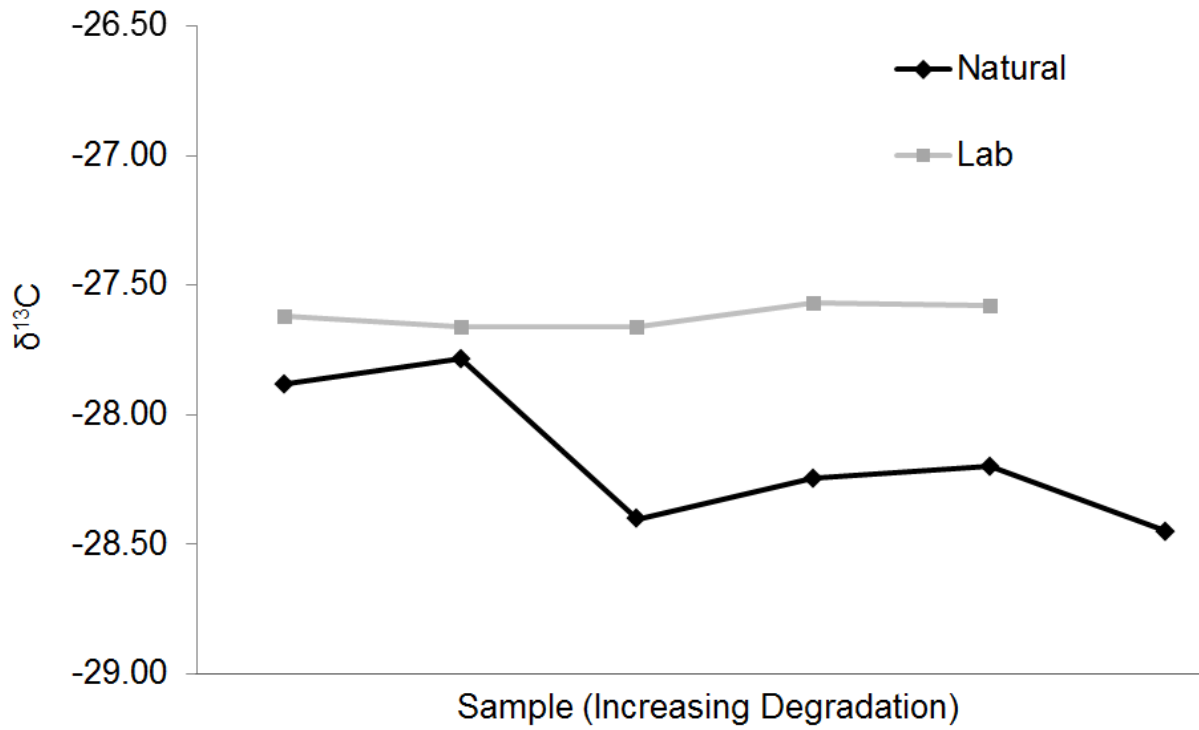


Figure 5. Leaf bulk tissue $\delta^{13}\text{C}$ of natural decay (black) and *Geotrichum candidum* laboratory decay (gray) samples of *Metasequoia glyptostroboides*, in order of increasing degradation where the natural decay numbers (M-M-B83-1 through 6) and the laboratory decay numbers (Day 0 through Day 25) are in order from left to right.

The natural decay series, however, does show change over time. A bulk $\delta^{13}\text{C}$ change ($\sim 1\%$) toward more negative values (from -27.2% to -28.2%) is seen along with the progress of natural decay (Figure 5). As expected, the most dramatic shift in isotopes is from M-M-83-B2 to M-M-83-B3, from early stages of senescence to late stages of senescence, respectively. M-M-83-B3 shows a significant N concentration drop by nearly 1%, resulting in a high C:N ratio. This suggests that senescence marks the onset of degradation on proteins and other N-containing molecules before the leaf has yet to fall from the tree (Figure 5 and Table 3). The last four samples in the natural decay series, M-M-83-B3 through M-M-83-B6, have resulted in lower C concentration, implying a significant tissue loss during progressive decay, as C is the primary element of all biomolecules (Table 3).

Typically, as seen in the natural decay series, ^{12}C enrichment occurs with age (and thus decreased $\delta^{13}\text{C}$ values over time). Contrary to the modern samples, the fossil *Metasequoia* samples demonstrate remarkably higher $\delta^{13}\text{C}$ values, ranging from -24.46 to -23.73% , approximately 3-4‰ more positive than the modern samples which range from -27.57 to -28.45% (Table 3). The reason for this enrichment will be discussed later in 7.2.2 and 7.3.3. Although $\delta^{15}\text{N}$ values were collected for the natural decay series, the results were inconclusive and are not discussed in great detail in this thesis.

Chapter 5. SEM Observations

5.1 Introduction

As further described in Chapter 1, the major physical means of using plant fossils as proxies is anatomically and morphologically. In order to study these features, microscopy is frequently used. Microscopy is the scientific investigation of microscopic objects, too small to be seen by the naked eye, with the aid of a microscope. Microscopes can be optical (light), electron, and scanning probe (Abramowitz and Davidson, 2004). The scanning electron microscope (SEM) is the major type of microscopy used for this research. The major tool used for paleobotany, not excluding this research, is scanning electron microscopy (SEM). This chapter explores the instrumentation, methods, and results for SEM observations.

Electron microscopy was developed by physicist Ernst Ruska and electrical engineer Max Kroll in the 1930s and is now widely used in scientific research (Watt, 1997). Electron microscopes are virtually identical to compound light microscopes in how they capture images, but as their name suggests, differ from the latter in that they use an electron beam instead of a light to produce a magnified image. Because electrons have wavelengths approximately one hundred thousand times shorter than visible light photons, magnification of an electron microscope is nearly ten million times greater than the typical light microscope (Watt, 1997). The two major types of electron microscope are the transmission electron microscope (TEM) and the scanning electron microscope (SEM). In contrast to TEM which directly transmits electrons through a thin slide of sample, SEM scatters electrons across the surface of the specimen in a scanning manner; as a result, SEM captures three-dimensional images (Rao et al., 2010).

SEM is applied in this study to observe plant cell wall structures for the determination of the preservation or degradation stage (Watt, 1997; Abramowitz and Davidson, 2004). It uses an electron gun which emits electrons through condenser lenses, deflection coils, and a final lens. The electrons then hit the surface of the specimen which is sitting on a stage in a vacuum chamber (Figure 6). When the electron beam traces over the surface of the specimen, two types of electrons, the backscattered electrons and secondary electrons, are detected to be generate different levels of brightness for the image (Abramowitz and Davidson, 2004).

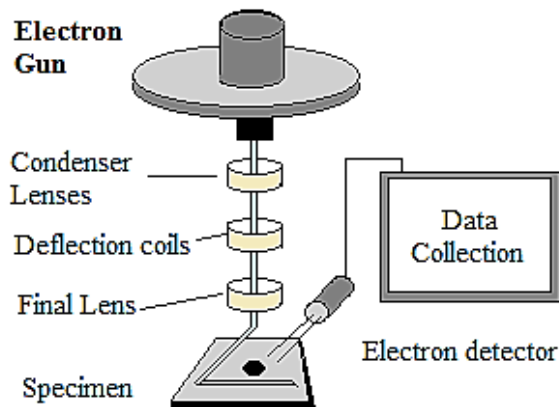


Figure 6. Flow diagram of scanning electron microscopy, starting from the electron gun and moving through to the electron detector and data collection.

5.2 Methods

A JEOL JSM-6010LA SEM was used to document morphological and anatomical changes of the leaf cell wall through decay in comparison with the fossil material. As leaf tissue at different positions of the leaf (from leaf base to apex), of the leafy branchlet, of the branch, and even of the tree height may have different anatomical features (Wang, 2010), for a standardized comparison, a 1mm long transverse section was cut from the middle portion of a leaf located at the middle portion of the branchlet using a single-edged razor blade. The sections were mounted on SEM stubs using double-sided tapes or a small drop of colorless nail polish with one of their cutting surfaces facing upward. Mounted samples were air-dried overnight and sputter coated with 17.5nm of gold by a Denton Desk V HP Cold-Sputter Coater for 60s under a current of 40mA. Samples were then observed and imaged by the SEM at accelerating voltage of 8 kV and a work distance of 2 mm.

5.3 Results

SEM results show an obvious and continuous decay of the three-dimensional structures within the *M. glyptostroboides* leaves throughout both the natural decay series and the laboratory decay series over the 25 d period of all sets of experiment no matter it is introduced with the single fungal culture or consortium. We here describe the morphological changes using *G. candidum* decayed *M. glyptostroboides* leaves as examples. We focus mainly on the vascular bundle, although other areas are also described.

In the control sample (Day 0, Figure 7A through C), all cells in the vascular bundle and the transfusion tissue (right area in Figure 7C) are three-dimensionally intact. All tracheids in the xylem and transfusion tissue show their primary walls, secondary cell walls which are unevenly deposited inside the primary cell walls, and solid middle lamella (mainly of pectin) between two cells (Figures 8B and C).

After the introduction of microbes, from Day 4 samples through Day 25 samples, leaf vascular bundles show a trend of increasing degradation. Day 4 samples display slight changes only observable in the phloem area while their xylem cells remain relatively intact (Figure 7D). Day 9 samples (Figure 7E and F) not only show the collapsing of some phloem cells (Figure 7E), but also some lignin-based secondary cell walls of the tracheids in the xylem have started to detach from the primary cell walls. Part of the middle lamella and primary cell walls can be seen decayed under high magnifications (Figure 7F), although tracheids still keep their three-dimensional structures. Day 21 samples display largely collapsed phloem cells (Figure 7G) and their xylem tracheid cells are no longer as rigid as in

previous samples as obvious detachment and unraveling of the unevenly deposited lignified secondary cell walls can be seen (Figure 7H and I). Day 25 samples, compared with Day 21 ones, as expected, demonstrate even more decay: Most of the cells in the vascular bundle, including some in the xylem, are collapsed (Figure 7K).

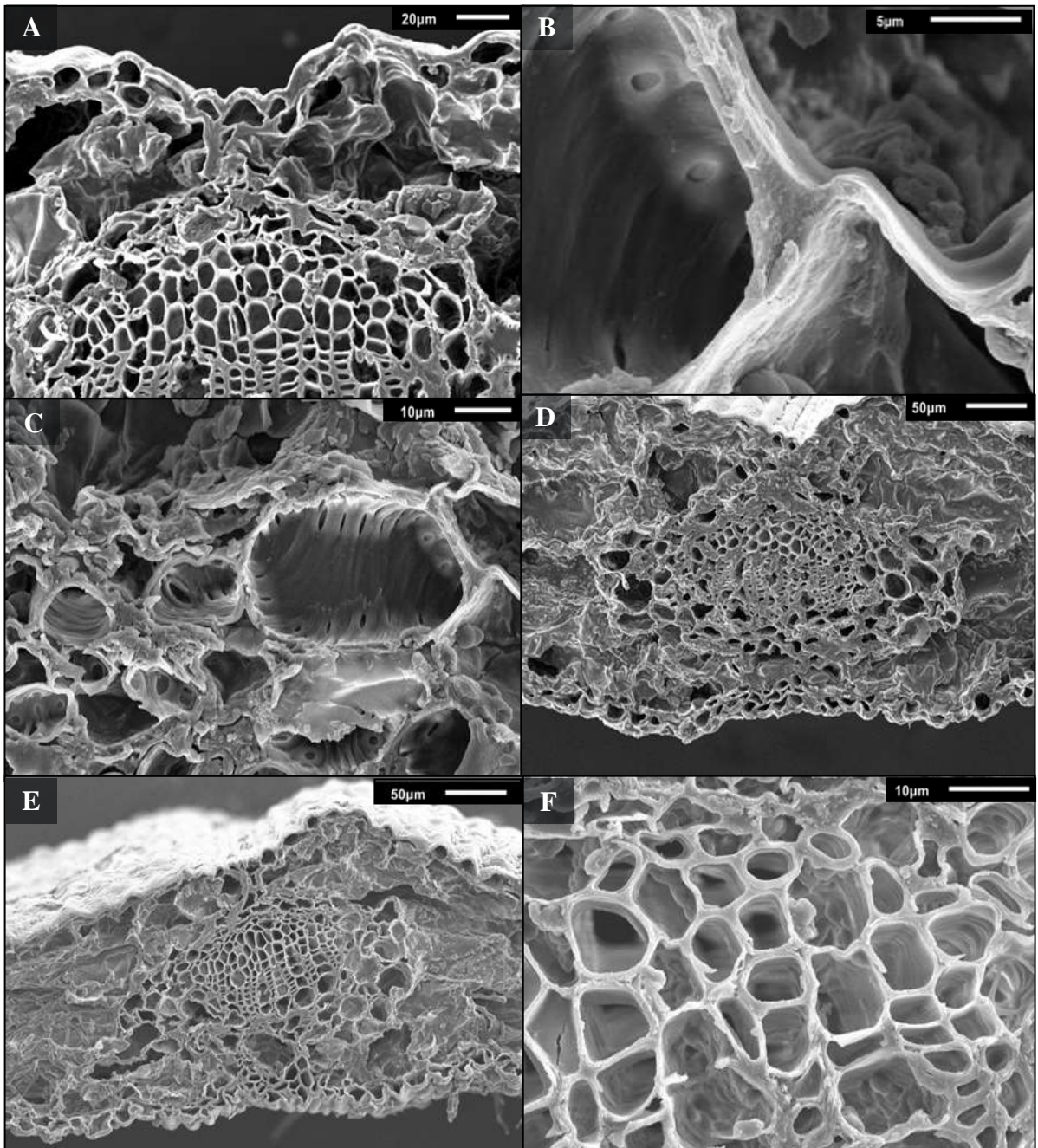


Figure 7. SEM observations of the transverse sections of the laboratory decay *Metasequoia glyptostroboides* leaf series introduced with *Geotrichum candidum*, showing the control sample (Day 0, A through C), and the decay series from Day 4 (D), Day 9 (E and F), Day 21 (G through J), and Day 25 (K through L) samples. J and L show the lateral sides of leaves with the leaf interiors filled with fungal hyphae, while or other images show the mid-vein area in the image center.

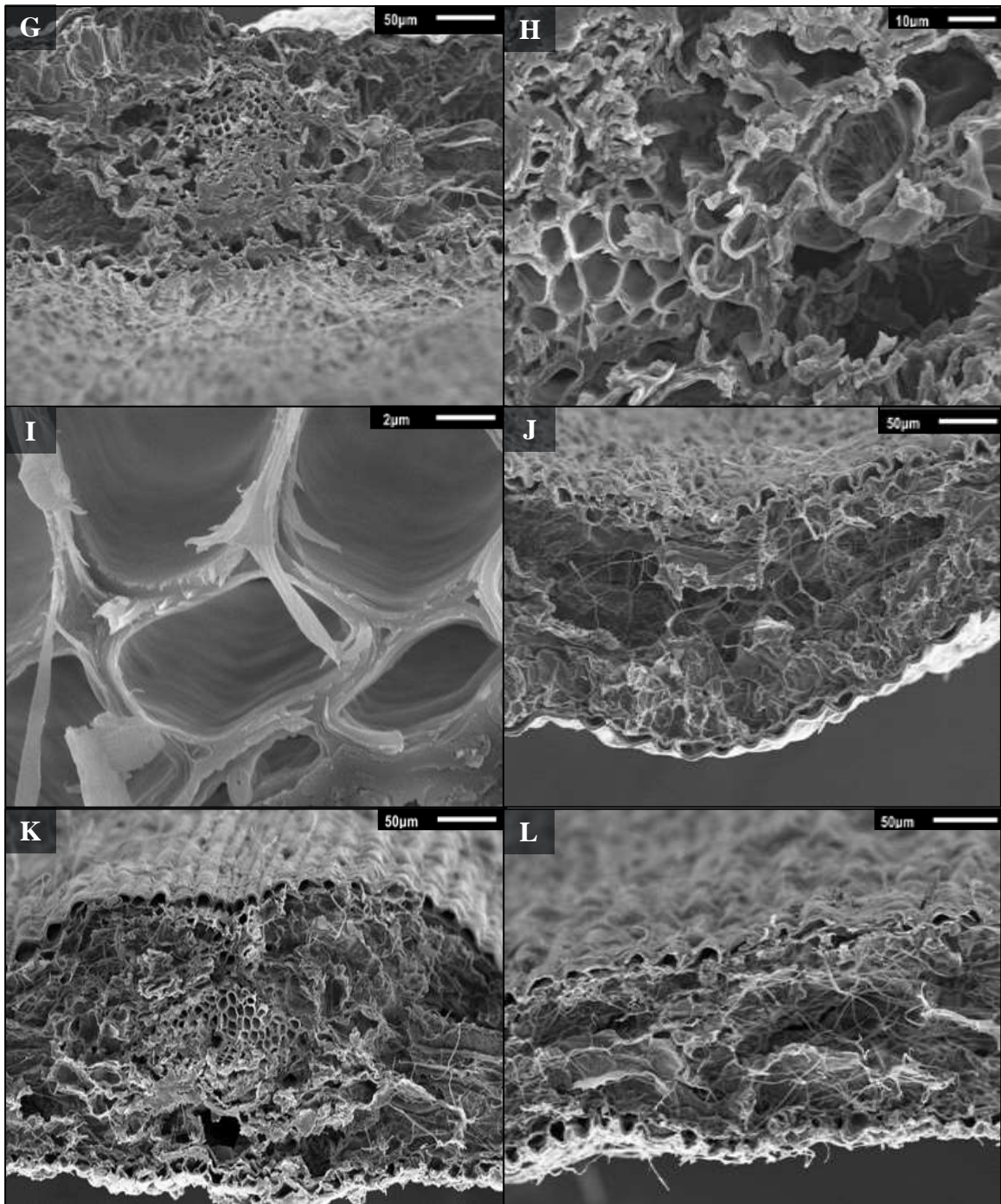


Figure 7, continued. SEM observations of the transverse sections of the laboratory decay *Metasequoia glyptostroboides* leaf series introduced with *Geotrichum candidum*, showing the control sample (Day 0, A through C), and the decay series from Day 4 (D), Day 9 (E and F), Day 21 (G through J), and Day 25 (K through L) samples. J and L show the lateral sides of leaves with the leaf interiors filled with fungal hyphae, while other images show the mid-vein area in the image center.

In addition to physical changes in the cell wall structures, fungal hyphae growth also shows an obvious changing pattern. There is no clear evidence of fungal growth in either the control samples, Day 0 (Figure 7A through C) or Day 4 samples (Figure 7D). However, in the following Day 9 samples large amount of fungal hyphae are seen successfully infiltrating in the leaf interior through stomata (Figure 8, B through D), the only openings on the leaf cuticular membrane arranged in the two stomatal zones of the lower leaf epidermis (shown on the clean cuticular membrane in Figure 8A).

Plant cuticle, the protective film covering the epidermis, is primarily made of large, complex soluble waxes composed of lipids, cutins, and hydrocarbon polymers. Epicuticular wax it is extremely difficult for microbes to decompose and/or penetrate. In the case of the modern laboratory decay, the *G. candidum* fungi could not penetrate the cuticle, but instead were able to infiltrate the leaf by penetrating through the stomata (Figure 8). Figure 8A illustrates the inner surface of the lower cuticle, showing the two stomatal zones known as bands and belts (image courtesy of Qin Leng, Vienna University, May 2006). The center of the image demonstrates the separation of the two stomatal bands by the mid-vein. Figure 8B through D exhibit this hyphal infiltration into the leaf via stomata for lab decay introduced with *G. candidum* on Day 9.

Once the *G. candidum* invaded the leaf, they quickly grow by decomposing leaf biomolecules and further developing their own hyphae, which have nearly reached the mid-vein of Day 9 samples (Figure 7E). The *G. candidum* fungal hyphae so are efficient in decomposing *M. glyptostroboides* leaf tissues that only after 21 d (Figure 7G through J), they

are seen everywhere in the leaf, including the vascular bundles, causing the decay of tracheid cell walls (Figure 7H and I). On Day 25 samples (Figure 7K and L), complete infiltration of fungal hyphae is obvious. Their long and string-like bodies are abundantly observable on both the surface of the leaves and within the leaves. Their dominant occupation is directly correlative with the disappearing leaf cell walls which have been decomposed by the microbes to extend their hyphae.

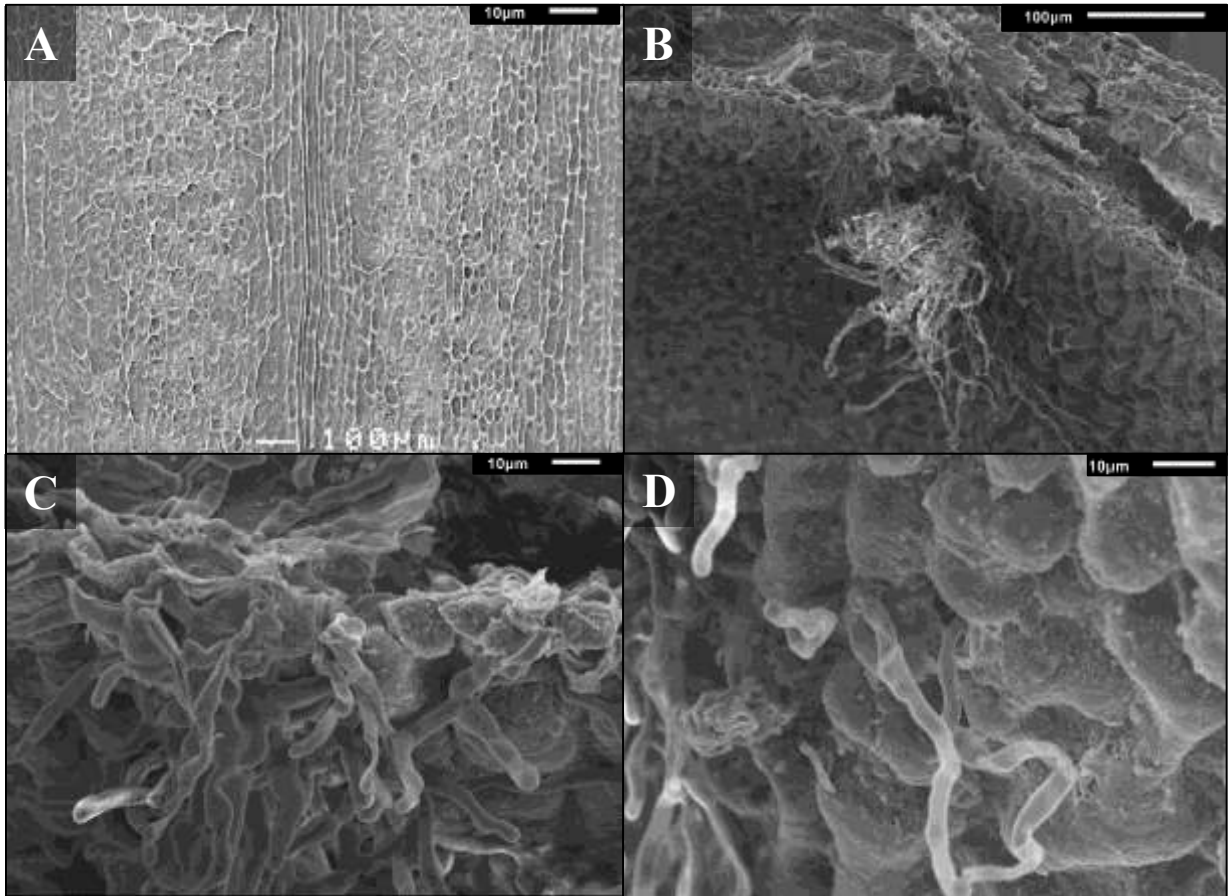


Figure 8. SEM observations of *Metasequoia glyptostroboides* leaf surfaces. (A) The inner surface of the clean cuticular membrane of the lower leaf epidermis of M-M-83-B1, showing the mid-vein area in the center and two stomatal zones. Leaf margins are not shown (image, courtesy of Qin Leng, Vienna University on May 2006). (B), (C), and (D) show external different views of leaf lower surface of Day 9 laboratory decay samples introduced with to *Geotrichum candidum*, at which time the fungal hyphae have infiltrated the leaf cuticle via stomata (arrows).

Chapter 6. Pixel-Count Evaluation

6.1 Introduction

A new pixel-count evaluation method has been developed specifically for the purposes of this research to quantify the degree of morphological tissue decay as seen in SEM images. It is the first research attempt at quantifying morphological degradation. The computer program mimics a hemocytometer, more commonly known as a counting chamber, a grid that biologists use to count cells in a culture. Hemocytometers are most common in microbiology, although they have occasionally been used in paleobotany to count large quantities of small particles such as pollen grains and mesofossils. This is the first study to apply the concept of a hemocytometer to a computer-based program.

This study applies hemocytometers to SEM images on the transverse sections of *M. glyptostroboides* leaves in two ways: first, as a manual count and second, as an automated computer program. In the "manual" method, if there is more cell wall than space shown in the grid box, it is given the value 1, and if there is more space than cell wall in the grid box, it is given a value 0. In the automated computer program, the grid values are obtained directly from the pixel values in the image. A pixel, abbreviated for picture element, is the smallest addressable element in a digital raster image. When an image has many pixels and is viewed at a distance, such as in Figure 9A, pixels are undetectable by the naked eye. However, once the image is enlarged, such as in Figure 9B, each individual box-shaped pixel is visible. Instead of using an arbitrary grid size, this automated program uses the smallest grid physically possible on a digital image, where each pixel acts as a box in a hemocytometer

grid. One major difference between the manual count and the automated computer count is that instead of labeling a grid box either 1 for “cell wall” or 0 for “space”, each pixel in an RGB digital photograph, an additive color model based on red, green and blue, is given a specific number value to indicate its grayscale, ranging from 0 (black) to 255 (white).

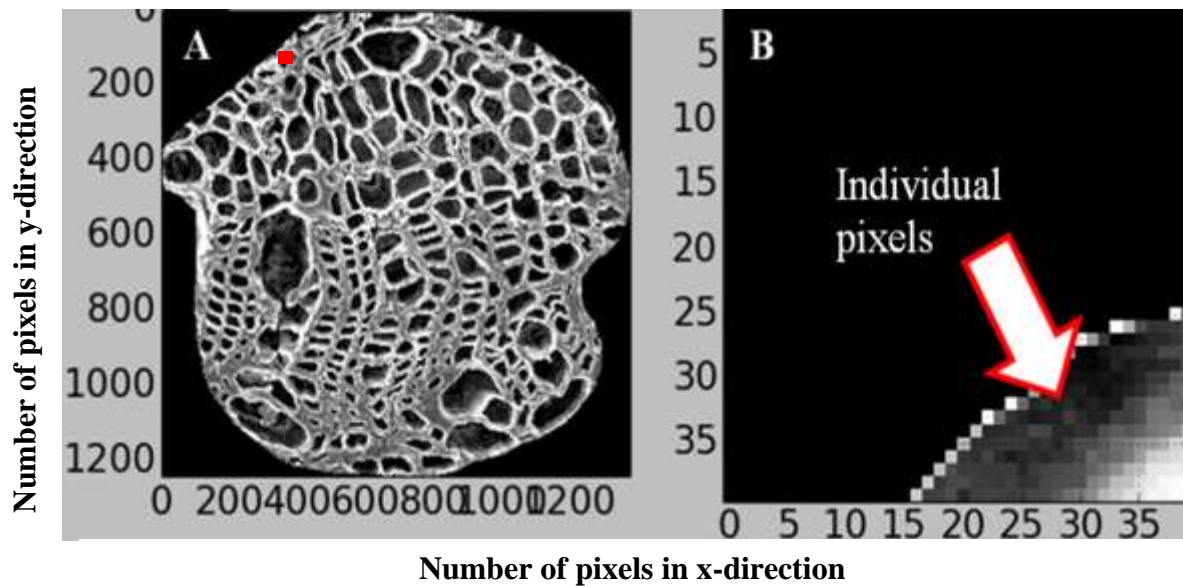


Figure 9. Example of the hemocytometer-like computer pixel-count evaluation method. (A) Pixel size of a selected region of interest on a SEM photograph on the transverse section of a *Metasequoia* leaf mid-vein. (B) 40x40 pixel grid cell used for both the conventional manual method and the computer pixel-count evaluation method.

In computer visualization problems, particularly when classifying images, there is a typical hierarchy approach of processes, which is shown in a flow-chart form in the Appendix A (Duda et al., 2001). A sensor converts images into signal data. In the case of this research, SEM takes digital images that are then converted to RGB values using a photo manipulation program. Images are then preprocessed through segmentation, in which a training set is devised. The training set images are representative of the groups being classified so that the computer can distinguish categories. For this research, samples were separated into either degraded (DG) or not degraded (NDG). Next, a feature extractor is used to reduce the data by measuring specific properties of the sample, such as the pixel values of an image. Next, the features (pixel values) are evaluated by a classifier which determines whether the sample is DG or NDG. Finally, post-processing is done, in which the overall program is adjusted and modified; for example, the feature extractor may be adjusted to add missing features or the classifier may be adjusted for new context (ex. cost-effectiveness) (Duda et al., 2001). A flow-chart of this process is in Appendix A.

The accuracy and reproducibility of this newly developed pixel-count evaluation method were tested in several ways. First, the method is applied to the same SEM images but with its photo conditions, such as brightness and contrast, changed. Second, the method was tested by a classifier, a software package used to identify and categorize samples. Third, the method was compared to the traditional quantitative approach frequently used in microbiology, the hemocytometer (essentially counting chamber consisting of a manually counted grid). Results of these tests were compared and discussed in 7.1.3.

6.2 Methods

To measure pixels on a SEM image of plant tissues, the precise region of interest (ROI), the mid-vein of *Metasequoia* leaf samples, is selected using the image editing program GNU© Image Manipulation Program (GIMP). The mid-vein was chosen as the ROI because it contains both the phloem (mainly sieve tube elements that have only primary cell wall) and the xylem (mainly tracheids that have both primary and secondary cell walls). Primary cell walls are primarily composed of polysaccharides, including cellulose and hemicellulose, whereas secondary cell walls not only contain cellulose and hemicellulose, but also lignin, a complex phenylpropanoid polymer (Boyce et al., 2003).

One of the fundamental goals of this research is to examine the effects of exclusively removing polysaccharide from leaf cell wall structures to observe structural changes. Although we cannot guarantee that the microbes will exclusively consume polysaccharide, microbes were chosen based on their *preferential* consumption. Theoretically, the sieve tube elements should collapse first because they only have a primary cell wall that is cellulose and hemicellulose-based, which will be decomposed by the introduced microbes, whereas lignin-strengthened tracheids should change at a slower rate. The ROI would provide insight into the morphological changes occurring over the degradation series.

Once the ROIs were selected, images were separated into DG and NDG. The program, written in the computer language Python, measured the pixel values where values range from 0 (black) to 255 (white), and collected those pixel values as data points. A visible difference in samples over time results in a difference in grayscale pixel values. Those changes can then

be quantitatively measured and analyzed. To analyze the pixel data, the grayscale pixel values of leaf cell walls in DG samples are compared to those in NDG samples. Tissue degradation is reflected in the dominant shades of gray on an SEM image. Regions without cell wall absorb electrons, and thus the spaces between cell walls have no backscatter, resulting in dark-colored pixels. Strong, thick, and intact NDG leaf cell wall structures display light-colored pixels for the cell wall because when the sample is cut, the robust cell wall structures reflect off more electrons which are detected. Therefore, NDGs demonstrate a distinct bimodal distribution, marked by relatively more black pixels and more white pixels. Contrary to NDGs, when DGs are cut, the degraded cell wall structures provide an uneven, deteriorating surface, causing electrons to scatter in many directions and resulting in primarily gray pixels.

Furthermore, the void where there was once black space has changed to gray. This is because as the cell wall structures are digested by microbes, the cell wall structures collapse and in part occupy the spaces with more uneven, crevassed surface (gray). When large amounts of cell wall are decayed, great voids (empty spaces) will be seen in the transverse sectional view of the sample, in which results in a bell-curve gray with a sharp black peak pixel-count. This can be readily identified and resolved by removing the voids in the ROI. Thus, overall there is a clear distinction between the NDG bimodal graph (mostly black and white) and the DG unimodal graph (mostly gray).

The pixel values of each image were then processed using a Gaussian mixture model (GMM), a standard statistical method used to determine the parametric probability density function of continuous data. The GMM for this research displays the distribution of data points in a two-peak model (shown in 6.3, Figure 10).

Data from the GMM can then be manipulated using the Bhattacharya distance to understand the similarity between the two resulting GMM distribution peaks. The Bhattacharya distance is the log of the overlap of the two peaks, where $D_B(p, q)$ is the Bhattacharyya distance between two distributions (p and q), μ is the mean, and σ is the standard deviation. The Bhattacharyya distance results in an accurate and quantified single-number index, summarizing the properties of the entire pixel distribution and can be used to compare samples (Equation 4).

Equation 4. Bhattacharyya distance.

$$D_B(p, q) = \frac{1}{4} \ln \left(\frac{1}{4} \left(\frac{\sigma_p^2}{\sigma_q^2} + \frac{\sigma_q^2}{\sigma_p^2} + 2 \right) + \frac{1}{4} \left(\frac{(\mu_p^2 + \mu_q^2)^2}{\mu_p^2 + \mu_q^2} \right) \right)$$

When the two distribution peaks are similar, meaning they have significant overlap, close means, and little covariance, they are considered DG. The pixel values congregate in the center of the graph because the pixel values are mostly uniformly gray, resulting in two close peaks. When the two peaks are not very similar, they are considered NDG. The pixel values are well-separated on the graph because the pixel values are primarily black and white, resulting in two distant peaks.

6.3 Results

Using the new Python-based methodology, we were able to demonstrate quantitative comparisons among leaf cell wall preservation, first by examining the laboratory decay samples, and then by adding the natural decay and fossil samples. Normal two-peak distribution using a GMM was applied to each sample (6.2, Figure 10).

As seen in Figure 10, two laboratory decay samples from different time-points throughout the experiment, Day 9 and Day 21, are compared using the method. The y-axis from 0.0 to 1.0 represents the percentage of each pixel value, as indicated by the grayscale below the distribution histogram, where 0 represents absolute black and 1.0 represents absolute white (explained in 6.1 and 6.2). As discussed in 5.3, Day 9 shows the start of hyphae infiltration of the leaf but has not yet reached the mid-vein and thus the mid-vein for Day 0, Day 4, and Day 9 displays NDG preservation (Figure 7, A, D, and E). In the Day 9 samples, there is a clear bimodal scale with one peak closer to black and one peak closer to white, which represents a typical NDG pixel distribution (Figure 10A).

Day 21 and Day 25, on the other hand, show complete infiltration of the mid-vein and thus display DG cell morphology in the mid-vein (Figure 7, G and K). This degradation demonstrates an observable difference in the pixel distribution using the pixel-count evaluation method as seen in Figure 10. In contrast to the Day 9 sample (Figure 10A), the Day 21 sample (Figure 10B) is primarily unimodal with both peaks closer to gray at the center of the graph. This represents a typical DG pixel distribution (Figure 10B).

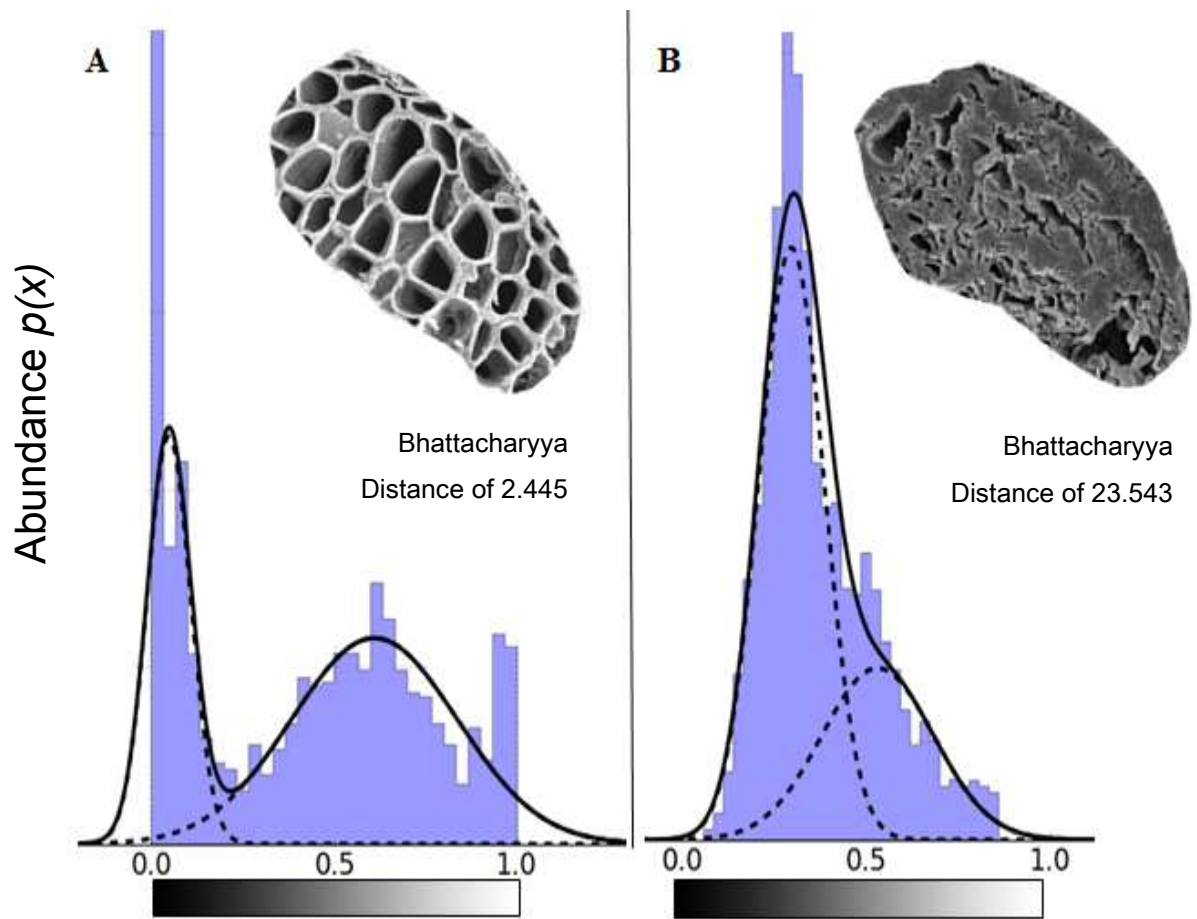


Figure 10. GMM of pixel values for *Geotrichum candidum* laboratory decay of *Metasequoia glyptostroboides*, where 0 represents black and 1.0 represents white. (A) Day 9 (image in upper right) shows a bimodal distribution of mostly black and white. (B) Day 21 (image in upper right) shows more unimodal distribution of mostly gray.

Because the GMM demonstrates a clear difference in pixel value distribution, the computerized pixel-count evaluation method showed strong evidence for being a promising quantification method (Figure 10). In order to test the computer program's ability to identify NDG and DG samples, the several million data points (pixel values) that were collected via the pixel-count evaluation method were then narrowed down to only five features of a normal two-peak continuous distribution, including the mean and standard deviation of each peak, as well as the overlap of the two peaks for every photograph.

To visualize the data, Figure 11 shows all the pixel values from the ROI (mid-vein from the modern laboratory decay, modern natural decay, and fossil *Metasequoia* images) funneled into only two features: the mean of the first distribution peak and the mean of the second distribution peak in the pixel value distribution (examples of a section from two of the samples in Figure 10). In Figure 11, the separation between NDG (red) and DG (green) is obvious, even on a two-dimensional plane. When the computer actually classifies and quantifies NDG and DG samples, it analyzes the data on the five dimensions aforementioned, which adds even clearer separation between the two sample types, but cannot be visualized.

NDG samples have clusters of more black and more white pixels, which lead to a much greater separation between the two-peak GMM distributions. This difference between means translates to the clustering seen in the upper left corner of the Figure 11. DG samples have primarily gray pixels, and thus the two-peak GMM distribution has overlapping peaks. The close means of these two distributions translates to the clustering seen at the bottom of the Figure 11.

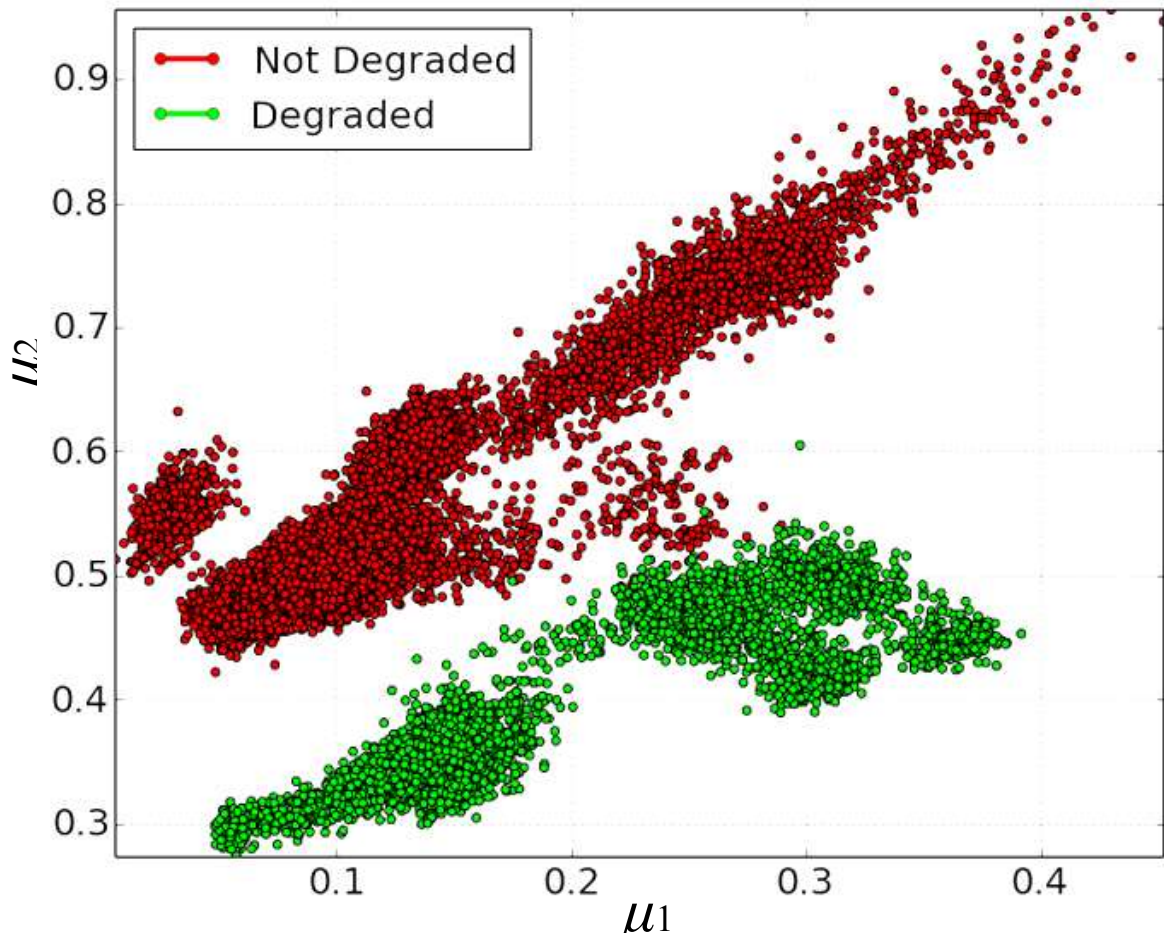


Figure 11. Scatterplot of the mean from the first peak against the mean of the second peak from the GMM distributions from the pixel-count evaluation. Red represents not degraded and green represents degraded samples.

Because the two targets (DG and NDG) are so well-distinguishable, the Bhattacharyya distance (Equation 5), the similarity of two distributions that considers the distance of means and covariance, is readily applied (Figure 12 through 16). Figure 12 demonstrates the Bhattacharyya distance for all DG (blue) and NDG (pink) samples as both a histogram and as a scatterplot. The variation among DG pixel values is small, being mostly gray and unimodal, so the Bhattacharyya distance (typically ranging from 8-13) is likewise much smaller than that of NDG (Figure 12 through 14). The variation among NDG pixel values is great, being more black and white and bimodal, so the Bhattacharyya distance (typically 22-28) is much larger. In general, DG samples have Bhattacharyya distances less than 15 and NDG samples have Bhattacharyya distances greater than 15 (Figure 14 and Figure 18).

In addition to displaying all of the DG and NDG samples, specific samples (green) were chosen to demonstrate the relative location of the sample's degradation among the entire sample set (Figure 12). As expected, Day 5 of the consortium laboratory decay is extremely well-preserved because it has only had several days exposed to the microbe, as seen by the morphologically well-preserved cell wall structures in Figure 12A. This preservation is confirmed by the location of Day 5 of the consortium laboratory decay among all samples, displayed both as a histogram and as a scatterplot (Figure 12, C and E). Figure 12B shows severe degradation in a Day 25 sample in the consortium laboratory decay. The location of Day 25 on the histogram and scatterplot is encouraging because the initial goal of the research was to mimic early stages of diagenesis which would thus be expected to be (and is) directly between the DG and NDG samples (Figure 12, D and F).

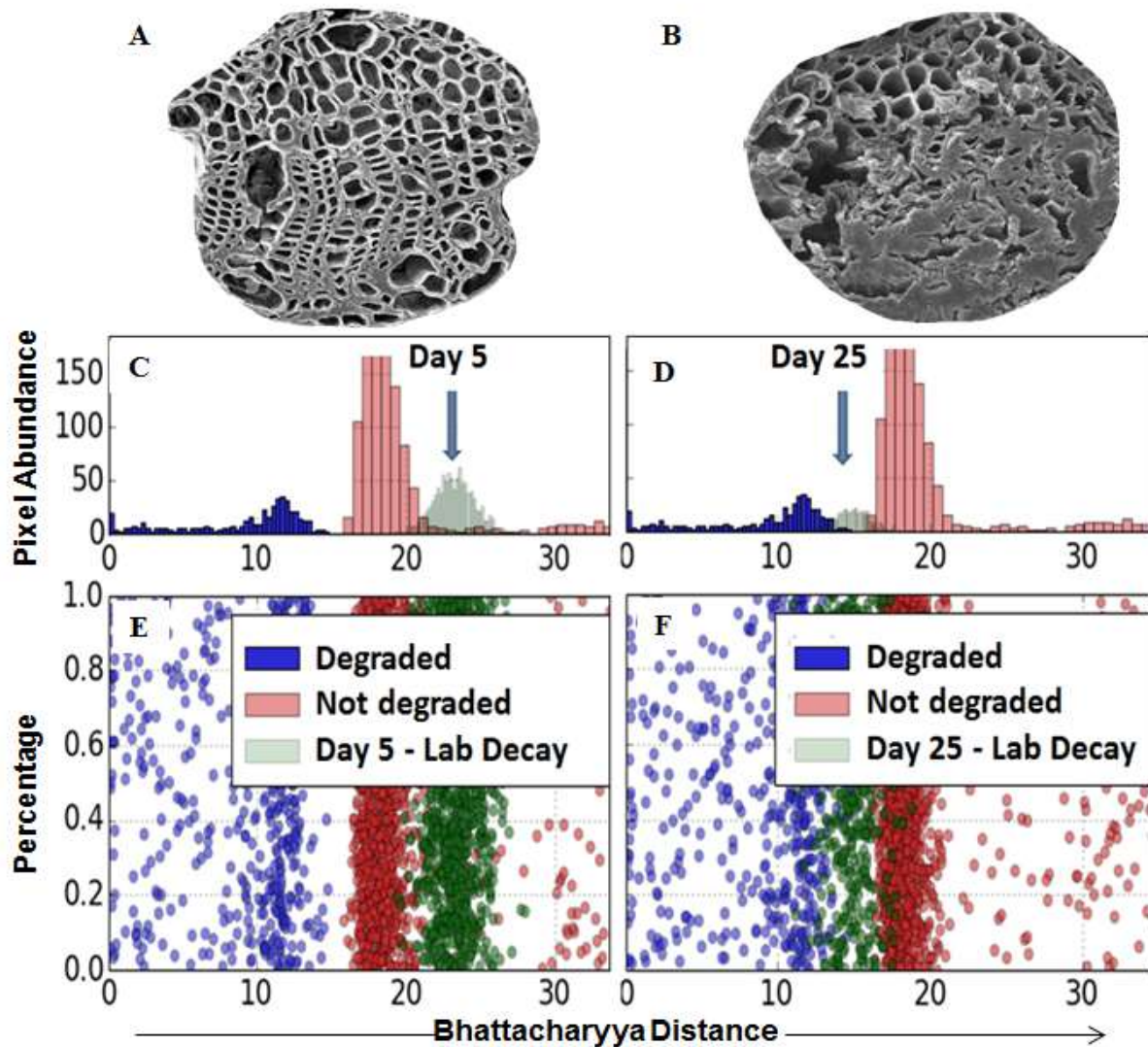


Figure 12. Bhattacharyya distance of GMM distributions from pixel-count evaluation using all samples (laboratory decay, natural decay, and fossil) showing degraded (blue) and not degraded (red). Day 5 (green) are seen in (A) region of interest, (C) histogram, and (E) scatterplot. Day 25 (green) are seen in (B) region of interest, (D) histogram, and (F) scatterplot.

As the program was being developed, several problems arose. One such problem which we soon address below involved partially degraded samples. When samples were remarkably well-preserved NDG samples (such as Day 0 in the laboratory decay) or extremely DG samples (such as Day 25 in the laboratory decay), the method works remarkably well because there are clear differences among pixel values distributions (99.98% accuracy using k-NearestNeighbor, discussed in 4.3.1). An NDG sample has two well-distinguished peaks and a DG sample has overlapped peaks (explained in 6.1 and 6.2).

However, partially degraded samples proved to be more difficult for the computer to distinguish. A partially degraded sample may still have well-preserved tracheid cells (demonstrating two distinguished peaks) and poorly preserved sieve tube elements (demonstrating two overlapped peaks), which results in a mix of three peaks. In order to address this problem, the random pixel collection was consecutively run twenty times and the mean was taken. This improved the margin of error from ± 4 to ± 2 on the Bhattacharyya distance. Because this margin of error was still not satisfactory, a second approach was tested which takes horizontal strips of the image and measures the quality of each strip. Horizontal strips (as opposed to vertical strips or quadrant pieces) were taken because the separation between the sieve tube elements in the phloem and the tracheid cells in the xylem, given no extreme and unusual cell warping, is horizontal (Figure 13 and 14). Strips of 40 pixel length (approximately 20-25 strips, depending on the image size) were measured using the GMM and Bhattacharyya distance.

As seen in Figure 13, an ROI image of Day 0 has been cut into strips. For reference, a transverse sectional view of the Day 0 mid-vein can be seen in Figure 7A. There are two distinguished peaks (many black and white pixels), resulting in high Bhattacharyya distances. High Bhattacharyya distances for Day 0 (and for any well-preserved sample) are consistent with previously discussed results (Figure 12 through 14). Specific regions of the cell wall have greater Bhattacharyya distances than others, but overall, the median distance is 34.421. In Figure 14, an ROI image of Day 25 has been cut into strips. For reference, a transverse sectional view of the Day 25 mid-vein can be seen in Figure 7K. Here, there are two indistinguishable peaks (mostly gray pixels) with small Bhattacharyya distances between the two peaks, which are consistent with previous results (Figure 12 through 14). Most of the values are very low, with an overall median of 15.099. However, as seen in the first several strips, there are large Bhattacharyya distances.

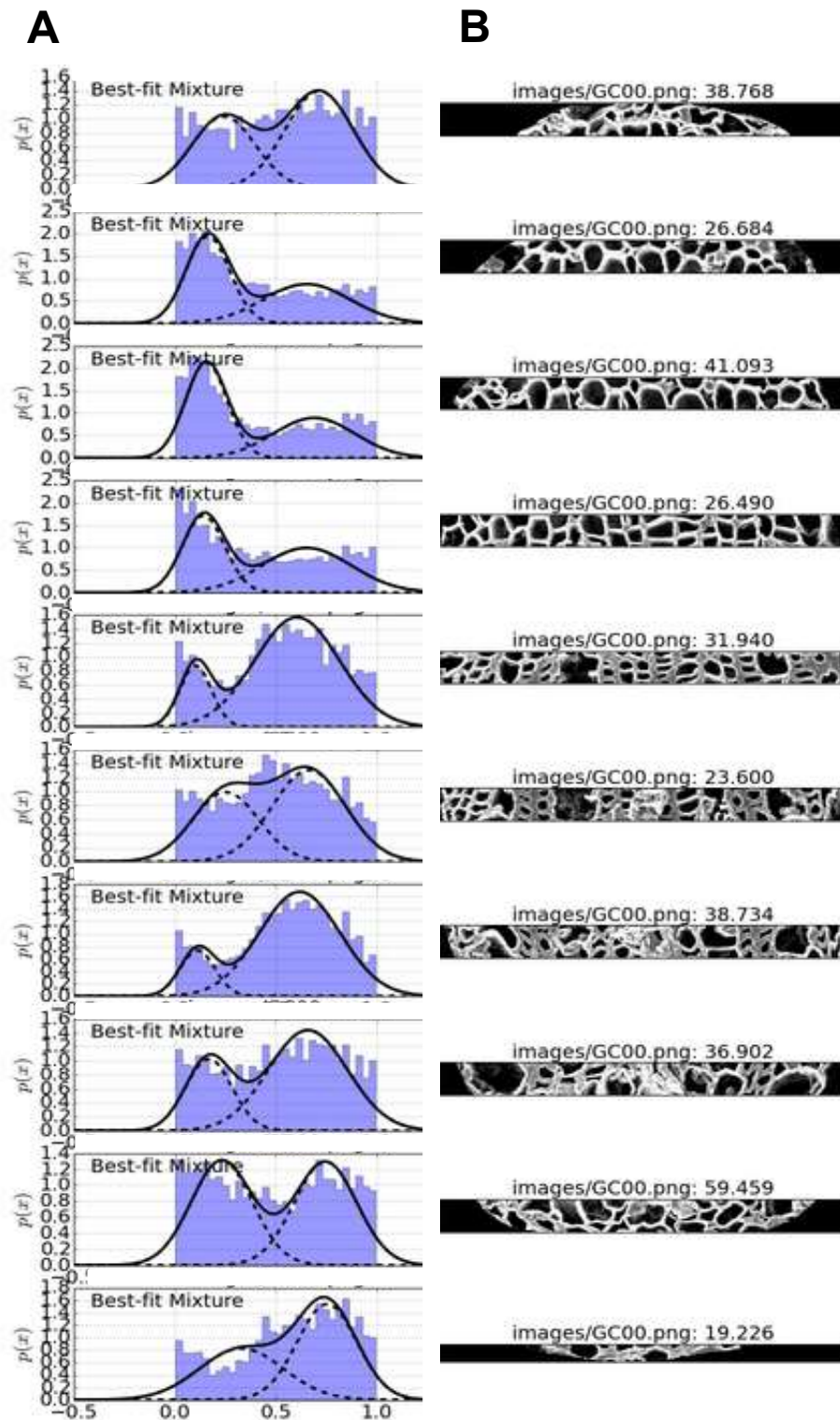


Figure 13. Pixel-count evaluation conducted on strips of the image for Day 0. (A) GMM showing the distributions of pixel values. (B) Strip image with Bhattacharyya distance.

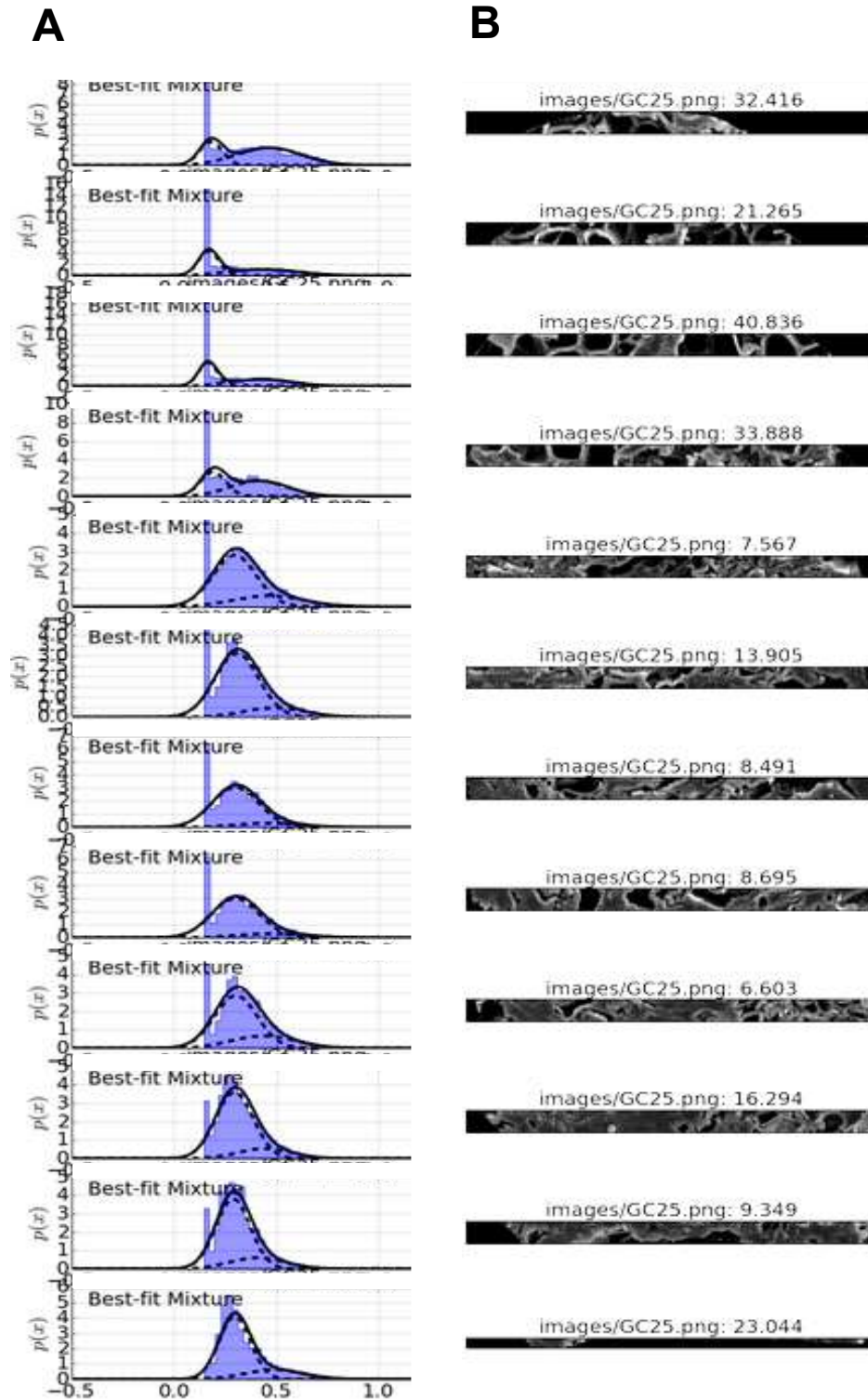


Figure 14. Pixel-count evaluation conducted on strips of the image for Day 25. (A) GMM showing the distributions of pixel values. (B) Strip image with Bhattacharyya distance.

The Bhattacharyya distance strips can be analyzed in two ways. The first way is to examine values within the same sample. In Figure 15, the highlight sections are based on the Bhattacharyya distance of each strip, where lighter strips demonstrate excellent preservation, whereas darker strips demonstrate degradation. This provides insight into 1) which regions and 2) to what extent those regions are degraded.

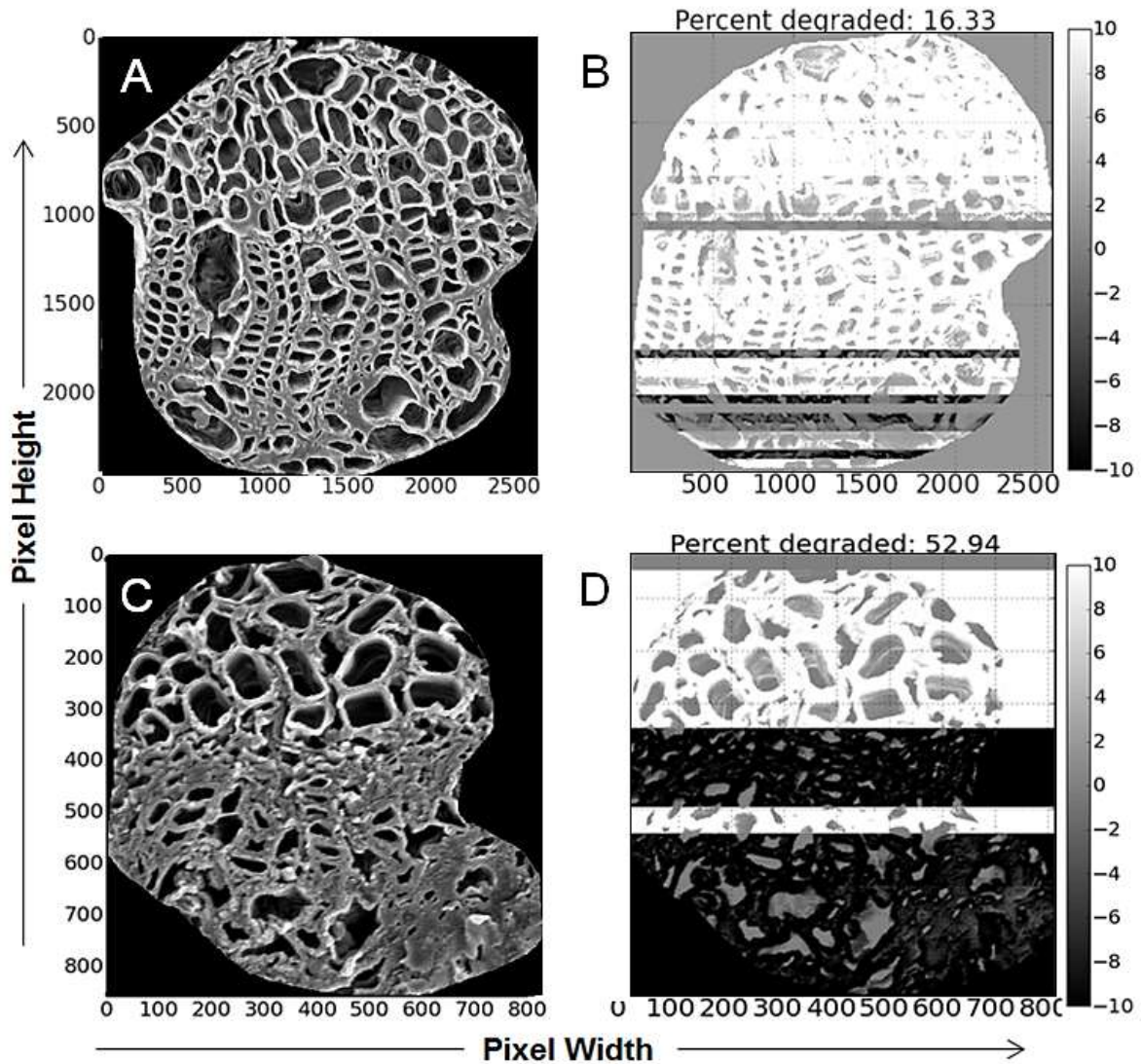


Figure 15. Pixel-count evaluation conducted on strips of the images for Day 5 (A and B) and Day 25 (C and D) of the consortium laboratory decay. (A) and (C) show the original image, whereas (B) and (D) show the strips color-coded based on how well-preserved (white) or poorly-preserved (black) the sample is, based on the Bhattacharyya distance.

The second way is to create greater accuracy for an individual sample's overall Bhattacharyya distance. The median was used as the overall distance, and then used to rank and compare samples. Figure 16 demonstrates all of the samples with their respective Bhattacharyya distances based on the strip-count method. On the x-axis, samples are in the order of degradation. In other words, the laboratory decay series moves left to right from Day 0 through Day 25, the natural decay series moves left to right from M-M-83-B1 through M-M-83-B6, and the fossils are shown as dashed lines. The fossil samples are not put in age order like the modern decays series because, as discussed in Witkowski et al. (2012), fossil age is not necessarily indicative of preservation. As seen in Figure 16, as seen in the laboratory decay series (particularly in the consortium laboratory decay series shown as circles), there is relatively little change in the first several samples and then a drastic decline in morphological preservation after approximately ten days. The fossil samples used for this study were comparable to the mid-point in the laboratory and natural decay experiments (Figure 16).

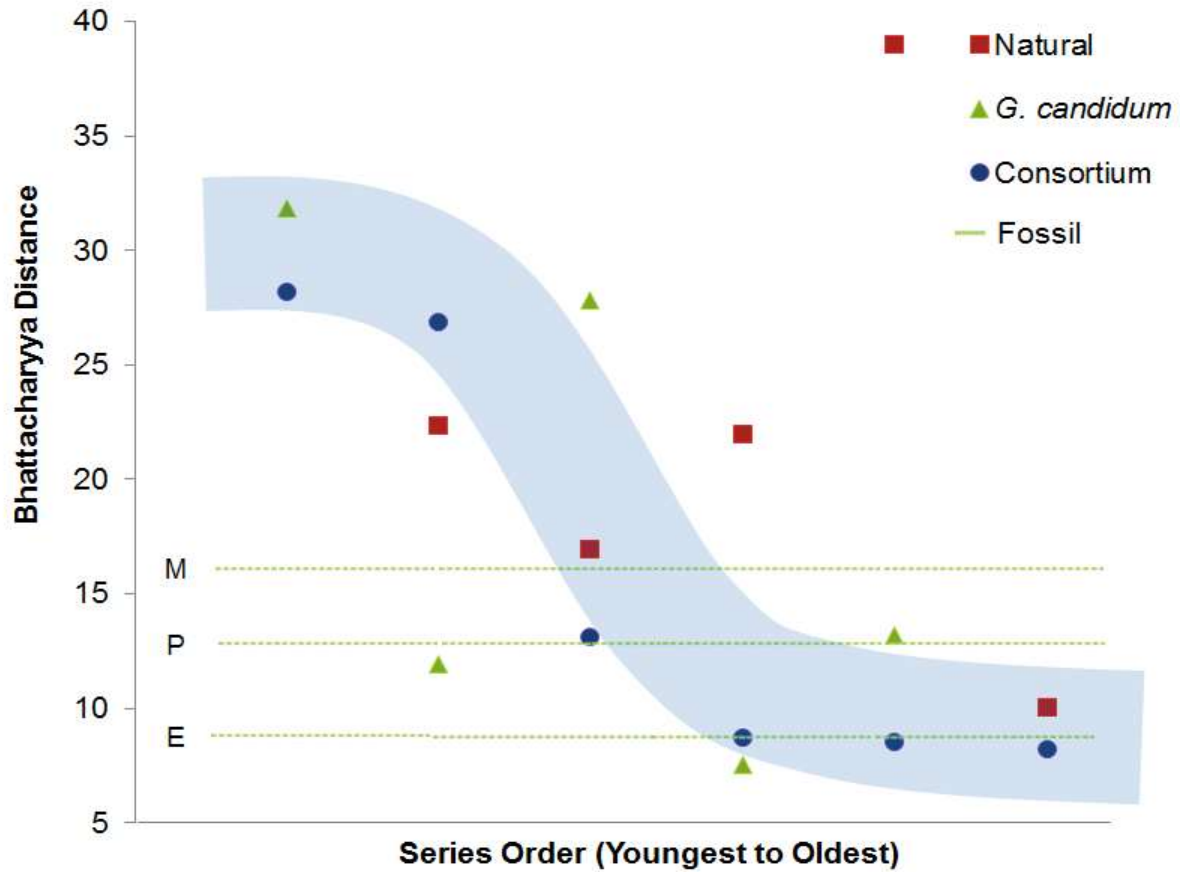


Figure 16. Bhattacharyya distance from the pixel-count evaluation method for consortium laboratory decayed (blue circles), *Geotrichum candidum* laboratory decayed (green triangles), and natural decayed series (red squares), as well as fossil *Metasequoia* leaves (gray dashed-line) marking Miocene (M), Paleocene (P), and Eocene (E) samples.

Chapter 7. Discussion

7.1 Quantified degradation

As aforementioned, to best understand the degradation process, an integrated approach of molecular, isotopic, and morphological analyses may play a more efficient role. Molecular and isotopic methods are primarily quantitative, with the exception of pyrolysis which can be considered semi-quantitative, whereas morphological methods are generally qualitative. Limiting morphological perspectives to only qualitative observations inhibit the scope and breadth of morphologically analytical potential and prevent the information readily compared with other forms of data. There are several benefits to the new pixel-count evaluation method, especially its quantitative nature (7.1.1), its automation (7.1.2), and its reliability (7.1.3), even given its limitations (7.1.4).

7.1.1 Quantification

The computerized quantitative method eliminates potential subjectivity of the observer and provides objective numerical ranking. Qualitative observations require an intimate relationship with the species being examined, which leads to biases. Two expert morphologists could have different rankings of degradation for the same leaf and arrive at different conclusions. Each morphologist could hold a reasonable opinion based on the individual's education and research experiences, but ultimately disagree because they had given weight to particular features instead of objectively examining the sample. Empirical investigations can be readily analyzed by anyone familiar with basic statistics. Non-morphologists can better grasp a numerical ranking system because it removes the jargon-based learning curve of interpreting sample preservation, distancing the researcher from the

experiment. Any biased observations in the traditional qualitative method are removed when relying on tangible numbers.

By framing the examination of a leaf cell wall away from an expert's opinion, a quantitative approach offers a new perspective on understanding the issue of three-dimensional preservation than one can gain from a qualitative approach. Once the pixel values are collected as data points, the problem is no longer limited to the issue of degradation. By examining degradation with pixel values, it can be cast as a problem in computer visualization or statistics, thus one can use well-established framework to which compare and analyze results (Fabio, 2003; Xiang and Berger, 2003; Nummiaro et al., 2003; Sfikas et al., 2005). Degradation is thus mapped on a large set of problems that have been previously explored.

Furthermore, by using these computer visualization, classification, and statistical tools on degradation, the features that can be explored are virtually limitless. For the sake of visualizing the data, there are several two-dimensional plots of the means of each distribution (Figure 11 and 12), but the program actually classifies using five features (the mean of each distribution, the standard deviation of each distribution, and the overlap), which allows for analyses in five dimensions. Finding features that were readily separable for this research was admittedly a fortunate guess, and there may actually be better features available that have yet to be explored. The program is readily modifiable based on new findings and allows for even more dimensions for analyses.

Not only is the method quantitative, but quantitative by several different tests. In this research, two quantitative methods have been used, and can be further expanded in future research. The first method used for this research was the Bhattacharyya distance which offers a quantitative measure based on the similarity of two-peak GMM distributions. The Bhattacharyya distance is based on features such as the distance between means and covariance. The second method for quantification is used when conducting classification, such as k-NearestNeighbor, (k-NN, described later in 7.3.1). The sample is given a probability of how likely it is DG (and thus also how likely it is NDG), which is a quantitative percentage. By having two readily available methods for quantification, there are measures for reaffirming the statistics for the degradation.

7.1.2 Automation

In addition to being quantitative, automation is another great benefit of the pixel-count evaluation method. An automated, computerized method is timesaving, both compared to qualitative methods and other potential quantitative methods. Qualitative methods require the same expert to examine all samples in order to determine the degree of leaf degradation. New sample must be examined by the same expert to determine the relation to previous data. Furthermore, a morphologist must examine every section of the sample. In the case of this research, it is time-consuming to examine from the overview transverse section of the leaf to the mid-vein to the individual cell wall structures to the leaf margin and cuticle. Quantified results offer a readily and immediate comparison between the new sample and the existing dataset, enabling the more efficient use of a morphologist's time.

An automated, computerized method is also timesaving and more reliable as compared to the alternative quantitative method, a hemocytometer, which requires one to manually count individual boxes of either DG or NDG (introduced in 6.1). Hemocytometers are time-consuming; for example, it took the author approximately four hours to count one image on a 40x40 grid, a total of 1581 boxes. In addition to the time factor, determining whether a box was more cell wall or more space was difficult, often requiring the author to examine the entire leaf in order to make the appropriate distinction. Furthermore, it was also prone to errors. Maintaining track of the grid cells and classifying the boxes were often difficult, and the monotony of the task offered more room for error. Comparison between manual and computer quantification is further discussed in 7.1.3.

7.1.3 Reliability

The pixel-count evaluation method was tested in several ways. First, the pixel-count evaluation method was tested to understand whether it could categorize the samples into either DG or NDG. The ROI images were classified using a classifier, a software package used to identify and categorize samples. Several classifiers were tested, although k-NearestNeighbor (k-NN) was the most successful. k-NN is a non-parametric method that classifies a sample based on its proximity to the pre-classified training data, the original separated DG and NDG ROI images (Cover and Hart, 1967; Toussaint, 2005; Hall et al., 2008). Because the DG and NDG images were well-distinguishable, k-NN readily identified which were DG images and which were NDG images. The program performed with 99.9852% accuracy the first time it was trained (taught). Once new data was added to the previous collection of images, the program's accuracy was 99.9803% on that test data. The more samples that are added to the training set, the better the computer will be able to perform. More data offers more patterns for the program to recognize when classifying samples, meaning that the program will only become more accurate over time.

Second, the automated program was tested against itself. For one, the exact same image was manipulated under different conditions (high/low contrast, high/low brightness, etc.) and ran through the program (Figure 17). The results were virtually the same (± 0.3 Bhattacharyya distance) regardless of photo conditions, suggesting that the lighting and contrast choices of the photographer do not affect the method and that the process is replicable (Figure 17).

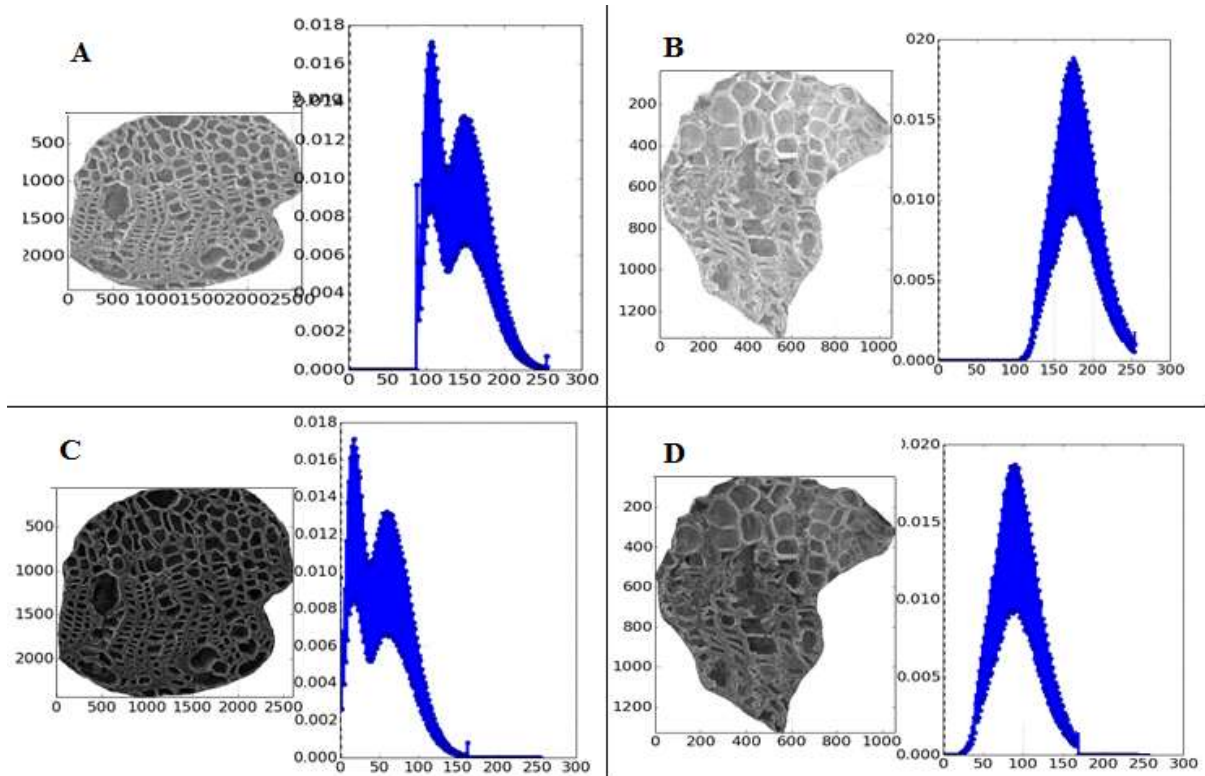


Figure 17. Different photo conditions to test the pixel-count evaluation effectiveness. (A) and (C) are low and high brightness for Day 5 consortium laboratory decay sample. (B) and (D) are low and high brightness for Day 25 consortium laboratory decay sample. The scale on the graph ranges from 0 (black) to 255 (white) pixel values.

Next, the pixel-based evaluation method was compared with the traditional hemocytometer quantitative approach (6.1, 7.1.2). Because the pixel-count evaluation uses the distribution of a continuous dataset, as opposed to the hemocytometer which uses only two values (either 1 or 0), comparing the two methods took slight modification. The hemocytometer method required manually counting $2.857\mu\text{m}$ -sized grid boxes on a 40×40 grid. Several images were manually counted for comparison with the computerized method. To compare with the manual method, the computerized method also used $2.857\mu\text{m}$ -sized boxes, each box equivalent to 30×30 pixels. The SEM ROI image was horizontally sliced into 30-pixel height strips to replicate the manual-count grid rows.

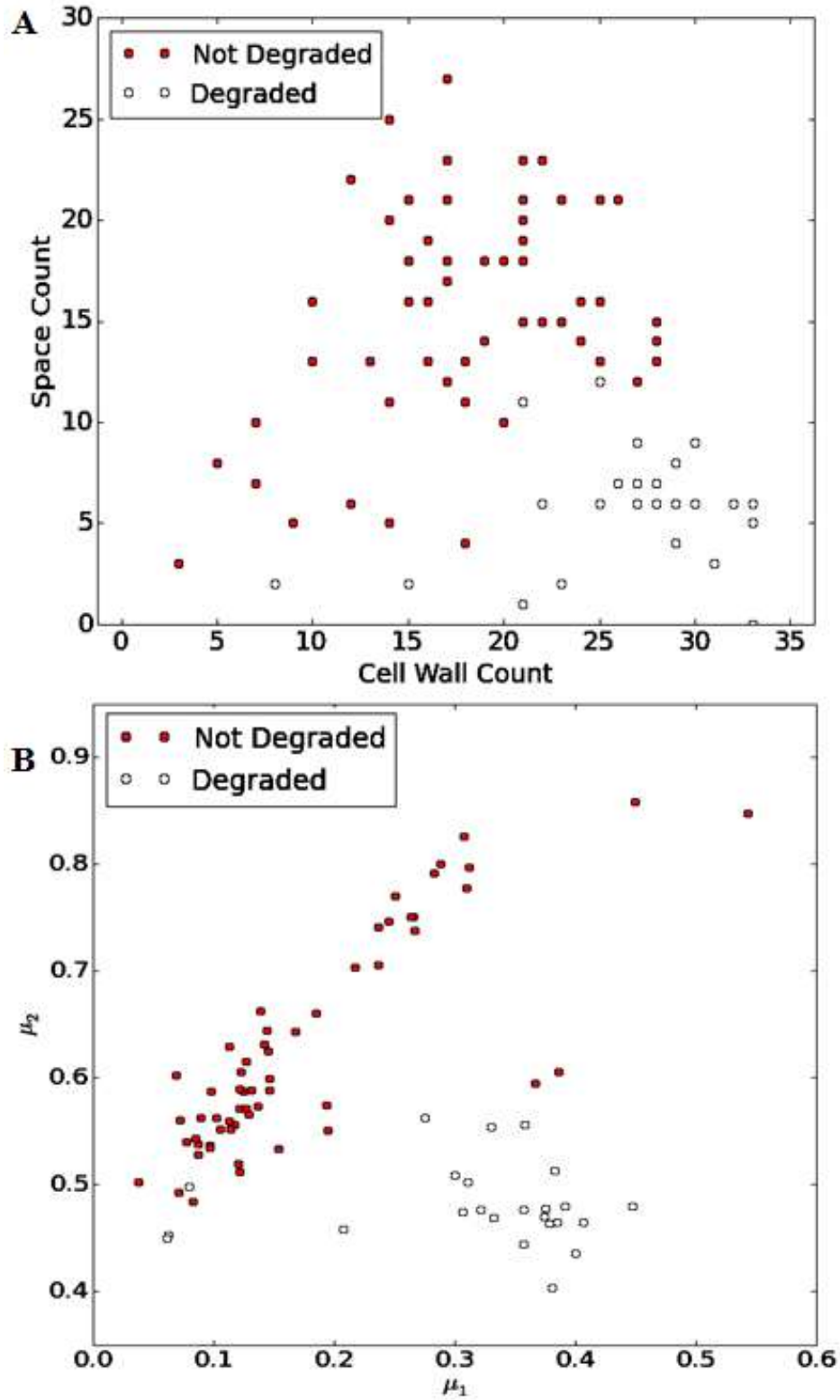


Figure 18. The same image of consortium laboratory decay Day 5 and Day 25 plot on the same graph, with not degraded (red circle) and degraded (open circle). (A) Traditional hemocytometer. (B) Computerized pixel-count evaluation method.

The computer program does the exact same function as a hemocytometers, but offers greater value. For one, the program is more accurate than traditional chamber counting because the program assigns specific number in a large range of values. It takes a distribution of many different values instead of simply classifying as either 1 or 0 (6.1, 6.2, and 7.1.2). As seen in Figure 18A, the hemocytometer has data points in rows and columns, indicative of the intrinsically discrete values in the manual method, whereas Figure 18B visibly has continuous values. Part due to the nature of the numbers and part due to the efficiency of the computer, the computerized method has clearly distinguished groupings of DG and NDG ROIs.

Moreover, the computerized pixel-count evaluation method removes human bias in determining how to mark 'gray', partially degraded plant cell walls that are neither 'black' space nor 'white' cell wall and removes human bias in determining how to mark a box that seems to contain equally half space and half cell wall. It further removes any human error in potentially missing or double-counting data. It is also more useful than the typical hemocytometer because it is automated. It has results for an image within fractions of a second, whereas manually counting takes many hours. This allows for large quantities of images to be processed, compared, and analyzed quickly and accurately.

7.1.4 Limitations

Currently, the new pixel-count evaluation method is in its beginning stages and as with any new method, it still requires minor adjustments. There are several limitations to the pixel-count evaluation method, namely, the inability to recognize specific cell wall features and the inherent problems involved with a new method. Despite the benefits of a quantitative approach, it lacks the subtlety of feature recognition used in a qualitative approach. A trained morphologist will always be able to verbally describe the exact regions of degradation (Figure 7 through 9), whereas the computer only numerically expresses the degree of degradation (Figure 12 through 16). For example, it cannot distinguish specific features of the plant cell wall, such as the type of cell wall (primary or secondary) nor what type of biomolecule (lignin or polysaccharide) is being degraded. A morphologist adds value not only in his or her ability to distinguish features, but also through his or her experience, particularly for the final interpretation of the computerized results and SEM observations. Thus, the method must be used in conjunction with traditional qualitative methods.

Furthermore, because the method is newly developed, the actual results and reliability of the pixel-count evaluation method were difficult to benchmark. No quantitative method has ever been tested on leaf cell wall structures. In order to demonstrate the effectiveness and efficiency of the new computerized method, a non-computerized method was developed specifically for this research (6.1, 7.1.2, 7.1.3). The manual method takes the concept of a hemocytometer from microbiology, but it must be noted that this has never been used for the purposes of this study. The manual method resolved the issue of testing the computerized method. However, the manual method itself is not a well-established and literature-supported standard.

As the program was being developed, several problems arose, although all have been addressed. One such problem, as described in 6.3, was that partially degraded samples proved to be more difficult for the computer to distinguish. A partially degraded sample may still have well-preserved tracheid cells (demonstrating two distinguished peaks) and poorly preserved sieve tube elements (demonstrating two overlapped peaks), which results in a mix of three peaks. In order to address this problem, the random pixel collection was consecutively run twenty times and the mean was taken. This improved the margin of error from ± 4 to ± 2 on the Bhattacharyya distance. Further, the horizontal strips method described in 6.3 was developed. By taking strips, we are able to see the quantified degradation of different sections of the mid-vein (Figure 13 through 15). Using the quantitative methods on the strips of SEM image offered an even greater value than the overall method, allowing for specific regions to be better quantitatively observed. The problem of unusual measurements was not only solved, but also offered greater quantitative insights into which portions of the mid-vein maintained structures (typically lignin-strengthened tracheids) and which portions were collapsed (6.3, Figure 13 through 15).

Although the pixel-count evaluation is still has tremendous room for improvement, overall, it is a useful additional method for paleobotanical analyses. The quantification and the automation of the program provide a ranking tool so that samples can be quickly and objectively analyzed. It can also determine the quantified degree of cell wall decay, highlighting regions of interest. These provide momentous advantages in prioritizing samples for qualitative morphological observations, as well as for molecular and isotopic analyses. Being able to quantify tissue decay and preservation allows us for direct comparison among other known fossil and modern samples, as well as readily determining whether a sample is

worth pursuing of molecular and/or isotope analysis. Quantifying the molecular and morphological mechanisms for preservation provides greater understanding of fossil degradation and, in turn, the utility of the well-preserved fossils as paleoclimate and paleoenvironmental reconstruction proxies. The method can be readily modified for studying the degradation of any other plant fossil *lagerstätten* and has the potential to be modified for any degradation studies.

7.2 Molecular evidence for plant decay and preservation

7.2.1 Explaining molecular degradation of *Metasequoia* samples

In the laboratory decay series, the molecular preservation of polysaccharides shows an initial decrease and later increase in total polysaccharide abundance, a final increase almost equivalent to that of the control (Figure 3, Figure 4, and Table 2). Having expected the concentration of polysaccharides to decrease throughout the entire experiments, we considered two possible hypotheses to interpret our data. 1) The experiment didn't degrade polysaccharides and thus there was actually little to no change in polysaccharide concentration. The observed change of polysaccharide concentrations through the laboratory decay experiment was simply an instrumentation artifact. 2) Decayed polysaccharides from plant leaves were utilized by the microbial growth and the reincorporation of polysaccharides into the microbe were counted along with the leaf polysaccharide (see Appendix D). The following evidence most strongly support the latter explanation: 1) multiple runs with consistent results among different molecular technologies, 2) microbiology literature, 3) consistent qualitative and quantitative morphological decay, and 4) the time of fungal entry into the leaf.

1) Two main molecular tools were used, Py-GC-MS and MBTH assay, both of which have consistent results. Both methods were run multiple times and yielded the same results. Pyrolysis is used for examining individual compounds within a sample. During pyrolysis in Py-GC-MS methodology, many of these polysaccharides are broken into smaller compounds (particularly chitin), which could be mistaken for the polysaccharides in the *Metasequoia* leaves. Py-GC-MS methodology demonstrates pyrolysates of larger polysaccharides but does

not distinguish the source of the original compound. Like pieces of a puzzle, analyses of pyrolysates can support hypotheses for original compounds, but cannot factually distinguish the source of polysaccharides or the kind of sugar (for example, glucose, mannose, galactose, etc.)

MBTH assay is used to examine bulk reducing sugars, as opposed to individual compounds. Although the method is very different from Py-GC-MS, the MBTH assay also yielded the same decrease and later increase in polysaccharide (Figure 4). MBTH assay is highly replicable and accurate, as seen in the standards of Glc and GlcNAc in Appendix B. In addition to Py-GC-MS and MBTH assay, nuclear magnetic resonance mass spectrometry (NMR) analysis was conducted on *G. candidum* decayed leaf samples on Day 0 and Day 25, and there is little difference in before and after decay (see Appendix C). Although this could support the first hypothesis, NMR is also highly reproducible and yielded differences among polysaccharides, which should not occur among the same sample. Because the microbes also contain polysaccharides, this likely affects the leaf bulk polysaccharides shown in NMR (see Appendix C). Running the same samples with the same methodologies multiple times and producing the same results makes the first hypothesis unlikely. In addition to the existing unlikelihood with one method, yielding the same results among *three* different methodologies (Py-GC-MS, MBTH, and NMR) makes the first hypothesis of the curve falling within the margin of error is *highly* unlikely.

2) Previous studies on the microbial polysaccharides indicate that *G. candidum* are primarily composed of glucose (28%), mannose (14%), galactose (12%), hexosamine (14%), lipid

(8%), and protein (7%), (Sietsma and Wouters, 1971), which has likely appeared in our molecular analyses. According to Sietsma and Wouters (1971), three major types of polysaccharides are present in *G. candidum* cell walls, namely galactomannan, a glucan with β -D-(1-3)- and β -d-(1-6)-linkages, and chitin. Likewise, the consortium contains many different sugars and polysaccharides, particularly from *T. reesei*, which is a fungus like *G. candidum* (2.1).

3) Furthermore, morphological evidence also most strongly supports the second hypothesis. Qualitatively, there are clear changes in leaf texture over the course of the experiment that suggests significant degradation, as seen in the SEM observations in Figure 7. A close-up of this decay is evident in the contrast between Day 0 (Figure 7B) and Day 21 (Figure 7I). On Day 0 (Figure 7B), the primary and secondary cell walls are indistinguishable due to their thickness, proximity, and all gaps filled with rich pectin. On Day 21 (Figure 7I), however, the primary cell wall is almost completely consumed, and there is visible detachment and peeling of the secondary cell wall. Furthermore, the pectin is almost entirely removed as seen by the clear gap and beginning separation between cell walls.

Quantitatively, the pixel-count evaluation method also shows evident morphological changes. The consortium decay in Day 5 has a Bhattacharyya distance of 28.223 for Day 0 and 26.871 for Day 5, demonstrating little change. However, post-hyphae penetration (Figure 8), Day 12 has a distance of 13.155 (Figure 16). The last several days in the consortium laboratory decay series stabilize to Bhattacharyya distances of 8.722 for Day 17, 8.511 for Day 20, and 8.252 for Day 25 (Figure 16). This supports that the decay was continual and rapid throughout the

laboratory decay series, and most definitely did not remain constant as the raw molecular analyses suggest.

4) Finally, the time at which there is observable evidence of the fungal hyphae entering the leaf stomata is consistent with the time at which the microbial population growth occurs (based on the second hypothesis). Fungi secrete enzymes that breakdown polysaccharides without the hyphae requiring contact. This would support the molecular decrease in polysaccharides at the beginning of the *G. candidum* laboratory decay experiment at Days 4 and 9 (Figure 4) in conjunction with the morphological decrease in cell wall (Figure 7 through 9) when the hyphae were still in slow growth.

Mycelium growth only occurs at the hyphae tips (Trinci, 1972; Prosser and Trinci, 1978; Bartnicki-Garcia et al., 2000). Until the mycelium is large and the Spitzenkörper (the intracellular organelle associated with the tip growth) is well-developed, initial growth is relatively slow. However, once the mycelia grow to a certain size with many hyphae tips, their growth increases rapidly. On Day 9 (Figure 7E and Figure 8B through D), the fungal hyphae have just entered through the stomata on the leaf epicuticular surface, but have not yet reached the polysaccharide-rich mid-vein. Once they reach the mid-vein where their enzymes have already begun to degrade the leaf cell walls, they are able to build up their own body structure, resulting in the fungi's exponential growth shown in molecular results (Figure 4).

7.2.2 The effects of open versus closed systems on the removal of carbohydrates

The extraordinary preservation of fossil material is greatly dependent on its rapid burial and lack of exposure to microbial growth (e.g., Briggs, 2003), as seen through both natural decay and laboratory-controlled experiments using modern *Metasequoia* leaves. The major difference between these two sets of decay environments is that the former is in a natural open system, whereas the latter is in a closed system in a highly controlled environment. In an open system of a small pond, microorganisms, water, minerals, and other matter can interact with the leaf and molecules, both agent of decay and decay products flow in and out of the leaf system in a constant and dynamic way. Although microbial life may appear, as seen in the pond samples (data not shown), microbes are rarely seen in large abundances within the leaf samples. In contrast to an open system like the natural decay experiment, the microbial life cannot leave the closed laboratory decay system within the confines of a petri dish.

Supporting evidence for the differences in an open versus a closed system is further evident in the molecular (Figure 4 and Table 2) and isotopic (Figure 5 and Table 3) data. In Py-GC-MS analysis, there is a clear difference between the natural decay and laboratory decay. As seen in Gupta et al. (2009), polysaccharides decrease over time in the natural decay series. For example, as seen in Figure 2 in Gupta et al. (2009), levoglucosan consistently decreases from sample M-M-83-B1 through M-M-83-B6. In this open system, once the polysaccharide was degraded, it was removed from the leaf system into the environment via microbial, hydrological, and/or other agents of exchange. Unlike the open-system natural decay, the laboratory decay demonstrated a decrease and later increase in both individual pyrolysates (Py-GC-MS) and bulk carbohydrates (MBTH assay) (Figure 4 and Table 2). The later

increase is due to the reincorporation of polysaccharides and products of polysaccharides into the hyphae of the microorganism (7.2.1). In a closed system, microbes remained in the system and were thus calculated into the overall polysaccharide abundances of the laboratory decay leaves.

Likewise, the bulk carbon isotope measurements of carbon isotope ratios demonstrate change in the open system and no change in the closed system. In an open system natural decay, the removal of carbon (primarily polysaccharides during early diagenesis) is more complete because the microbes leave after partially digesting the carbon-based compounds in the leaves. The removal of polysaccharides during early diagenesis in natural decay series resulted in a net 1‰ negative shift of bulk leaf carbon isotope ratios (Figure 5 and Table 3). This negative shift is consistent with the result in Schweizer et al. (2009), in which grasses and legumes were decayed for 119 days.

Concurrent with 7.2.1, there is no isotopic change in the closed system because the microbes cannot leave. Carbon remains in the closed system as the microbes consume and reincorporate compounds into their own bodies. The data not only suggests the exchange of carbon between plant leaf and microbe but also implies the lack of significant carbon isotope fractionations during the process of carbon incorporation into the microbe's system. When all reactants are consumed and converted to product in an irreversible system, such as CO₂ fixation in a closed system, there is no fractionation (Berry and Troughton, 1974; O'Leary, 1981; Farquhar et al., 1989).

Bulk carbon isotope from fossil *Metasequoia* are far more positive (~ -24.5 ‰) than modern samples signatures (~ -27.7 ‰), as seen in Table 4. Molecular analyses show that fossil *lagerstätten* samples have only partial removal of polysaccharides and resistant molecules such as lignin largely remained (Yang et al., 2005; 2007). As explained in 4.3, plant material becomes more enriched in ^{12}C through degradation because it is more resistant in compounds like lignins and lipids, whereas it is readily depleted in less resistant compounds like polysaccharides. Because morphological observations show remarkably preserved, thick polysaccharide-based leaf cell walls, this means the ^{12}C enrichment must come from the environment and not degradation. Implications of these results and discussion will be further explained in 7.3.3.

7.2.3 Polysaccharide concentration as a structural keystone

All samples sets (laboratory decay, natural decay, and fossil samples) support the hypothesis that polysaccharides are the key molecule group for the preservation of three-dimensional structures in *Metasequoia* leaves. After removing polysaccharides in the laboratory decay, we observed the progressive collapse of cellulose and hemicelluloses-based cell walls (Figure 7, Figure 15, and Figure 16).

Specifically, the progressive collapse of primary cells walls can be observed in the laboratory decay (Figure 7). Responsible for the transportation of carbohydrates (primarily sucrose) throughout the plant, the phloem of *Metasequoia* is mainly composed of sieve tube elements and parenchyma cells, both of which have cell walls predominantly made of cellulose and hemicellulose. After 25d of decay, these cells are all collapsed (Figure 7K) as their cellulose has been digested by the fungus. Figure 7 shows that over the course of the laboratory decay series (from Day 0 to Day 25). There is a continual removal of polysaccharides which maintain the structural integrity of those cells in the vascular bundle.

Additionally, there is a partial collapse of tracheid cells in the xylem and transfusion tissue of the laboratory decay samples, as seen by the comparison from Day 9 (Figure 7C) to Day 21 (Figure 7H). In contrast with the phloem cells, the tracheids are elongated sclerenchyma cells with a secondary cell wall deposited further within the primary cell wall, and the unevenly deposited secondary cell wall is largely strengthened by lignin. Thus, overall they firstly have remained well-intact, and gradually (but in a much slow pace compared with parenchyma cells) showed a certain degree of deformation due to cellulose loss as well as the pectin loss in the middle lamella. Sooner or later, they will also finally collapse along with the further

decomposition of polysaccharides (in the middle lamella, primary cell wall, and also in the secondary cell walls) by microbes (Figure 7). As seen in Figure 7F, the Day 9 secondary cell wall is beginning to peel in some places and by Day 21 (Figure 7H), there is obvious unraveling of the secondary cell wall from the tracheids.

Interestingly, as seen in Figure 7, H and I, although the secondary cell walls in the xylem tracheids have begun to peel, they seem having not totally lost their structure (remaining in long string-like ravel), very likely due to the existence of lignin which are not consumable to the introduced microbes. Because both primary and secondary cell walls are composed of polysaccharides, particularly primary cell walls which are almost entirely polysaccharides (mainly cellulose and some hemicellulose), the molecular and morphological analyses suggest that polysaccharides are essential to preserving the three-dimensional structure of the leaf cell walls. Without the complex mesh-like polysaccharide structures present, the walls are no longer strengthened.

The change in preservation in laboratory decay is also apparent in the pixel-count evaluation method. As explained in 7.2.1 and as seen in Figure 16, there is a rapid decline in preservation as indicated by the Bhattacharyya distance, consistent with both molecular and morphological analysis. Taking the consortium laboratory decay series as an example in Figure 16, the first several samples remain relatively well-preserved, with a Bhattacharyya distance of 28.223 for Day 0 and 26.871 for Day 5. Once the fungal hyphae penetrate the stomata on the leaf surface, as indicated by SEM observations (Figure 7 through 9), there is a dramatic change in preservation, from 26.871 for Day 5 to 13.155 for Day 12. The rapid

degradation is concurrent with the hyphae penetration. Thus, the slow start followed by quick degradation is mostly due to the fact that the microbes initially lacked access to the inner leaf and as soon they penetrated the leaf via stomata, quickly devoured the leaf cell wall polysaccharides. Major degradation slows for the last several days of the series, where the Bhattacharyya distance for Day 12 at 13.155, and then stabilizes for Day 17 at 8.722, Day 20 at 8.511, and Day 25 at 8.252 (Figure 16). This is likely due to the fact that the simpler carbohydrates and polysaccharides are exhausted in the leaf cell wall, only leaving more complex lignin-based secondary cell wall structures behind.

7.3 Insights for paleobotanical studies

7.3.1 Cross-examination

Had only the molecular and isotope analyses been conducted, the degradation of the laboratory experiment would have been poorly understood or misinterpreted. Moreover, both molecular and isotopic results of the laboratory decay experiment could have implied a very different experimental outcome: Consistent among all molecular data, both from individual polysaccharide pyrolysates in Py-GC-MS and from bulk carbohydrates in the MBTH assay, there is a glycomic decrease and later increase in the laboratory decay series (Figure 4 and Table 2). Isotopic data demonstrating no change throughout the laboratory decay series (Figure 5 and Table 3) might have suggested a similar explanation: no polysaccharide decay occurred.

Qualitative and quantitative analyses of SEM images of the *M. glyptostrobooides* leaves in the laboratory decay, however, demonstrate that polysaccharides but not lignin were degraded in the leaves, as expected in determining the appropriate microbial strains for the experiment (Figure 7 and Figure 16). The laboratory decay demonstrates an extreme scenario which would unlikely occur in nature, and so within the 25 d experiment series, the role polysaccharide plays in preserving three-dimensional structures is profound.

Nevertheless, morphological analyses cannot stand alone. Both the qualitative and quantitative methods required molecular and isotopic data to understand the mechanisms behind the observed morphological changes and distinguish the differences between different decay systems. Both the laboratory decay and natural decay appeared remarkably similar at

the morphological level. However, using molecular (Figure 4 and Table 2) and isotopic findings (Figure 5 and Table 3), we were able to understand the difference between open and closed systems and their effects on the rate of decay. Overall, molecular cross-reference with morphological tools provided insights into the realistic degradation patterns, whereas morphological cross-reference with molecular and isotopic tools provided the bases for understanding open versus closed systems.

7.3.2 Implications for molecular mechanisms

Although previous studies have examined early diagenesis and degradation (Hedges et al., 1985; Tegelaar et al., 1989; Hayes, 1993; Bland et al., 1998; Opsahl and Benner, 1999; Poinar and Stankiewicz, 1999), both the natural and laboratory decay series in the current study provide a unique opportunity to examine the fate of a leaf during fossilization, particularly the changes during early diagenesis with post-introduction to microbes. Furthermore, no study has examined this in *Metasequoia*, one of the most well-studied higher plants, which also gives this research a unique perspective for paleo-studies. The molecular mechanisms for morphologically well-preserved fossils became more apparent in the current study.

As soon as the hyphae are able to reach the cellulose-rich mid-vein, particularly the sieve tube elements in the vascular bundle which have only a cellulose-based primary cell walls, there is a drastic change, both molecular and morphologically. As discussed in 5.2.1, Day 9 is the turning point in the molecular degradation where there is the lowest amount of polysaccharide pyrolysates and bulk carbohydrates measured before there is a rapid growth of hyphae (Figure 6 and Table 2). Morphologically, as observed in Figure 8 and Figure 9, the hyphae are nearly at the mid-vein in Day 9 of the *G. candidum* laboratory decay. The amount of degradation was also quantified using the new method, in which the same trend is seen again. The consortium laboratory decay, for example, shows little change in the Bhattacharyya distance for the first several days and then a drastic increase from Day 12 of the consortium laboratory decay (Figure 16).

After only nine days after introduction, the *G. candidum* were able to penetrate the cuticle via stomata and infiltrate the entire leaf and gradually collapse the cell wall structures (Figure 7). This provides three major findings. 1) Previous morphological and geochemical studies, the way in which hyphae physically attack leaf tissues was poorly understood, and is now better understood. We directly observed that the microbe penetrated the leaf epidermis via stomatal entry (Figure 8). 2) The time needed for penetration was explored. In both laboratory decay experiments, inoculated with either *G. candidum* or a consortium, took approximately ten days for hyphae to infiltrate the leaf (Figure 8). 3) The rate of degradation post-penetration was divulged. After leaf epidermis penetration, the microbes were able to quickly and efficiently remove polysaccharide from the leaf cell wall structures within days (Figure 7 and Figure 16). Microbial growth stabilized towards the end of the 25 d period, suggesting the microbes had exhausted all sugars, carbohydrates, and polysaccharides in the leaf, leaving only complex lignin and waxes behind (2.2.3, Figure 16).

In addition to polysaccharide playing a major role in the preservation of the laboratory decay, the amount of polysaccharide directly relates to morphological preservation in the natural decay and fossil samples, confirming a previous observation based upon limited fossil materials (Yang et al., 2007). Polysaccharide decay occurs quickly during early diagenesis when samples are exposed to microbial life, as seen in the laboratory and natural decay samples.

7.3.3 Impact on fossilization

While morphological evidence can be congruent with molecular data (e.g. Yang et al., 2005), morphological preservation is not always reflected at molecular and/or isotopic levels and thus must be viewed tentatively when considering the proxy-value of the given sample (Tegelaar et al., 1989; Poinar and Stankiewicz, 1999; Nguyen Tu et al., 2004; Tipple et al., 2010). However, the examination of three different sample sets (modern laboratory decay, modern natural decay, and fossils) provided insights into which biomolecules play critical roles in maintaining three-dimensional structures at the stage of early diagenesis.

As the laboratory decay has demonstrated that the mid-vein cell wall structures are impossible to maintain without the presence of polysaccharide in the leaf cell wall, especially in the sieve cells and other cellulose-based cells that are observed in fossil samples (4.2.2). Supporting the established hypothesis that microbe-restricted depositional environments are correlated to excellent preservation (Eglinton and Logan, 1991; Briggs and Eglinton, 1994; Gupta et al., 2009), the morphologically intact structures and polysaccharide-rich pyrolysates of the readily-degradable, cellulose-based cell walls in fossil materials (Benner et al., 1990; van der Heijden and Boon, 1994; Franchini et al., 2002) suggest that well-preserved fossil samples were rapidly buried, thus subsequently prevented the typical microbial degradation.

Given that the fossils were rapidly buried (due to lack of observable microbial activity, large molecular polysaccharide abundances, and three-dimensionally preserved structures), the positive isotope shift (up to ~4‰) in the Arctic fossil *lagerstätten* is not likely due to isotope fractionations associated with microbial degradation, but instead due to the change of

environmental parameters (Farquhar et al., 1989; Hayes, 1993; Jahren and Sternberg, 2003; Yang et al., 2011).

Although other plants typically produce different homologues throughout various stages of the growing season (El-Otmani and Coggins, 1985; Gülz et al., 1991; Nguyen Tu et al., 2004), the modern natural decay series demonstrates that *M. glyptostroboides* leaves have little $\delta^{13}\text{C}$ variation during different stages of senescence (Figure 5 and Table 3). It isn't until the modern natural decay leaves are exposed to aquatic microbes that there is a significant 1‰ negative shift in $\delta^{13}\text{C}$ (Figure 5 and Table 3). Thus, the approximately -24‰ $\delta^{13}\text{C}$ value in *Metasequoia* fossil *lagerstätten* is highly likely from biosynthetic pathways associated with ancient atmospheric isotopes, and not due to the time during the growth season or microbial decay during diagenesis (O'Leary, 1981; Farquhar et al., 1982; Nguyen Tu et al., 2004; Schweitzer et al., 2009).

The relationship of C_3 higher plants assimilating of $\delta^{13}\text{C}$ is approximately 20‰ less than the atmosphere (Bender, 1971; Osmond, 1978; Tipple et al., 2010), where isotopic composition of modern air is generally -7.8‰ compared to PDB (Keeling et al., 1979). However carbon isotope ratios of ancient atmospheric conditions allow for conversion of fossil bulk carbon isotopes to atmospheric CO_2 conditions at the time of fossil deposition (Troughton et al., 1974; Farquhar et al., 1982). To determine the atmospheric changes in CO_2 concentrations (δ_{atm}) during the time of the fossil plant's burial, a modified Farquhar et al. (1982) equation can be implemented (Equation 5).

Equation 5. Relationship between plant tissue carbon isotope value $\delta^{13}\text{C}$ and intercellular CO_2 concentrations.

$$\delta^{13}\text{C} = \delta^{13}\text{C}_{atm} - a - (b - a)c_i/c_a + br$$

The equation takes into account the carbon discrimination associated with the diffusion of air (a), the discrimination in the carboxylation reaction (b), partial pressures of CO_2 (c) in the external atmosphere (c_a) and intercellular spaces (c_i), and the drop in concentration as a proportion of the ambient CO_2 concentration (r). In the case of the fossil *Metasequoia*, the relationship of the extreme positive $\sim 3\text{-}4\text{‰}$ shift in $\delta^{13}\text{C}$ thus suggests a different carbon isotope value of ancient atmospheric CO_2 during the growth of these plant fossils. Given the burning of fossil fuels (with average carbon isotope values of $\sim -28\text{‰}$), the carbon isotope values of modern air ($\delta^{13}\text{C}_{atm}$) is perhaps at its lowest level compared with its geological past. Thus, given *Metasequoia*'s physiological conditions are consistent through geological times, the different CO_2 conditions are likely responsible for the observed carbon isotope changes in fossil *Metasequoia* tissues (Tippie et al., 2010). Higher CO_2 concentrations are associated with higher temperatures, which are likewise indirectly linked to many environmental and climatic features, providing insights into ancient ecosystems (Tippie et al., 2010).

Chapter 8. Conclusion

Modern *Metasequoia glyptostroboides* samples were degraded under two different conditions, laboratory-controlled and natural environment, in order to mimic the early stages of diagenesis in its plant fossil *lagerstätten* counterpart. By using combined molecular, isotopic, and morphological methodologies, we have arrived at several major conclusions, including new insights in to molecular mechanism for the preservation of three dimensional cell structures, the potential for a new quantitative morphological approach, and implications for better understanding fossil taphonomy and their isotopic records.

1) Morphological and molecular changes of *Metasequoia* leaves during early diagenesis are evident in all three samples sets of modern laboratory decay, modern natural decay, and fossil samples. Mimicking early diagenesis in the modern samples was achieved, as seen by the continual anatomical deformation at the cellular level along with the reduction of total polysaccharides. Our evidence suggests that polysaccharide is in fact a keystone in maintaining three-dimensional structures, confirming previous observations based on fossil material. Samples with more abundant polysaccharides are better morphologically preserved and ranked higher on the quantitative pixel-count evaluation method, which offered new insights on the degradation process.

2) The quantitative pixel-count evaluation method offers a new morphological tool to aid morphologists in ranking samples with different degrees of degradation. Not only did the method offer similar final results as molecular, isotopic, and traditional morphological tools, but offers new perspectives in its quantification of degradation. The method can be readily

modified to examine the degradation of other materials, as well as be modified for any use in which there are visible differences in the sample image.

3) Because both modern decay series provide evidence that polysaccharide-induced diagenesis occurs quickly in leaves, as seen by the qualitative and quantitative morphological observations, fossil samples that maintained three-dimensional cellulose-based structures were likely rapidly buried and thus not exposed to microbial degradation. Removal of polysaccharides in the open-system natural decay led to a small shift ($\sim -1\text{‰}$) in bulk carbon isotopes, an indication of bulk carbon isotope fractionation due to microbial decay in the pond samples. As decay in *Metasequoia* fossil *lagerstätten* was held only at early stage, the large positive isotope shift ($\sim 3\text{-}4\text{‰}$) in the fossils is likely due to environmental causes.

Acknowledgements

I'd like to thank the committee for their time and efforts in helping me complete my Master's Thesis. Thank you to my advisor for the past seven years, Dr. Hong Yang, for all of his persistent guidance, insights, and opportunities he has provided in my emerging science career. His leadership has taught me the difference between a scientist and a technician. Thank you to Dr. Qin Leng for her meticulous observations and unparalleled morphological expertise, to Dr. Gaytha Langlois for paving the road for my undergraduate and graduate degrees, and to Dr. Dan McNally for his unique perspectives and constant support.

Dr. John Dietrich's many years of advice has helped me grow as a writer, as an academic, and as a person – I can never thank him enough. I am grateful to the Bryant University Department of Science and Technology, especially Dr. Brian Blais for help with the new pixel-count evaluation method, but more importantly for intellectual stimulation, generous advice, and enduring friendship. I thank Drs. Julie Crowley-Parmentier and Chris Reid for their kindness, advice, and instrumental expertise. I am also grateful to the Department of Microbiology at China University of Geosciences, particularly to Dr. Feng Liang for help with the laboratory decay series and Dr. Hongmei Wang for the use of her lab. Thank you to Dr. George E. Cody for NMR and Dr. Weiguo Liu for offline bulk carbon isotope analysis.

This research was funded by a NASA Experimental Program to Stimulate Competitive Research (EPSCoR) Grant for Bryant University and Hanban Scholarship for the one year study at CUG Wuhan. This manuscript represents the contribution of 201402 in the Laboratory of Terrestrial Environments at Bryant University.

References

- Abramowitz, M., and Davidson, M. W. (2004). Introduction to Microscopy. Retrieved March 3, 2014, from the *Optical Microscopy at the National High Magnetic Field Laboratory* website: <http://micro.magnet.fsu.edu/primer/anatomy/introduction.html>.
- Anthon, G.E., and Barrett, D.M. (2001). Colorimetric Method for the Determination of Lipoxygenase Activity. *Journal of Agriculture and Food Chemistry*. 49:1, 32–37.
- Bartnicki-Garcia, S., Bracker, C.E., Gierz, G., Lopez-Franco, R., Lu, H. (2000). Mapping the Growth of Fungal Hyphae: Orthogonal Cell Wall Expansion during Tip Growth and the Role of Turgor. *Biophysical Journal*. 79:5, 2382–2390.
- Barber, K.E., Chambers, F.M., Maddy, D. (2003). Holocene palaeoclimates from peat stratigraphy: macrofossil proxy climate records from three oceanic raised bogs in England and Ireland. *Quaternary Science Reviews*. 22:5–7, 521–539.
- Basinger, J.F. (1991). The fossil forest of the Buchanan Lake Formation (early Tertiary), Axel Heiberg Island, Canadian Arctic Archipelago: preliminary floristics and paleoclimate. *Geological Survey of Canada Bulletin*. 403, 39–66.
- Berry, J.A., Troughton, J.H. (1974). Carbon isotope fractionation by C₃ and C₄ plants in ‘closed’ and ‘open’ atmospheres. *Carnegie Institute Washington*. 73, 785–90.
- Blanchette, R.A., Cease, K.R., Abad, A., Burnes, T. (1991). Ultrastructural characterization of wood from Tertiary fossil forest in the Canadian Arctic. *Canadian Journal of Botany*. 69, 560–568.
- Briggs, D.E., Eglinton, G. (1994). Chemical traces of ancient life. *Chemistry in Britain*. 31, 907–912.
- Briggs, D.E.G. (2003). The role of decay and mineralization in the preservation of soft-bodied fossils. *Annual Review of Earth and Planetary Science*. 31, 275–301.
- Chaney, R.W. (1951). A revision of fossil *Sequoia* and *Taxodium* in western North America based on the recent discovery of *M. glyptostrobooides*. *Transaction of the American Philosophical Society*. 40, 171–239.
- Charmen, D.J., Blundell, A., Chiverrell, R.C., Hendon, D., Langdon, P.G. (2006). Compilation of non-annually resolved Holocene proxy climate records: stacked Holocene peatland palaeo-water table reconstructions from northern Britain. *Quaternary Science Reviews*. 25:3–4, 336–350.
- Chaverri, P., Samuels, G.J. (2003). Hypocrea/Trichoderma (Ascomycota, Hypocreales, Hypocreaceae): Species with green ascospores. *Studies in Mycology*. 48, 1–116
- Cover, T., Hart, P. (1967). Nearest neighbor pattern classification. *Information Theory*. 13:1, 21–27.

- Davies, T.J., Barraclough, T.G., Chase, M.W., Soltis, P.S., Soltis, D.E., Savolainen, V. (2004). Darwin's abominable mystery: a supertree of the angiosperms. *Proc National Academy of Science USA*. 101, 1904–1909.
- Dilcher, D. (2000). Toward a new synthesis: Major evolutionary trends in the angiosperm fossil record. *PNAS*. 97:13, 7030–7036.
- Dilcher, D.L. (2001). Paleobotany: some aspects of non-flowering and flowering plant evolution. *Taxon*. 50, 697–711.
- Doyle, J.A., Hickey, L. J. (1976). in *Origin and Early Evolution of Angiosperms*, ed. Beck, C. B. (Columbia Univ. Press, New York), pp. 139–206.
- Duda, R.O., Hart, P.E., Stork, D.G. (2001). *Pattern Classification*. Wiley-Interscience Publication. 1–24.
- Eglinton, G., Logan, G.A. (1991). Molecular preservation [and Discussion]. *Philosophical Transactions of the Royal Society of London*. 333, 315–328.
- El-Otmani, M., Coggins Jr., C.W. (1985). Fruit development and growth regulator effects on normal alkanes of “Washington” naval orange fruit epicuticular waxes. *Journal of Agriculture and Food Chemistry*. 33, 656–663.
- Endress, P.K., Igersheim, A. (2000). Gynoecium structure and evolution in basal angiosperms. *International Journal of plant Science*. 161:6, 211–223.
- Fabio, R. (2003). From point cloud to surface: The modeling and visualization problem. *International Archives of the Photogrammetry, Remote Sensing and Spatial Information Sciences*. 34, 5–10.
- Farquhar, G.D., O’Leary, M.H., Berry, J.A. (1982). On the relationship between carbon isotope discrimination and the intercellular carbon dioxide concentration in leaves. *Australian Journal of Plant Physiology*. 9, 121–137.
- Farquhar, G.D., Ehleringer, J.R., Hubick, K.T. (1989). Carbon isotope discrimination and photosynthesis. *Annual Review of Plant Physiology and Plant Molecular Biology*. 40, 503–537.
- Felton, M.J. (2004). Looking for Isotopes: Three varieties of MS have become the technologies of choice in determining isotope ratios. *American Chemical Society Technology and Tools*. 39–41.
- Florin, R. (1963). The distribution of conifer and taxad genera in time and space. *Acta Horti. Berg*. 20, 121–312.
- Franchini, J.C., Gonzalez-Vila, F.J., Rodriguez, J. (2002). Decomposition of plant residues used in no-tillage systems as revealed by flash pyrolysis. *Journal of Analytical and Applied Pyrolysis*. 62, 35-43.

- Friis, E.M., Pedersen, K.R., Crane, P.R. (2005). When Earth started blooming: insights from the fossil record. *Current Opinion in Plant Biology*. 8, 5–12.
- Gülz, P.G., Müller, E., Prasad, R.B.N. (1991). Developmental and seasonal variations in the epicuticular waxes of *Tila tomentosa* leaves. *Phytochemistry*. 30, 769–773.
- Gupta, N.S., Pancost, R.D. (2004). Biomolecular and physical taphonomy of angiosperm leaf during early decay: Implications for fossilization. *Palaeo*. 19, 428–440.
- Gupta, N.S., Yang, H., Leng, Q., Briggs, D.E.G., Cody, G.E., Summons, R.E. (2009). Diagenesis of plant biopolymers: Decay and macromolecular preservation of *M. glyptostrobooides*. *Organic Geochemistry*. 40, 802–809.
- Hall, P., Park, B.U., Samworth, R.J. (2008). Choice of neighbor order in nearest-neighbor classification. *The Annals of Statistics*. 36:5, 2025–2550.
- Harris, D. C. (1999). Gas Chromatography. In *Quantitative chemical analysis*, 5th ed.; W. H. Freeman and Company. 675–712.
- Hayes, J.M. (1993). Factors controlling ^{13}C contents of sedimentary organic compounds: Principles and evidence. *Marine Geology*. 113, 111–125.
- Hedges, J.L., Cowie, G.L., Ertel, J.R., Barbour, R.J., Hatcher, P.G. (1985). Degradation of carbohydrates and lignins in buried woods. *Geochimica et Cosmochimica Acta*. 49, 701–711.
- Hickey, L. J. (1973). Classification of the architecture of dicotyledonous leaves. *American Journal of Botany*. 60, 17–33.
- Hickey, L.J., Wolfe, J. A. (1975). The bases of angiosperm phylogeny: the woody dicots. *Ann. Missouri Botany Gard*. 62, 538–589.
- Hu, H.H. and Cheng, W.C. (1948). On the new family *M. glyptostrobooides* and on *M. glyptostrobooides*, a living species of the genus *M. glyptostrobooides* found in Szechuan and Hupeh. *Bulletin of the Fan Memorial Institute of Botany*. 2, 153–162.
- Hughes, N.F. (1994). The enigma of angiosperm origins. Cambridge: Cambridge University Press. 230–242.
- Jahren, A.H., Sternberg, L.S.L. (2003). Humidity estimate of the middle Eocene Arctic rainforest. *Geology*. 31, 463–466.
- Kohn, M.J. (2010). Carbon isotope compositions of terrestrial C3 plants as indicators of (paleo)ecology and (paleo)climate. *PNAS*. 107:44, 19691–19695.
- Kuhls, K., Lieckfeldt, E., Samuels, G. J., KoVacs, W., Meyer, W., Petrini, O., Gams, W., Börner, T., Kubicek, C.P. (1996). Molecular evidence that the asexual industrial fungus *Trichoderma reesei* is a clonal derivative of the ascomycete *Hypocrea jecorina*. *Proceedings of the National Academy of Sciences*. 93: 7755–7760.

- Leng, Q., Yang, H., Yang, Q., Zhou, J. (2001). Variation of cuticle micromorphology of *M. glyptostrobooides* (Taxodiaceae). *Botanical Journal of the Linnean Society*. 136:2, 207–219.
- Leng, Q., Langlois, G.A., Yang, H. (2010). Early Paleogene Arctic terrestrial ecosystems affected by the change of polar hydrology under global warming: Implications for modern climate change at high latitudes. *Science China Earth Sciences*. 53:7, 933–944.
- Li, C., Yang, Q. (2003a). Polymorphism of ITS sequences of nuclear ribosomal DNA in *Metasequoia glyptostrobooides*. *Journal of Genetics and Molecular Biology*. 13: 264–271.
- Li, C., Yang, Q. (2003b). Phylogenetic relationships among the genera of *Taxodiaceae* and *Cupressaceae* from 28S rDNA sequences. *Heredity*. 25: 177–180.
- Liang, M.M., Bruch, A., Collinson, M., Mosbrugger, V., Li, C.S., Sun, Q.G., Hilton, J. (2003). Testing the climatic estimates from different paleobotanical methods: an example from the Middle Miocene Shanwang flora of China. *Palaeogeography, Palaeoclimatology, Palaeoecology*. 198: 3–4, 279–301.
- Liu, Y., Li, C., Wang, Y. (1999). Studies on fossil *M. glyptostrobooides* from north-east China and their taxonomic implications. *Botanical Journal of the Linnean Society*. 130, 267–297.
- Liu, W., Ning, Y., An, Z., Wu, Z., Lu, H., Cao, Y. (2005). Carbon isotopic composition of modern soil and paleosol as a response to vegetation change on the Chinese Loess Plateau. *Science in China Series D: Earth Sciences*. 48:1, 93–99.
- Martin, A. and Synge, R. (1941). Applications of Partition Chromatography. *American Chemical Society and the Chemical Heritage Foundation*. 35, 1358–1366.
- McDermott, F. (2004). Palaeo-climate reconstruction from stable isotope variations in speleothems: a review. *Quaternary Science Reviews*. 23: 7–8, 901–918.
- McIver, E.E., Basinger, J.F. (1999). Early Tertiary floral evolution in the Canadian high Arctic. *Annals of the Missouri Botanical Garden*. 86, 523–545.
- McMaster, M. and McMaster, C. (1998). GC/MS: a practical user's guide. Wiley: New York. 12–13.
- Moberg, A., Sonechkin, D.M., Holmgren, K., Datsenko, N.M., Karlen, W. (2005). Highly variable Northern Hemisphere temperatures reconstructed from low- and high-resolution proxy data. *Nature*. 433, 613–617.
- National Institute for Standards and Technology (NIST) (2010). Electron Ionization Library Component of the NIST Mass Spectral Library and NIST GC Retention Index

- Database. Retrieved January 5, 2014 from NIST website:
http://www.nist.gov/mml/chemical_properties/data/electionlibcomp.cfm.
- The Nobel Foundation (2002). The Nobel Prize in Chemistry 2002: Information for the Public. Retrieved from the Nobel Prize website:
http://nobelprize.org/nobel_prizes/chemistry/laureates/2002/public.html.
- Nobel Media (2014). The transmission electron microscope—Preparation of specimen. Retrieved March 5, 2014 from the Nobel Prize website:
<http://www.nobelprize.org/educational/physics/microscopes/tem/preparation.html>.
- Nguyen Tu, T.T., Derenne, S., Largeau, C., Bardoux, G., Mariotti, A. (2004). Diagenesis effects on specific carbon isotope composition of plant *n*-alkanes. *Organic Geochemistry*. 35, 317–329.
- Nummiaro, K., Koller-Meier, E., Van Gool, L. (2003). An adaptive color-based particle filter. *Image and Vision Computing*. 21:1, 99–110.
- O’Leary, M.H. (1981). Carbon isotope fractionation in plants. *Phytochemistry*. 20, 553–567.
- Opsahl, S. and Benner, R. (1999). Characterization of carbohydrates during early diagenesis of five vascular plant tissues. *Organic Geochemistry*. 30:1, 83–94.
- Peulve, S., de Leeuw, J.W., Sicre, M., Bas, M., Saliot, A. (1996). Characterization of macromolecular organic matter in sediment traps from the northwestern Mediterranean Sea. *Geochimica et Cosmochimica Acta*. 60, 1239–1259.
- Poinar, H.N., Stankiewicz, B.A. (1999). Protein preservation and DNA retrieval from ancient tissues. 96:15, 8426–8431.
- Prosser, J.I. and Trinci, A.P.J. (1978). A model for hyphal growth and branching. *Microbiology*. 111:1, 153–164.
- Rao, D. V. S., Muraleedharan, K., Humphreys, C. J. (2010). TEM specimen preparation techniques. In *Microscopy: Science, Technology, Applications and Education*. Mendez-Vilas, Ed., Diaz, Ed. 1232–1244.
- Schweitzer, M., Fear, J., Cadisch, G. (2009). Isotopic ($\delta^{13}\text{C}$) fractionation during plant residue decomposition and its implications for soil organic matter studies. *Rapid Communications in Mass Spectrometry*. 13, 1284–1290.
- Sfikas, G. Constantinopoulos, C., Likas, A., Galatsanos. (2005). An analytic distance metric for Gaussian mixture models with application in image retrieval. *Lecture Notes in Computer Science*. 3697, 835–840.
- Shetty, P. H., Archer, J., Porter, M. (1993). In *Nobel Laureates in Chemistry 1901–1992*; James, L. K., Ed.; Washington, DC: American Chemical Society and the Chemical Heritage Foundation. 352–355.

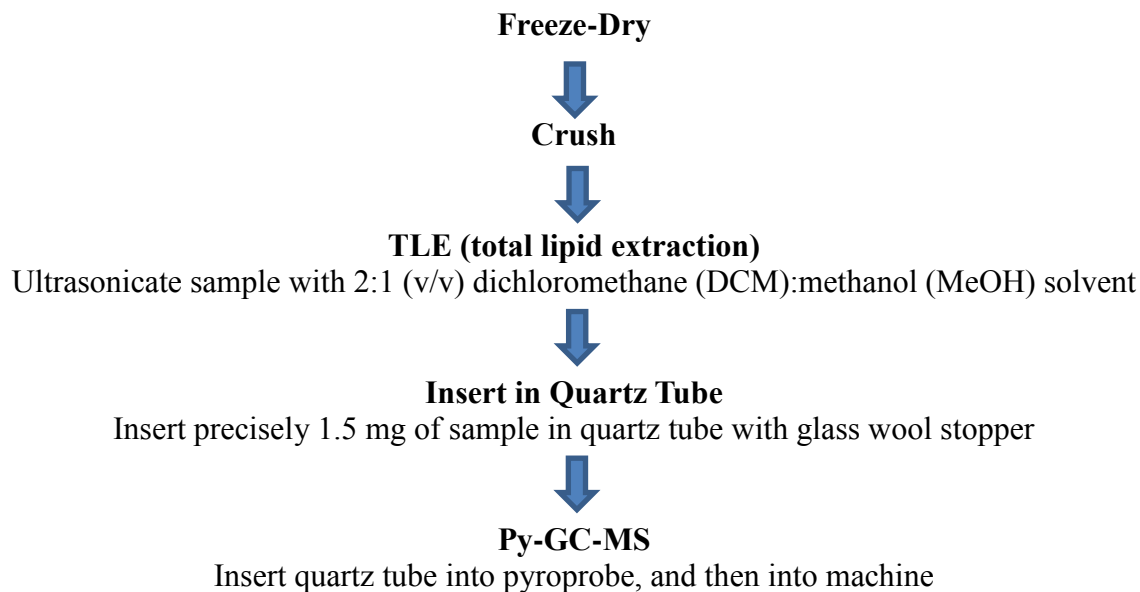
- Sietsma, J.H. and Wouters, J.T.M. (1971). Cell wall composition and “Protoplast” formation of *G. candidum*. *Archiv für Mikrobiologie*. 79:3, 236–273.
- Soltis, D.E., Soltis, P.S., Zanis, M.J. (2002). Phylogeny of seed plants based on evidence from eight genes. *American Journal of Botany*. 89, 1670–1681.
- Stevens, T., Thomas, D.S.G., Armitage, S.J., Lunn, H.R., Lu, H. (2007). Reinterpreting climate proxy records from late Quaternary Chinese loess: A detailed OSL investigation. *Earth-Science Reviews*. 80:1–2, 111–136.
- Stocker, T.F., Mysak, L.A. (1992). Climatic fluctuations on the century time scale: A review of high-resolution proxy data and possible mechanisms. *Climatic Change*. 20:3, 227–250.
- Tegelaar, E.W., de Leeuw, J.W., Derenne, S., Largeau, C. (1989). A reappraisal of kerogen formation. *Geochim Cosmochim. Acta*. 53, 3103–3106.
- Tipple, B.J., Meyers, S.R., Pagani, M. (2010). Carbon isotope ratio of Cenozoic CO₂: A comparative evaluation of available geochemical proxies. *Paleoceanography*. 25, 1–11.
- Toussaint, G. (2005) Geometric proximity graphs for improving nearest neighbor methods in instance-based learning and data mining. *International Journal of Computational Geometry*. 15:2, 101–150.
- Trinci, A.P.J. and Collinge, A.J. (1975). Hyphal wall growth in *Neurospora crassa* and *G. candidum*. *Microbiology*. 91:2, 355–361.
- Trinci, A.P.J. (1972). A study of the kinetics of hyphal extension and branch initiation of fungal mycelia. *Microbiology*. 81:1, 225–236.
- Uhl, D., Mosbrugger, V. (1999). Leaf venation density as a climate and environmental proxy: a critical review and new data. *Palaeogeography, Palaeoclimatology, and Palaeoecology*. 149: 1–4, 15–26.
- van den Brink, J. and de Vries, R.P. (2011). Fungal enzyme sets for plant polysaccharide degradation. *Applied Microbiology and Biotechnology*. 91:6, 1477–1492.
- van der Heijden, E., Boon, J.J. (1994). A combined pyrolysis mass spectrometric and light microscope study of peatified Calluna wood isolated from raised bog peat deposits. *Organic Geochemistry*. 22, 903-919.
- van Fossen, A.L., Lewis, D.L., Nichols, J.S., Kelly, R.M. (2008). Polysaccharide degradation and synthesis by extremely thermophilic anaerobes. *Annals of the New York Academy of Sciences*. 1125, 322–337.
- Verschuren, D. (1999). Sedimentation controls on the preservation and time resolution of climate-proxy records from shallow fluctuating lakes. *Quaternary Science Reviews*. 18:6, 821–837.

- Wang, L. (2010). Morphology and anatomy of *M. glyptostrobooides* leaves and their environmental indicative values: Evidence from the comparative studies of “living fossil” and fossils. *Nanjing Institute of Geology and Paleontology*. Nanjing: The Graduate School of Chinese Academy of Sciences. 423.
- Watt, I. M. (1997). The principles and practice of electron microscopy. Second edition. Press Syndicate of the University of Cambridge.
- Witkowski, C., Gupta, N.S., Yang, H., Leng, Q., Williams, C.J., Briggs, D.E.G., Summons, R.E. (2012). Molecular preservation of Cenozoic conifer fossil *lagerstätten* from Banks Island, the Canadian Arctic. *Palaios*. 27:5, 279–287.
- Wolf, J.A. (1971). Tertiary climatic fluctuations and methods of analysis of Tertiary floras. *Palaeogeography, Palaeoclimatology, Palaeoecology*. 9, 27–57.
- Wolf, J.A. (1977). Paleogenen Floras from the Gulf of Alaska Region. *US Geological Survey Professional Paper*. 997, 1–108.
- Xiang, B., Berger, T. (2003). Efficient text-independent speaker verification with structural Gaussian mixture models and neural network. *Speech and Audio Processing*. 11:5, 447–456.
- Xiao, L., Yang, H., Sun, B., Li, X., Guo, J. (2013). Stable isotope compositions of recent and fossil sun/shade leaves and implications for paleoenvironmental reconstruction. *Review of Palaeobotany and Palynology*. 190, 75–84.
- Yang, H., Jin, J. (2000). Phytogeographic history and evolutionary stasis of *Metasequoia*: Geological and genetic information contrasted. *Acta Palaeontologica Sinica*. 39, 288–307.
- Yang, H. (2005). Biomolecules from *Metasequoia*. In: B.A. LePage, C.J. Williams and H. Yang., eds. The geobiology and ecology of *Metasequoia*. Dordrecht: Springer.
- Yang, H., Huang, Y., Leng, Q., LePage, B.A., Williams, C.J. (2005). Biomolecular preservation of Tertiary *M. glyptostrobooides* fossil *lagerstätten* revealed by comparative pyrolysis analysis. *Review of Palaeobotany and Palynology*. 134:3–4, 237–256.
- Yang, H., Leng, Q., LePage, B.A. (2007). Laboratoryile biomolecules in three-dimensionally preserved early Tertiary *M. glyptostrobooides* leaves from Ellesmere Island, Canada. Biological and geological applications. *Bulletin of the Peabody Museum of Natural History Yale University*. 48, 317–328.
- Yang, H., Leng, Q. (2009). Molecular hydrogen isotope analysis of living and fossil plants—*Metasequoia* as an example. *Natural Science*. 19, 901–912.

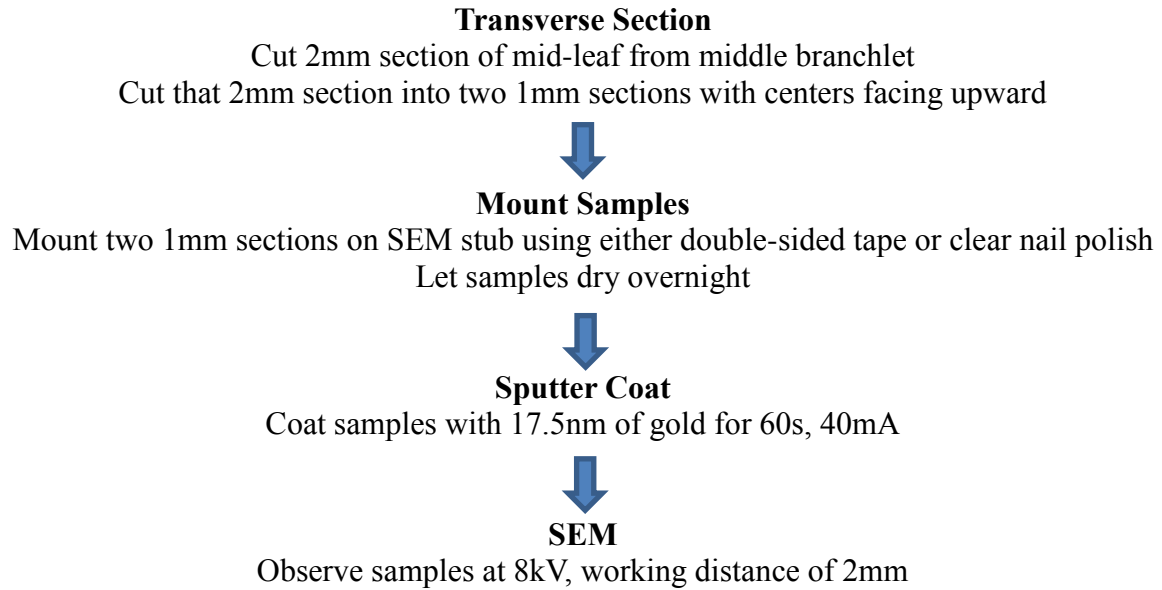
Yang, H., Blais, B.S., Leng, Q. (2011). Stable isotope variations from cultivated *Metasequoia* trees in the United States: A statistical approach to assess isotope signatures as climate signals. *Japanese Association of Historical Botany*. 19:1–2, 75–88.

Appendix A – Flow Charts

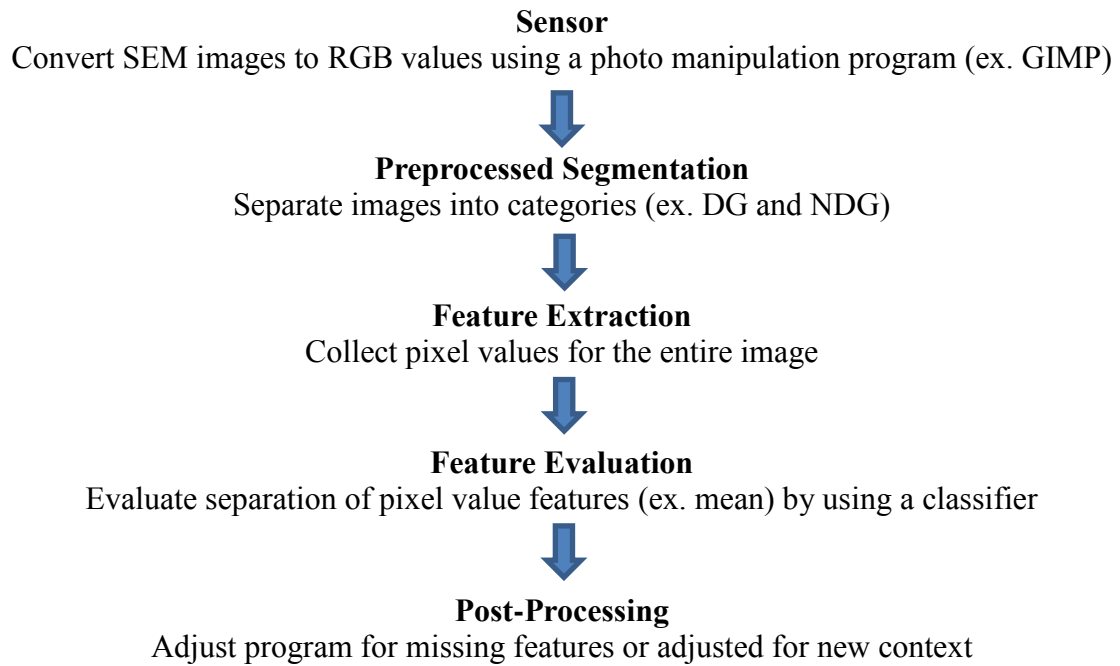
Flow-chart of pyrolysis-gas chromatography-mass spectrometry (modified from Yang et al., 2005; Gupta et al., 2009; Witkowski et al., 2012).



Flow-chart of scanning electron microscopy process (modified from Yang et al., 2005; Leng et al., 2009).

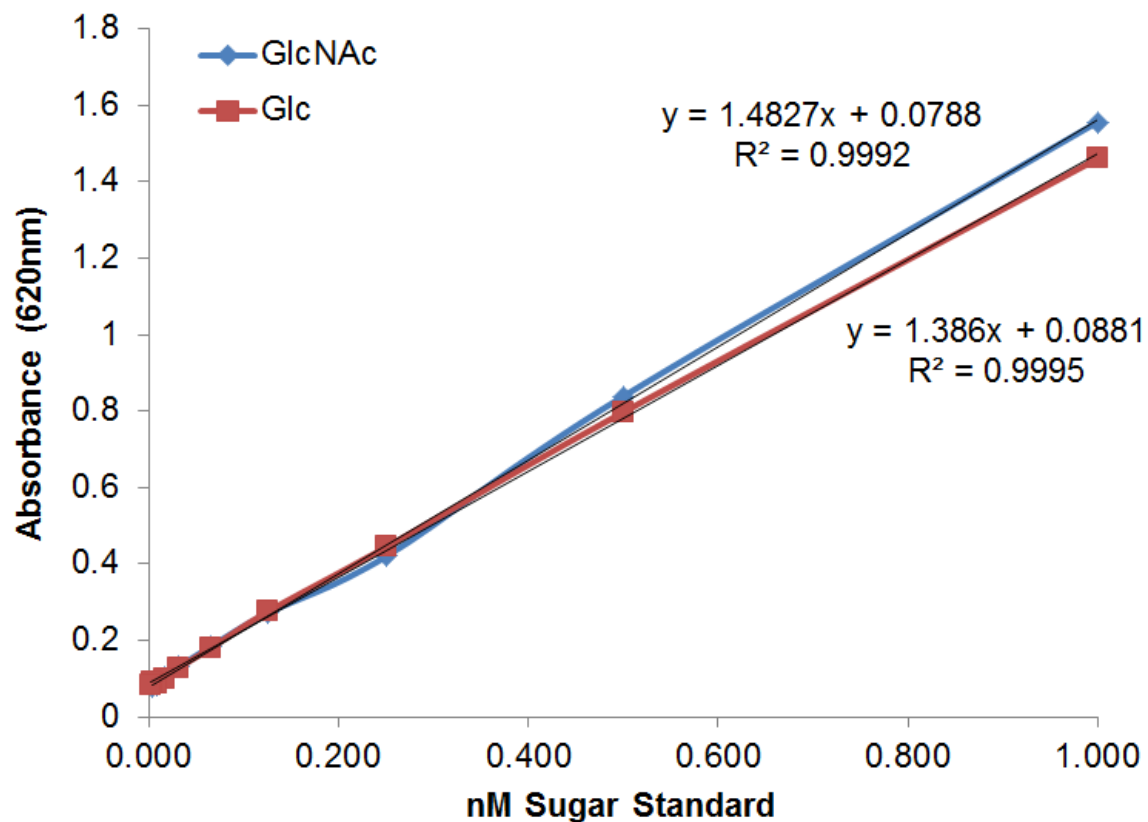


Flow-chart of classification process (modified from Duda et al., 2001).



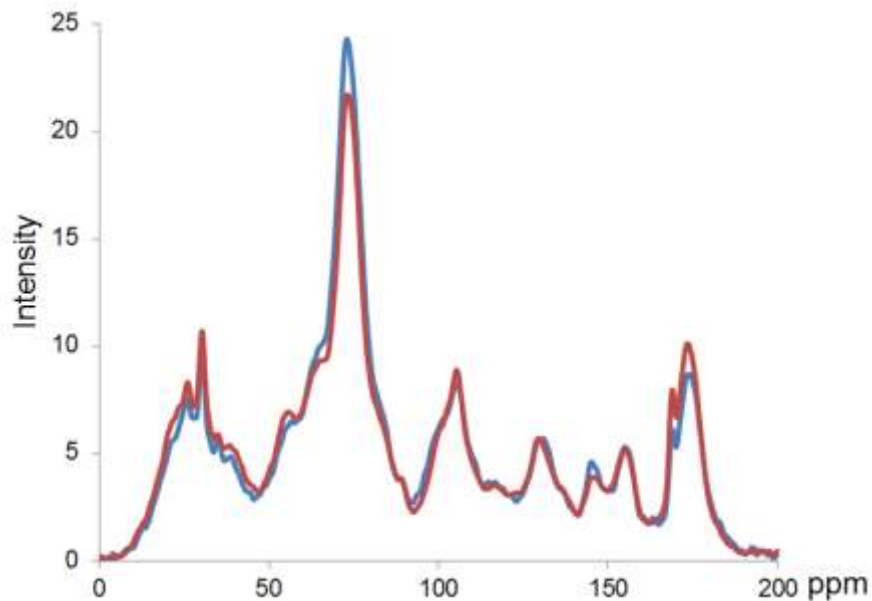
Appendix B – Standards

Standard for 3-methyl-2-benzothiazolinone hydrazone (MBTH) colorimetric assay using N-Acetylglucosamine (GlcNAc, shown in blue) and Glucose (Glc, shown in red), including equations and R^2 values for both.

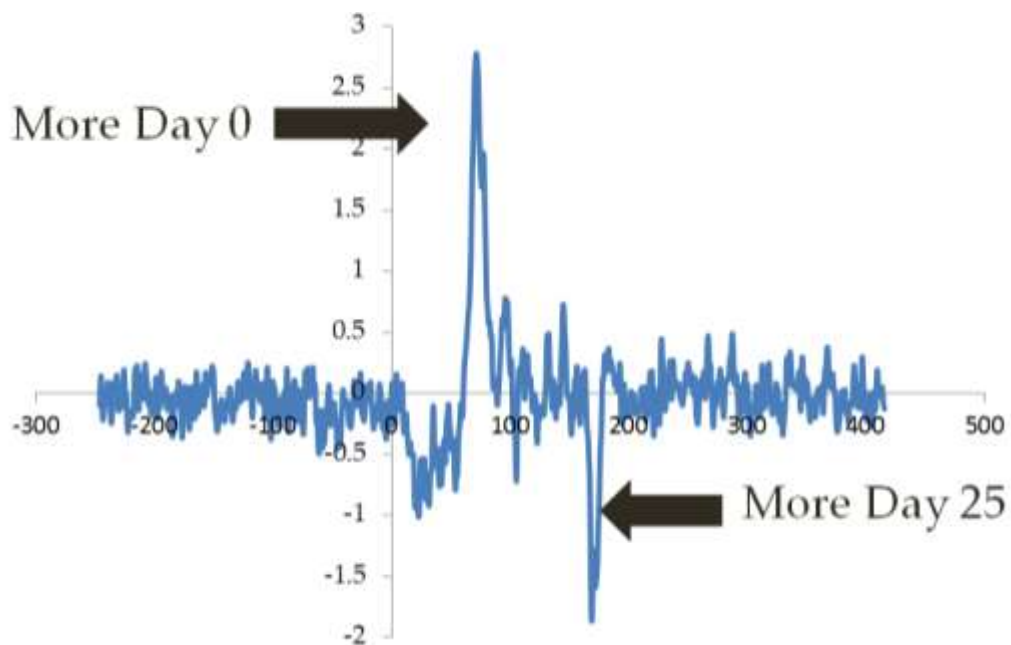


Appendix C – NMR Results

Nuclear magnetic resonance mass spectroscopy (NMR) for Day 0 (blue) and Day 25 (red).



Nuclear magnetic resonance mass spectroscopy (NMR) for difference between Day 0 (positive) and Day 25 (negative), indicating which sample has greater abundance at specific frequencies.



Appendix D – Polysaccharide in Lab Decay

Hypothesis B, the supported hypothesis for this research on why there is a decrease and later increase in polysaccharides in the laboratory decay series, shows that the leaf polysaccharide decreases constantly throughout the experiment, while the microbial growth explodes around Day 9 when the microbes gain access to the polysaccharide-rich mid-vein of the *Metasequoia* leaves.

